Analysis of cytoplasmic organization and compartmentalization in syncytial *Drosophila* embryo

A Thesis
submitted in partial fulfilment of the
requirements of the degree of

DOCTOR OF PHILOSOPHY
by

SAMEER THUKRAL
20133257

INDIAN INSTITUTE OF SCIENCE EDUCATION AND RESEARCH
PUNE

CERTIFICATE

It is certified that the thesis entitled **"Analysis of cytoplasmic organization and compartmentalization in syncytial *Drosophila* embryo"** submitted by **Mr. Sameer Thukral** represents his original work which was carried out by the candidate at IISER, Pune, under my guidance and supervision during the period from **July 2013 to July 2019**.

The work presented here or any part of it has not been included in any other thesis submitted previously for the award of any degree or diploma from any other University or institution. I further certify that the above statements made by him in regard to his thesis are correct to the best of my knowledge.

Dr. Richa Rikhy
(Supervisor)
Date:

DECLARATION

I declare that this written submission represents my idea in my own words and where others' ideas have been included; I have adequately cited and referenced the original sources. I also declare that I have adhered to all principles of academic honesty and integrity and have not misrepresented or fabricated or falsified any idea/data/fact/source in my submission. I understand that violation of the above will be cause for disciplinary action by the Institute and can also evoke penal action from the sources which have thus not been properly cited or from whom proper permission has not been taken when needed. The work reported in this thesis is the original work done by me under the guidance of Dr. Richa Rikhy.

Sameer Thukral
Reg.no. 20123257
Date:

Table of Contents

Abstract

Syncytial nuclei found in fungi, plant endosperm, insect embryos and muscles maintain an autonomous 'nuclear-cytoplasmic region of influence', thereby generating compartments within a seemingly shared cytoplasm. Molecular diffusion across syncytial nucleo-cytoplasmic domains may be constrained by binding to different components of the cytoarchitecture. The syncytial *Drosophila* blastoderm embryo provides a paradigm to test the impact of binding to the cytoarchitecture on cytoplasmic diffusion. We have analyzed the organization of the cytoplasm and further tested the extent of diffusion of molecules that bind differentially to the cytoarchitecture across nucleo-cytoplasmic domains. We find that the cytoplasm is enriched in a phase separated manner at the cortex of the syncytial *Drosophila* embryo above the yolk. Photobleaching analysis shows that molecules are more constrained above the nuclei as compared to below the nuclei in the syncytial embryo. We generated ectopic diffusion sources of photoactivatable-GFP (PA-GFP) or PA-GFP-Tubulin by photoactivation in the antero-posterior axis.We found that PA-GFP-Tubulin which is incorporated in the tubulin cytoskeleton, spreads less than PA-GFP in the anterior-posterior direction. Using anteriorly localized ectopic probes,we have tested how molecules of different sizes or with different cyto-architectural interactions spread in embryo. Expression of heavier fluorescent molecules at the anterior showed a shallow linear gradient in the antero-posterior axis as compared to RFP that spread uniformly throughout the embryo. Expression of anteriorly PH-PLC-CFP that has an attachment to plasma membrane phospholipids however, created an exponential gradient. We have further tested what cyto-architectural components can restrict these gradients, using Bicoid gradient as a functional readout. Mutants affecting the cytoarchitecture of the syncytial embryo differentially affect these gradients and our study proposes a role of the cytoarchitecture in differentially constraining gradients based on their molecular properties.

Synopsis

Name of the Student: **Sameer Thukral**
Registration number: **20133257**
Name of Thesis advisor: **Dr. Richa Rikhy**
Date of Registration: **24th July 2013**
Place: **Indian Institute of Science Education and Research (IISER), Pune**
Title: **Analysis of cytoplasmic organization and compartmentalization in syncytial *Drosophila* embryo**

Introduction

Cytoplasm is defined as all the material present inside the cell membrane excluding the nucleus (Shepherd, 2006).Our understanding of the cytoplasm has evolved over the past decades, from that being of an aqueous dilute homogenous medium with infinite volume and free diffusion to that of a crowded heterogeneous medium which is complex.

In the cytoplasmic space, various forms of subcellular organization exist in both prokaryotic and eukaryotic cells.These include some well studied forms of cellular organization like active transport,enclosed membranes (organelles and vesicles) or binding to intracellular/extracellular landmarks like the centrosome or extra cellular matrix (ECM). The cytoplasm,on the other hand, is traditionally considered to be unorganized and homogenous,allowing free mixing of components. The property of crowdedness and presence of cytoskeletal elements can cause steric hindrance to the solutes present in the cytoplasm.The confinement,which divides the cytoplasm into various ‘compartments’ without the presence of obvious membrane based restriction, may be termed as cytoplasmic compartmentalization.This compartmentalization may be due to transient binding to existing structures or due to size exclusion. There have been various studies on cytoplasmic compartmentalization (Janson et al., 1996a; Luby-Phelps et al., 1986a; Luby-Phelps et al., 1987; Provance et al., 1993) and it’s functional implications in both prokaryotes (Parry et al., 2014a; Parry et al., 2014b) and eukaryote (Baum et al., 2014; Kuimova et al., 2009).

Syncytial systems provide an interesting opportunity to study cytoplasmic compartmentalization and restriction. A syncytium can be defined as a cell where multiple nuclei are contained within a single common plasma membrane. Cytoplasmic compartmentalization gains importance in the syncytia because each nucleus has to maintain its separate functional identity by separating its products from those produced by other nuclei, in the absence of plasma membrane boundaries. Such compartmentalization in syncytia has been reported in fungi (Gladfelter, 2006; Gladfelter et al., 2006; Lee et al., 2013), muscle cells (Cutler et al., 2018; Pavlath et al., 1989; Windner et al., 2019) and plant cells (Brown et al., 2003; Pickett-Heaps et al., 1999) in the context of restricted diffusion of either mRNA or proteins.

Drosophila embryogenesis begins with 9 nuclear division cycles deep within the embryo during the pre-blastoderm stage.Nuclei along with centrosomes migrate to the cortex in nuclear cycle 10 and the nuclear division cycles 11-14 occur beneath the cortex forming the syncytial blastoderm embryo (Foe and Alberts, 1983; Foe,Odell and Edgar, 1993; Karr, 1986; Sullivan and Theurkauf, 1995; Warn, 1986).The Bicoid and Dorsal morphogens spread across the antero-posterior and dorso-ventral axis respectively to form gradients in the syncytial *Drosophila* embryo.Restriction and compartmentalization of ER, Golgi, plasma membrane and mitochondria to energids has been reported in the syncytial embryo (Chowdhary et al., 2017; Frescas et al., 2006; Mavrakis et al., 2009a)

In this study, we focussed on cytoplasmic compartmentalization in the *Drosophila* early embryo syncytium and have used the Bicoid morphogen system as a paradigm to study our observations in a functional context.

Results

Cortical enrichment of the cytoplasm during syncytial blastoderm stage

The syncytial blastoderm consists of nuclear cycles 10 to 13 which take place near the cortex of the embryo, just below the plasma membrane. Using maternally expressed fluorescent tags, like mRFP, Tubulin and Dynamin, we find that rather than uniformly spreading all across the embryo, the cytoplasm is present in a narrow band of 30 to

40µm layer near the cortex. Further, this enrichment increases across nuclear cycles. We also observe gradual movement of yolk platelets towards the centre of the embryo, forming two phases of the cortical cytoplasm and bulk yolk.

Greater restriction in cytoplasmic exchange above the nuclei than in the nuclear plane or below the nuclei

In order to test the extent of exchange of cytoplasm between individual energid during the blastoderm stages, we conducted FLIP experiments in the plane of or above the nuclei during interphase of nuclear cycle. We found that there is greater restriction to exchange of cytoplasm between energids, above the nuclei rather than in the nuclear plane. Further, this restriction was greater during metaphase. This could be either due to increased crowding due to the presence of centrosomes or due to the presence of nascent membrane/pseudo-cleavage furrows.

Photoactivation as a tool to study cytoplasmic restriction

We have used photoactivation of cytoplasmic PA-GFP to analyze its distribution and diffusion across nucleo-cytoplasmic domains of the syncytial *Drosophila* embryo and further compared it to PA-GFP-Tubulin, which is present in the cytoplasm and is also incorporated in microtubules. We find that PA-GFP spreads to a greater distance (as inferred from its length scale) than PA-GFP-Tubulin, at steady state concentrations. Thus, diffusion is constrained by interaction with the cyto-architecture components of the syncytial blastoderm embryo.

Photoactivation of cytoplasmic probes suggests cortical enrichment and difference in local diffusion

Photoactivation of both these components showed diffusion to a greater distance in the antero-posterior axis in the cortex as compared to the depth of the embryo, thus confirming that the cytoplasmic components have an increased concentration at the cortex near the nucleo-cytoplasmic domains. Further, photoactivated cytoplasmic components diffused less when generated at the center of the embryo as compared to the anterior, a difference which exists in the pre-blastoderm embryo as well,thus

suggesting inherent differences in diffusion either due to architecture or geometry. Posterior and anterior activations lead to similar length scales for PA-GFP-Tubulin.

Using anterior localization of fluorescent probes with different properties to assess compartmentalization

We analyzed the extent of diffusion of free cytoplasmic proteins and plasma membrane associated PH-PLC-CFP when expressed anteriorly like Bicoid using the *bcd*-3'UTR. This gave us the opportunity to study restriction to energids based on varying molecular properties. We found that even though anteriorly expressed 5X/8XGFP created a gradient as compared to mRFP, it was not sufficient to form the exponential spread. The steeper gradient observed for anteriorly expressed PH-PLC-CFP showed an exponential spread. This suggests that the spread of proteins in the syncytial *Drosophila* embryo could be restricted depending on their interaction with the cytoarchitecture within each energid, than just size alone.

Using Bicoid gradient as a paradigm to study cytoplasmic compartmentalization

We have used the Bicoid gradient paradigm in syncytial *Drosophila* embryos as a paradigm to test functional implications of cytoplasmic restriction and compartmentalization. We have compared it to plasma membrane associated PH-PLC-CFP which is expressed anteriorly like Bicoid. Anteriorly expressed PH-PLC-CFP and Bicoid gradient remained at the cortex even across the change in cytoarchitecture during each syncytial division cycle. Actin remodelling regulated both PH-PLC-CFP and Bicoid gradients while pseudocleavage furrows affected the restriction of PH-PLC-CFP and not Bicoid.

References

Baum, M., Erdel, F., Wachsmuth, M. and Rippe, K. (2014). Retrieving the intracellular topology from multi-scale protein mobility mapping in living cells. *Nat. Commun.***5**, 4494.

Brown, R. C., Lemmon, B. E. and Nguyen, H. (2003). Events during the first four rounds of mitosis establish three developmental domains in the syncytial endosperm of Arabidopsis thaliana. *Protoplasma* **222**, 167–174.

Chowdhary, S., Tomer, D., Dubal, D., Sambre, D. and Rikhy, R.(2017). Analysis of mitochondrial organization and function in the Drosophila blastoderm embryo.*Sci. Rep.***7**, 5502.

Cutler, A. A., Jackson, J. B., Corbett, A. H. and Pavlath, G. K.(2018). Non-equivalence of nuclear import among nuclei in multinucleated skeletal muscle cells.*Journal of Cell Science***131**, jcs207670.

Foe, V. E. and Alberts, B. M.(1983). Studies of nuclear and cytoplasmic behaviour during the five mitotic cycles that precede gastrulation in Drosophila embryogenesis.*J. Cell Sci.***61**, 31–70.

Foe,Odell and Edgar (1993). Mitosis and morphogenesis in the Drosophila embryo: point and counterpoint. In *The Development of Drosophila melanogaster* (ed. Michael Bates, A. M. A.), pp. 149–300.Cold Spring Harbor Laboratory Press.

Frescas, D., Mavrakis, M., Lorenz, H., Delotto, R. and Lippincott-Schwartz, J. (2006). The secretory membrane system in the Drosophila syncytial blastoderm embryo exists as functionally compartmentalized units around individual nuclei. *J. Cell Biol.***173**, 219–230.

Gladfelter, A. S. (2006). Nuclear anarchy: asynchronous mitosis in multinucleated fungal hyphae. *Curr.Opin.Microbiol.***9**, 547–552.

Gladfelter, A. S., Hungerbuehler, A. K. and Philippsen, P.(2006). Asynchronous nuclear division cycles in multinucleated cells.*J. Cell Biol.***172**, 347–362.

Janson, L. W., Ragsdale, K. and Luby-Phelps, K.(1996). Mechanism and size cutoff for steric exclusion from actin-rich cytoplasmic domains.*Biophys.J.***71**, 1228–1234.

Karr, T. L.(1986). Organization of the cytoskeleton in early Drosophila embryos.*J. Cell Biol.***102**, 1494–1509.

Kuimova, M. K., Botchway, S. W., Parker, A. W., Balaz, M., Collins, H. A., Anderson, H. L., Suhling, K. and Ogilby, P. R. (2009). Imaging intracellular viscosity of a single cell during photoinduced cell death. *Nat. Chem.***1**, 69–73.

Lee, C., Zhang, H., Baker, A. E., Occhipinti, P., Borsuk, M. E. and Gladfelter, A. S. (2013). Protein aggregation behavior regulates cyclin transcript localization and cell-cycle control. *Dev. Cell***25**, 572–584.

Luby-Phelps, K., Taylor, D. L. and Lanni, F. (1986). Probing the structure of cytoplasm. *J. Cell Biol.***102**, 2015–2022.

Luby-Phelps, K., Castle, P. E., Taylor, D. L. and Lanni, F.(1987). Hindered diffusion of inert tracer particles in the cytoplasm of mouse 3T3 cells.*Proc. Natl. Acad. Sci. U. S. A.***84**, 4910–4913.

Mavrakis, M., Rikhy, R. and Lippincott-Schwartz, J. (2009). Plasma membrane polarity and compartmentalization are established before cellularization in the fly embryo. *Dev. Cell***16**, 93–104.

Parry, B., Surovtsev, I., Cabeen, M., O'Hern, C., Dufresne, E. and Jacobs-Wagner, C. (2014a). Cellular Metabolism Fluidizes the Glassy Bacterial Cytoplasm. *Biophysical*

*Journal***106**, 313a.

Parry, B. R., Surovtsev, I. V., Cabeen, M. T., O'Hern, C. S., Dufresne, E. R. and Jacobs-Wagner, C. (2014b). The bacterial cytoplasm has glass-like properties and is fluidized by metabolic activity. *Cell***156**, 183–194.

Pavlath, G. K., Rich, K., Webster, S. G. and Blau, H. M.(1989). Localization of muscle gene products in nuclear domains.*Nature***337**, 570–573.

Pickett-Heaps, J. D., Gunning, B. E., Brown, R. C., Lemmon, B. E. and Cleary, A. L. (1999). The cytoplast concept in dividing plant cells: cytoplasmic domains and the evolution of spatially organized cell. *Am. J. Bot.***86**, 153–172.

Provance, D. W., Jr, McDowall, A., Marko, M. and Luby-Phelps, K.(1993). Cytoarchitecture of size-excluding compartments in living cells.*J. Cell Sci.***106(Pt 2)**, 565–577.

Shepherd, V. A. (2006). The cytomatrix as a cooperative system of macromolecular and water networks. *Curr.Top. Dev. Biol.***75**, 171–223.

Sullivan, W. and Theurkauf, W. E. (1995). The cytoskeleton and morphogenesis of the early Drosophila embryo. *Curr.Opin. Cell Biol.***7**, 18–22.

Warn, R. M. (1986). The cytoskeleton of the early Drosophila embryo. *J. Cell Sci. Suppl.***5**, 311–328.

Windner, S. E., Manhart, A., Brown, A., Mogilner, A. and Baylies, M. K. (2019). Nuclear Scaling Is Coordinated among Individual Nuclei in Multinucleated Muscle Fibers. *Dev. Cell***49**, 48–62.e3.

List of abbreviations

3’UTR	3’ UnTranslated Region
AP	Anterior-Posterior
CFP	Cerulean Fluorescent Protein
EGFP	Enhanced Green Fluorescent Protein
ER	Endoplasmic Reticulum
FCS	Fluorescence Correlation Spectroscopy
FLIP	Fluorescence Loss in Photobleaching
FP	Fluorescent Protein
FRAP	Fluorescence Recovery After Photobleaching
LD	Lipid Droplet
mRFP	monomeric Red Fluorescent Protein
NC	Nuclear Cycle
NC	Nuclear Cycle
NCD	Nuclear Cytoplasmic Domains
NLS	Nuclear Localization Signal
PA	Photo Activation
PA-GFP	PhotoActivatable-GFP
PH-PLC	PH domain of PhosphoLipase C-δ
PM	Plasma Membrane
ROI	Region of Interest
SDD	Synthesis Diffusion Degradation
SEM	Scanning Electron Microscopy
WT	Wild Type

List of Tables

List of Movies

All movies have been uploaded chapter wise at this google drive link:
https://bit.ly/39d9lYJ

Chapter 3

Mov3.S1: mCherry-Tubulin: mCherry-Tubulin expressed with *mat*-Gal4 is imaged in the syncytial division cycles. Note mCherry-Tubulin incorporation into centrosome, spindle and cortical microtubules.

Mov3.S2: Lipid Droplets (LD-2.6-GFP): Lipid Droplets tagged with the LD-2.6-GFP marker expressed with *mat*-Gal4 is imaged in the syncytial division cycles. Note lipid droplets move gradually below the nuclei, towards the centre of the embryo across nuclear cycles.

Mov3.S3: FLIP of Dynamin-GFP above the nuclei. Note the discernable boundaries of the energids and rates of fluoresence depletion within and outside the energids.

Mov3.S4: FLIP of Dynamin-GFP in the nuclear plane. Note that there are no discernable boundaries of the energids and rates of fluoresence depletion near and far from the ROI are only dependent on the distance from the ROI.

Mov3.S5: Yolk movement across cycles in time and depth. Yolk can be seen as black circles in this embryo containing mRFP expressed under *nanos*-Gal4. Notice the gradual movement of yolk towards lower Z sections across cycles.

All movies (except S5) are in shown in 16 color intensity rainbow scale where Blue represents the lowest intensity and red represents the highest intensity. Scale bar=10μm or 50μm as mentioned.

Chapter 4

Mov4.S1: Cytoplasmic GFP: GFP expressed under the *ubi* promoter is imaged across the syncytial division cycles. Note that GFP enters the nuclei in interphase.
Mov4.S2: mCherry-Tubulin: mCherry-Tubulin expressed with *mat*-Gal4 is imaged in the syncytial division cycles. Note mCherry-Tubulin incorporation into centrosome, spindle and cortical microtubules.
Mov4.S3: PA-GFP anterior photoactivation: Region of interest at the anterior is photoactivated to create a source of PA-GFP. Note that PA-GFP enters the nuclei in interphase.
Mov4.S4: PA-GFP-Tubulin anterior photoactivation: Region of interest at the anterior is photoactivated to create a source of PA-GFP-Tubulin. Note PA-GFP-Tubulin incorporation into centrosome, spindle and cortical microtubules.
Mov4.S5: PA-GFP middle photoactivation: Region of interest in the middle of the embryo is photoactivated to create a source of PA-GFP.
Mov4.S6: PA-GFP-Tubulin middle photoactivation: Region of interest in the middle of the embryo is photoactivated to create a source of PA-GFP-Tubulin.
Mov4.S7: PA-GFP anterior photoactivation in RhoGEF2-OE embryos: Region of interest at the anterior is photoactivated to create a source of PA-GFP in RhoGEF2-OE embryos.
Mov4.S8: PA-GFP-Tubulin anterior photoactivation in RhoGEF2 mutants: Region of interest at the anterior is photoactivated to create a source of PA-GFP-Tubulin in RhoGEF2-OE embryos.
Mov4.S9: PA-GFP anterior photoactivation in *eb1* mutant embryos: Region of interest at the anterior is photoactivated to create a source of PA-GFP in *eb1* RNAi expressing embryos

Mov4.S10: PA-GFP-Tubulin anterior photoactivation in EB1 mutants: Region of interest at the anterior is photoactivated to create a source of PA-GFP-Tubulin in *eb1* RNAi expressing embryos. Note the undulations caused by yolk contractions and that the cytoplasm remains peripheral, without mixing with the embryo yolk region.

Chapter 5

Mov5.S1: *mat-Gal4*>UASp-RFP-*bcd*-3'UTR

Anteriorly localized UASp-RFP containing the bicoid *(bcd)* 3'UTR localization signal expressed using the *maternal*-Gal4 and imaged across the syncytial division cycles 11-14. Anterior is to the left. Note that RFP enters the nucleus.

Mov5.S2: *mat*-Gal4>UASp-5x-GFP-*bcd*-3'UTR

Anteriorly localized UASp-5X-GFP containing the bicoid *(bcd)* 3'UTR localization signal expressed using the maternal Gal4 and imaged across the syncytial division cycles 11-14. Anterior is to the left. A linear gradient could be seen.

Mov5.S3: *mat*-Gal4>UASp-PH-PLC-CFP-*bcd*-3'UTR

Anteriorly localized UASp-PH-PLC-CFP containing the bicoid *(bcd)* 3'UTR localization signal expressed using the maternal Gal4 and imaged across the syncytial division cycles 12-14. Anterior is to the left. PH-PLC-CFP labels the complete apical and lateral membrane.

Mov5.S4: Bicoid-Venus

Bicoid tagged to Venus under the Bicoid endogenous promoter imaged across the syncytial division cycles 10-14. Anterior is to the left. Bicoid gradient can be seen in the AP axis. Bicoid signal can be seen in the nucleus in interphase and cytoplasmic in metaphase.

Chapter 6

Mov6.S1: Bicoid-Venus-DeltaK

BicoidΔK50-57 tagged to Venus under the Bicoid endogenous promoter imaged across the syncytial division cycles 11-14. Anterior is to the left. BicoidΔK50-57 gradient can be

seen in the AP axis. BicoidΔK50-57 signal is seen in the cytoplasm in both interphase and metaphase.

Mov6.S2: Bicoid-Venus in Act-RFP OE

Bicoid-Venus expressed and imaged in an embryo over expressing Actin-RFP across syncytial cycles 11-13. Anterior is to the left. The embryo undergoes many rounds of contraction and the gradient is disrupted.

Mov6.S3: *nos*-Gal4>UASp-PH-PLC-CFP-*bcd*-3'UTR in Act-RFP OE

UASp-PH-PLC-CFP-*bcd*-3'UTR expressed and imaged in an embryo over expressing Actin-RFP across syncytial cycles 11-13. Anterior is to the left. The interphase and metaphase furrows are absent in most of the embryo. The embryo undergoes contraction and the gradient is disrupted.

Mov6.S4: Bicoid-Venus in *ralA* RNAi

Bicoid-Venus expressed and imaged in an embryo expressing *ralA* RNAi across syncytial cycles 12-14. Anterior is to the left. Even though the embryo undergoes many rounds of contraction, the gradient is not disrupted.

Mov6.S5: BicoidΔK50-57-Venus in *ralA* RNAi

BicoidΔK50-57-Venus expressed and imaged in an embryo expressing *ralA* RNAi across syncytial cycles 12-14. Anterior is to the left. Even though the embryo undergoes many rounds of contraction, the gradient is not disrupted.

Mov6.S6: *mat*-Gal4>UASp-PH-PLC-CFP-*bcd*-3'UTR in *ralA* RNAi

UASp-PH-PLC-CFP-*bcd*-3'UTR expressed and imaged in an embryo expressing *ralA* RNAi across syncytial cycles 11-14. Anterior is to the left. The interphase and metaphase furrows are absent in most of the embryo. The embryo undergoes contraction and the gradient is disrupted.

List of Figures

Chapter 1: Introduction

Chapter 2: Methods and Materials

Chapter 3: Cytoplasmic distribution and dynamics in the early *Drosophila* syncytial embryo

Chapter 4: Photoactivation as a tool to test cytoplasmic distribution and dynamics by creating ectopic localized gradients

Chapter 5: Estimation of the role of molecular size and interaction with cyto-architecture in formation of antero-posterior gradient

Chapter 6: Bicoid gradient as a paradigm to study the cytoplasmic compartmentalization

Acknowledgement

“Where there is challenge, there is joy of progress.
Where there is challenge, a moving drama is born.
Where there is challenge, there shines a glorious future.

All things in the universe are constantly engaged in challenge.
Flowers strive to break through the deep snows to send up new sprouts.
Waves crash tirelessly against rocks on the shore, wearing them down.
Day after day, the sun bursts forth from the darkness and emerges joyously.

All things quietly and tenaciously persevere,
working unceasingly to fulfil their unique mission,
whether seen or unseen.
Challenge! Challenge! Challenge!
That is what it means to be alive.

I will keep moving forward--
for my single, small step today
will eventually forge a great path!
I will not be defeated--
for I know that, even after dark nights of raging blizzards,
the sun of victory will rise again tomorrow without fail!”

-Dr Daisaku Ikeda, The New Human Revolution, Vol26

I would like to deeply express my gratitude to my guide, Dr Richa Rikhy. I had been very worried about choosing the right institute and then the right lab with the right temperament of the guide and what luck I have to have been in Richa’s lab. I am grateful for her amazing personality of taking everyone along, of having a dialogue to resolve issues and of great attention to detail. I’m glad that even when having scientific differences of opinions, she ensures people feel respected and still have the freedom to pursue what they find convincing. For this, I’m truly awed by her.

I've been lucky to have great friends in the lab, specially my close friends, Bipasha and Swati. Their scientific inputs and inputs on life have kept me going through these years. Bipasha has been my closest friend since the past 12 years and I've learnt a lot from her grit and sincerity and her love of food, movies and art. Swati has helped me remain creative by her injections of randomness into the normalcy of daily life.

Our lab atmosphere has always been such an amazing place to be. I've never felt judged or talked behind my back or side stepped and such an environment in the rough world of science is a rare find. Thanks to Darshika for permeating the lab with her fun, Dnyanesh for his random songs, Tirthosree for her excitement, Sayali for her ultra-bad jokes, Bhavin for his sincerity and the new kids, Soumya and Debasmita for their willingness to learn and contribute.

Our collaborators at IIT Mumbai, Mithun, Amitabha and Bivash have really been such a stroke of good fortune. We have learnt so much from them and their depth and uniqueness have brought a different flavour to this work. I am deeply grateful to have Dr. Girish Deshpande as a scientific advisor to whom I have been able to turn to for any scientific and non-scientific advice. It is rare to find such mentors who are genuinely interested in other's success.

I'm so proud to be part of Bharat Soka Gakkai, an NGO working for peace, culture and education, based on humanistic principles of Buddhism. Their close support in Pune, especially Sapna, Shamit, Varsha and Karna have made me learn so much in life. My deepest gratitude to my mentor in life, Dr Daisaku Ikeda, whose writings have sustained me through the ups and downs of life. I would like to quote some lines, which pulled me up through months of feeling under confident.

"No successful person has ever led a life that was only smooth sailing without exerting great effort. No one has ever triumphed in life without experiencing failures and setbacks. True victors in life are those who have persevered arduously through

hardship, stoop on the edge of despair many times, yet pressed forward tenaciously, again and again."
-Dr. Ikeda in The New Human Revolution, Vol26.

I'm also glad that I could pursue my interests in singing and theatre along with my scientific endeavours. A big shout out to the folks at Drama club, Dhriti, Shweta, Amogh and Akanksha, who have become amazing friends. Shweta has been there for over 8 years and I have so much to learn from her, despite her jokes. Dhriti's boldness, Amogh's focus on perfection and Akanksha's fun, are all things I will cherish. I owe a great deal to Prof John Mathew for being who he is and teaching me not only theatre but an amazing approach to life.

The faculty at IISER Pune have been extremely supportive and encouraging. I owe many discussions and perspectives to interactions with Dr Sudha Rajamani, Dr. Girish Ratnaparkhi, Dr Ramana Athreya, Prof. N.K. Subhedar and Dr M.S.Madhusudhan. I also would like to thank Dr Aurnab Ghose, Dr Thomas Pucadyil and Dr Chetan Gadgil for their helpful suggestions as members of my advisory committee.

Members of Girish lab, especially Vallari and my batch mates, especially Shrikant and Raunaq have provided much needed respite when needed. My summer student, Anjana Madhosoodhan also made me undergo training about how to guide students effectively and humanely to bring out their best.

Three cheers to the support staff at IISER Pune. Tushar from the Dean's office, Mahesh, Kalpesh, Piyush, Shabnam and Mrinalini are the best support ever in getting things done. I'm amazed by their sense of responsibility and how they ensure that students never suffer due to lack of reagents or by too much paperwork. Snehal, Ashwini and Yashwant from the fly lab are known for their diligence and I'm thankful for their focus on always supporting the work over their own convenience. Vijay from Microscopy has been such a great support. If you're stuck with microscopy, he will

make you unstuck and somehow make it work. Kudos to him and the microscopy team at IISER.

The mess food, the mess servers (who have often given me extra sweets or an extra portion), Surendra Pujari anna from G1 canteen, the security guards who have always identified me on the gate and never asked for a register entry, have made my experience at IISER so much more meaningful and richer.

Lastly, I would like to offer deep gratitude to my parents, Mr Satish and Sunita Thukral, my brother, sister-in-law and my nephew, Saurabh, Mukti and Sahaj Thukral, for persevering through the long period of my absence at home, for supporting my studies and for always being there for me and allowing me to work without any pressures or distractions. I owe so much to you.

Chapter 1: Introduction

Chapter 1 summary: *In this chapter, we discuss the basic motivation for studying cytoplasm. Further, we discuss how syncytial systems provide an ideal setup to study the various cytoplasmic properties, namely, restricted diffusion and compartmentalization. We also look at compartmentalization in the early Drosophila embryo in the context of morphogens.*

Cytoplasm is defined as all the material present inside the cell membrane excluding the nucleus and other membrane bound organelles. Our understanding of the cytoplasm has evolved over the past decades from that being of an aqueous dilute homogenous medium with infinite volume and free diffusion to that of a crowded complex heterogeneous medium.

In this chapter, we discuss our current understanding of the nature of cytoplasm from various perspectives. We will look at cytoplasmic constituents, diffusion in cytoplasm, factors influencing cytoplasmic diffusion, functional and metabolic changes to cytoplasmic properties and finally consider how syncytia provide a unique system to study cytoplasmic properties.

1.1 Cytoplasm is a complex medium which restricts diffusion in a differential manner

Spatial organization is one of the hallmarks of a cell and is not dissociable from functional regulation. Various forms of subcellular organization exist in both prokaryotic and eukaryotic cells. These include some well-studied forms of cellular organization like active transport, enclosed membranes (organelles and vesicles) or binding to intracellular/extracellular landmarks like the centrosome or extra cellular matrix (ECM). The cytoplasm, on the other hand, is traditionally considered to be unorganized, allowing free mixing of components.

However, the cellular interior is extremely crowded. Illustrations drawn to scale using ultra-structural data provide a sense for how crowded the cellular interior is in both prokaryotes (Goodsell, 2009) and eukaryotes (Goodsell, 2011) (Figure 1.1). The protein

content of cells ranges from 17 to 35% by weight (Luby-Phelps, 2000). Moreover, the eukaryotic cytoplasm is not simply a solution of high protein concentration, but also contains membrane bound organelles of different sizes, which are supported & organized by a network of self-assembling polymers, called the cytoskeleton. The cytoskeletal elements include actin filaments, microtubules and intermediate filaments, which are all interconnected and anisotropically distributed (Luby-Phelps, 2000).

Figure 1.1: Illustrating crowding and heterogeneity in the cytoplasm. (Left) Cross section through an Escherichia coli cell, showing all macromolecules. (**Middle)** Protein sorting in the golgi. **(Right)**Transport of a vesicle through the cytoplasm. Images are drawn to scale at a magnification of X 1,000,000. Reproduced from (Goodsell, 2009; Goodsell, 2011)

Considering these properties, cytoplasm is subject to two emergent properties. Firstly, crowdedness and presence of cytoskeletal elements causes steric hindrance to the solutes present in the cytoplasm. This increases the travelling distance between any two points in the cell leading to a decrease in the effective translational diffusion. Secondly, the reduction in available free space may confine cytoplasmic components to a restricted region, even in the absence of binding to other components. This restriction in available free space can be brought about due to transient binding to existing structures or due to size exclusion. This confinement divides the cytoplasm into various ‘compartments’ without the presence of obvious membrane based restriction and is termed as cytoplasmic compartmentalization.

1.1.1 Differential crowdedness results in restricted diffusion of cytoplasmic components

To illustrate size based compartmentalization, inert tracers of various sizes were injected into a Swiss 3T3 cell and their distribution was monitored (Janson et al., 1996b). Unexpectedly, these inert tracers distributed unevenly throughout the cell suggesting that different regions permit or restrict access to molecules of different sizes (Figure1.2). Confirming these findings, a series of studies using Dextrans (Luby-Phelps et al., 1986b), Ficoll (Luby-Phelps et al., 1987) and ratio imaging (Luby-Phelps et al., 1988) established that the cytoplasm retards the motion of inert tracer molecules in a size dependent manner.

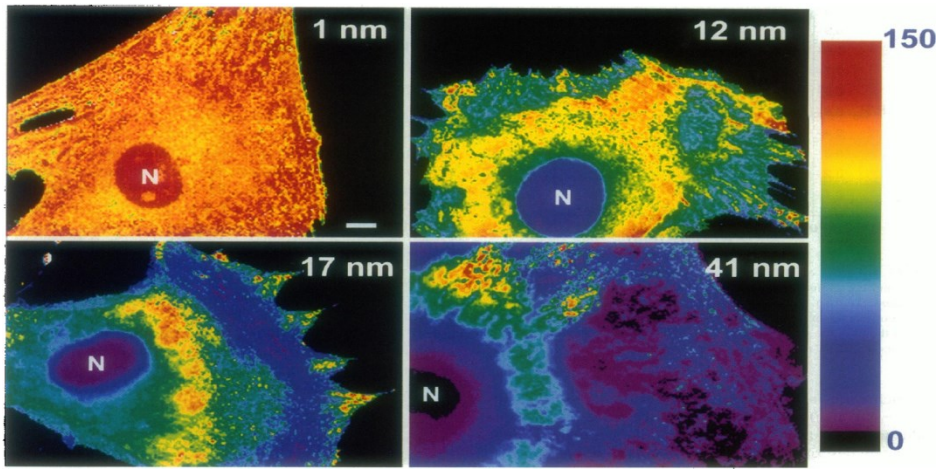

Figure 1.2: Size based compartmentalization of inert tracers. Pseudocolor ratio image maps of the intracellular concentration variations for four different fractions of FTC-Ficoll in single, living Swiss 3T3 cells. Relative intensities are encoded as shown by the color wedge at the right. Warm colors are regions of high concentration and cool colors are regions of low concentration. It can be seen that regions of low intensity (excluding compartments) appear and grow in area as the mean radius of particles in the FTC-Ficoll fraction increases. Bar=10μm. Reproduced from (Janson et al., 1996b).

What cellular component could be involved in mediating size exclusion? Towards this, the ultra-structure of the confining regions was elucidated (Provance et al., 1993). Using TEM, they found that size-excluding compartments lacked membrane-bound organelles and had a dense cytoplasm consisting of numerous, long bundles. The mean 'mesh-size' of the excluding compartments was 31 nm, compared to 53 nm in adjacent non-excluding portions, hence leading to the size cut-off (Figure 1.2).Thus physical

occlusion mediated by cytoskeletal elements and corresponding to lack of membrane bound compartments, created the conditions for such compartmentalization. The term “cyto-architecture” is used for actin, microtubule and intermediate filament networks, along with any other features like phase separating compartments and organellar structures which hinder diffusion and make the cytoplasm heterogenous (Provance et al. 1993; Luby-Phelps 1999).

What cytoskeletal elements made up these bundles? Immunofluorescence experiments showed presence of filament bundles containing F-actin, nonmuscle filamin (ABP280) and α-actinin in distal excluding compartments (Figure1.3), while microtubules and intermediate filament-vimentin were usually absent.

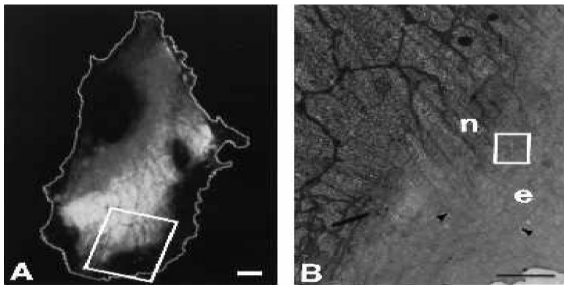

Figure 1.3: Ultrastructural analysis of size excluding compartments. Ultrastructure of distal excluding compartments in a PtK1 cell. (**A)** Fluorescence ratio image of the relative distribution of large and small tracer particles in the living cell. Areas of low intensity are compartments that exclude large particles. (**B)** Electron micrograph of a region of the same cell. Excluding (e) and non-excluding compartments (n) are clearly distinguishable by their ultrastructure. Note the numerous filament bundles in the excluding compartments (arrowheads). Reproduced from (Provance et al., 1993).

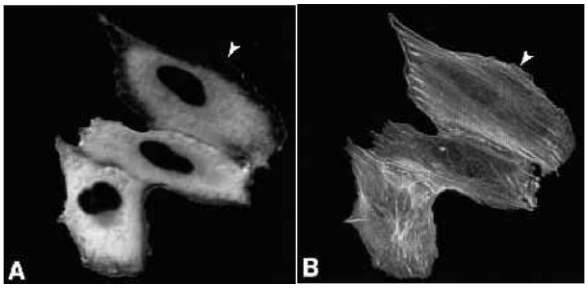

Figure 1.4: Molecular characterization of size excluding compartments. (A) Ratio map of excluding compartments (arrowheads) in a group of CV1 cells immediately before fixation. **(B)** Rhodamine-phalloidin image of F-actin. Reproduced from (Provance et al., 1993).

Moreover, it was found that the regions excluding tracers change both spatially and temporally. For example, upon induction of cellular motility in Swiss 3T3 cells, leading

lamellipodia were found to exclude large tracer molecules (radius >24nm), while allowing entry of smaller (radius<3.5nm) tracers (Luby-Phelps et al., 1988). This illustrates how cytoplasm is restricted by the cytoarchitecture depending on the size of probes and how this property is dynamically modulated as per cellular conditions.

1.1.2 Studying cytoplasmic diffusion and factors influencing it

Knowing the extent of crowding inside cells, it is interesting to ask how diffusion of cytoplasmic components changes in various regions of the cell.

Fluorescence Correlation Spectroscopy (FCS) is a tool to measure the diffusivity in small confocal volume. It measures the correlation of fluorescent molecules moving in and out of the volume and thereby provides information on the diffusivity of the molecule in question. FCS performed at various locations inside a cell can yield differences in diffusivity, which can then be used as a readout of the local heterogeneity in cellular substructures.

Another approach is using Mutli-scale Fluorescence Cross- Correlation Spectroscopy (mFCCS), which involves performing FCCS simultaneously across a series of various confocal volumes. mFCCS is used to measure mean-squared displacement (MSD) values on various time scales, to avoid averaging over long & short time scales, and hence predict the detailed topology of the cell (Figure 1.4a,b). By measuring diffusion coefficients of GFP_1, GFP_3 (3 GFP molecules in tandem) and GFP_5 (5 GFP molecules in tandem), it was found that diffusion in cells deviated from free diffusion. The viscosity of the cytoplasm was found to be 1.3-fold larger than that of water, using GFP_1 as a probe.In the cytoplasm, protein mobility was found to be reduced at a subset of positions, portraying local structural heterogeneity of free spaces separated by obstacles (Baum et al., 2014).

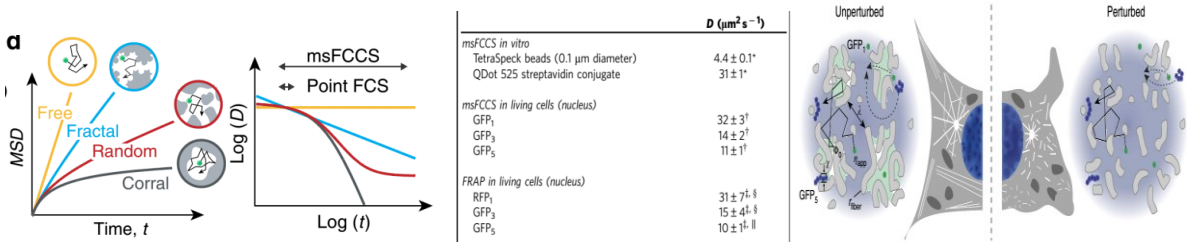

Figure 1.5: Characterizing cellular topology using msFCCS. a (Left). The diffusion coefficients determined for different distances can be used to reconstruct the molecules' Mean Squared Displacement (MSD) as a function of the diffusion time t. The time dependence of the diffusion coefficient reflects the nanostructure 'seen' by the diffusing protein. **Figure 1.5 b (Middle,Table)** Mobility parameters obtained for different tracer molecules *in vitro* and in the nucleus of living cells. **Figure 1.5 c (Right)** Cellular interior appears as a porous medium formed by random obstacles. The correlation length λ for the distance between obstacles 'sensed' by a given protein is derived from the time dependence of its diffusion coefficient. Reproduced from (Baum et al., 2014).

For how long do various sizes of molecules get trapped due to local topology? It was found that GFP3 and GFP5 were significantly (6 to 8%) immobile on the 100ms timescale, while remaining mobile on the minute time scale. The time dependence observed for the average diffusion coefficients showed that the cytoplasm has a multi-scaled random organization. Using mathematical modelling and assuming a polymeric fibre-like structure, it was found that 15% of the cellular space is occupied by obstacles. The mean obstacle diameter of about 12±4nm in the nucleus and 8±4 nm in the cytosol has been reported. The presented observations suggestthat smaller molecules are able to diffuse better because they see the surface of obstacles andbarriers with higher resolution and are able to access smaller pores and channels than larger molecules (Baum et al., 2014) (Figure 1.5c).

In general, the diffusion of various probes is hindered to different extents. Larger probes are trapped due to cytoarchitectural networks more often and easily and therefore show greater retardation in their diffusion when compared to diffusion in water (Figure 1.6).

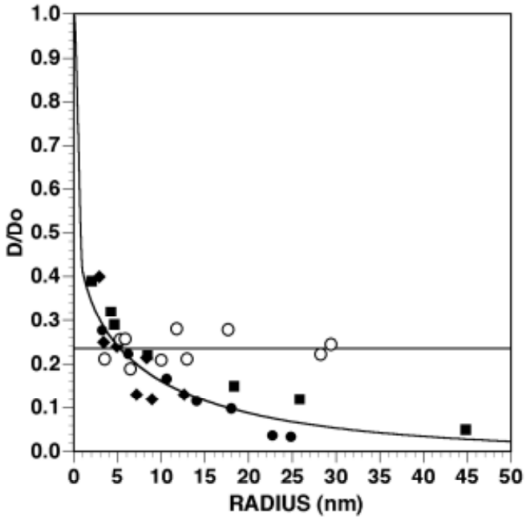

Figure 1.6: Retardation of diffusion in cytoplasm is dependent on the probe size. Relative diffusion coefficients of inert fluorescent tracers in fibroblasts (filled circles, open circles), neurons (squares) and myotubes (diamonds). D/D_0 represents the ratio of diffusion coefficient measured in the system versus that in water for the fluorescent tracer. The nonlinearity in the change of this value suggests the cytoplasmic probes of different sizes are hindered to different extents, suggesting cytoplasmic compartmentalization.Reproduced from (Luby-Phelps, 2000).

1.1.3 Relevance of cytoplasmic compartmentalization in a biological context

Does cytoplasmic compartmentalization and size-dependent diffusion have any role in biological context? How does cytoplasmic crowding change with time or with cell-cycle? What mediates this change and what are the implications of such changes? In this section, we summarize some studies of biological implications of cytoplasmic compartmentalization.

The bacterial cytoplasm provides a different and interesting context to study these properties. Bacterial cytoplasm is crowded, poly-disperse (i.e. has components of wide ranging sizes) and in the absence of known motors, mixingfor metabolic activities, takes place largely due to diffusion. The bacterial cytoplasm has two regimes of viscosity. For particles below a certain size scale ($\leq$ 30nm), the cytoplasm behaves like a simple viscous fluid and for particles above this size the cytoplasm is like a glass-forming liquid (Figure 1.7 (C)). Under natural conditions, this behaviour might reduce diffusion of large macromolecules & hinder cellular activities, yet surprisingly it does not. It was found that metabolic activity suppresses this glassy behaviour by fluidizing the cytoplasm (Figure 1.7 (A), (B)) (Parry et al., 2014b).

This is remarkable as even though the cytoplasm behaves like glass-forming liquid to macromolecules above a size threshold, yet local metabolic activities can fluidize it and allow for faster diffusion locally. Fluidization due to metabolism helps the cell to achieve the delicate balance of maintaining high concentrations of biomolecules without compromising macromolecular motion (Parry et al., 2014a).
Implication of this finding also suggests that the surrounding environmental conditions can dramatically alter cytoplasmic properties.

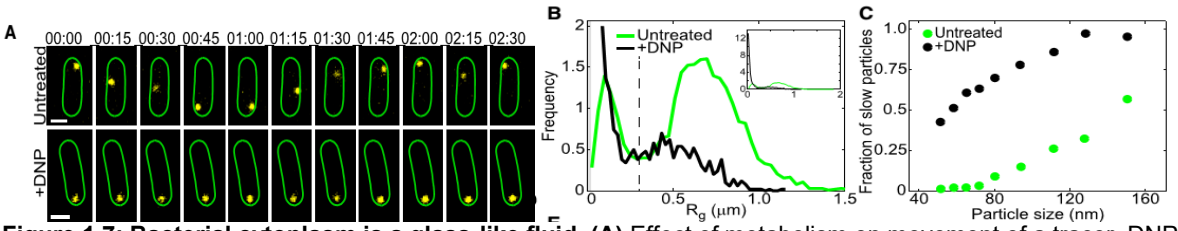

Figure 1.7: Bacterial cytoplasm is a glass-like fluid. (A) Effect of metabolism on movement of a tracer. DNP (2, 4-dinitrophenol) was used to arrest bacterial metabolism. (**B)** Upon DNP treatment, the population of tracers exhibiting larger radius of gyration (R_g) reduces significantly, i.e. tracers become more confined. (**C)** The confinement due to absence of metabolism (DNP), is much more for large particles (~≥30nm) than for smaller particles, observed as fraction of slow particles. Reproduced from (Parry et al., 2014b)

In another study of intracellular viscosity, a porphyrin- dimer-based molecular rotor was used. This molecule exists in two spectrally separable states: planar and twisted. The planar state predominates at dilute solutions, while the twisted conformation predominates in viscous material, thus acting as a viscosity probe. Does cytoplasmic viscosity change on cell death? Using this probe, it was found that local intracellular viscosity increases significantly during irradiation induced cell death, from 50cP to >300cP (Figure 1.8) (Kuimova et al., 2009).

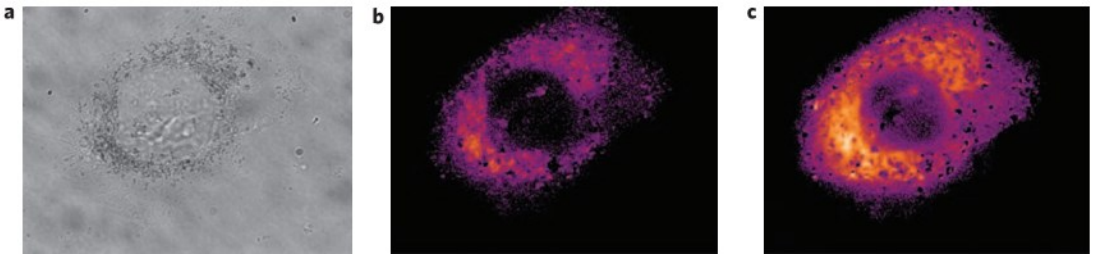

Figure 1.8: Characterizing cellular viscosity during apoptosis. Imaging changes in intracellular viscosity using ratiometric approach. Transmission image (**a)** and ratiometric fluorescence (**b,c)** images of the rotor in a cell obtained during initial (**b)** and advanced (**c)** stages of irradiation; violet corresponds to lower viscosity and orange to higher viscosity, and all viscosities are in the range >>1cP. Reproduced from (Kuimova et al., 2009).

1.1.4 Modelling approaches implicate microtubules in cytoplasmic compartmentalization

Direct or indirect association with cytoskeletal elements is one of the hypothesised ways in which cells can achieve compartmentalization. Another hypothesis is size dependent

entrapping and/or slowing down of macromolecules, such that their mobility is limited around the nucleus where they were produced.

Using computational modelling, it is possible to test whether microtubule networks by themselves can cause cytoplasmic compartmentalization. A study based on mitotic spindles, it was noted that many components of the cytoplasm bind directly or indirectly to the microtubules. Further, the microtubule density is sufficiently high to cause concentration of molecules.Using simulations, it has been suggested that components can concentrate on a particular centrosomal pole by their association with minus ended motors like Dynein. Further, variations in localization can be achieved by regulating binding affinities or mobility & association with multiple motors. The whole process may be modulated since microtubules are regulated drastically across cell cycle. This concentration of components is not necessarily motor dependent, but can also be achieved simply by direct or indirect association with microtubules, thus strongly suggesting that microtubule networks can themselves cause cytoplasmic compartmentalization (Chen et al., 2012).

1.2 Syncytia as a model to study cytoplasm dynamics and distribution

Studies discussed so far have established the extent of cytoplasmic restriction and the cellular context where it might play a role. Next, we turn our attention to a special cellular system, the syncytium, where cytoplasmic restriction on diffusion might play a significant role.

A syncytium can be defined as a cell where multiple nuclei are contained within a single common plasma membrane (non-linear) or where individual cells have connecting channels, allowing transfer of cytoplasmic material (linear). Multinucleated fungi, the *Drosophila* early embryo, skeletal muscle syncytia and plant early endosperm are examples of non-linear syncytia. On the other hand, the nurse cells of the *Drosophila* ovary have connected channels, forming linear syncytia.

The concept of entrapment and cytoplasmic compartmentalization gains importance in the syncytia because each nucleus has to maintain its separate functional identity by separating its products from those produced by other nuclei, in the absence of plasma membrane boundaries. Cytoplasmic compartmentalization may be a way to achieve this. In the following sections, we explore compartmentalization in the context of various syncytial systems and the functions of such compartmentalization.

1.2.1 Inside out model of the cell

Traditional models of the origin of the eukaryotic cell suggest that the formation of various organelles inside the cell is a result of phagocytosis and subsequent symbiosis. For example, the cytoplasm is derived from the host while the nucleus was phagocytosed (Baum and Baum, 2014).Similarly, the mitochondria were phagocytosed by the host. While the endosymbiosis theory has been tested thoroughly, the phagocytosis theory has its origins in the assumption that the plasma membrane was already formed and thus engulfed other organelles. Therefore, the formation of the eukaryotic cell is proposed to be via the ‘outside-in’ mechanism (Baum and Baum, 2014).

Another viewpoint is that of the ‘inside-out’ model of eukaryotic cell origin. In this model, a primitive nucleus existed and formed protrusions using membrane extensions and cytoskeleton. This network of protrusions engulfed mitochondria and other organelles, eventually forming a separate plasma membrane (Baum and Baum, 2014). One of the predictions of this model is that nuclei can retain distinct domains of action in the context of a syncytium.

Julius Sachs introduced the concept of “energids” in 1892 by describing an energid as a nucleus with an associated portion of cytoplasm (“sphere of influence”) (Baluska et al., 2006; Sachs, 1892). Further elaboration of this concept by Daniel Mazia and Baluska led to the concept of the “cell body”, where the smallest autonomous and self-reproducing unit of eukaryotic life is formed by the nucleus and perinuclear microtubules (Baluska et al., 2004).

Thus, syncytial systems provide the opportunity to check this experimentally. By testing whether organelles, cytoplasm and plasma membrane domains maintain nucleus-associated individuality, the two models can be distinguished.

1.2.2 Plant early endosperm develops as a syncytium with different ‘mitotic-domains’

Endosperm develops from one of the two products of the double fertilization process in flowering plants. It develops as a syncytium within a few days after fertilization and comprises a few hundred nuclei. This syncytium is a large cell that ultimately divides into individual cells by the process of cellularization. Even before cellularization, the multinucleate cytoplasm is organized into nuclear-cytoplasmic domains (NCD), essentially a cytoplasmic region in the vicinity of each nucleus. The radial microtubule system emanating from each nucleus “claims” the NCD. The microtubule network also defines the location of future cell boundaries (Figure 1.9 Left and Centre) (Otegui and Staehelin, 2000).

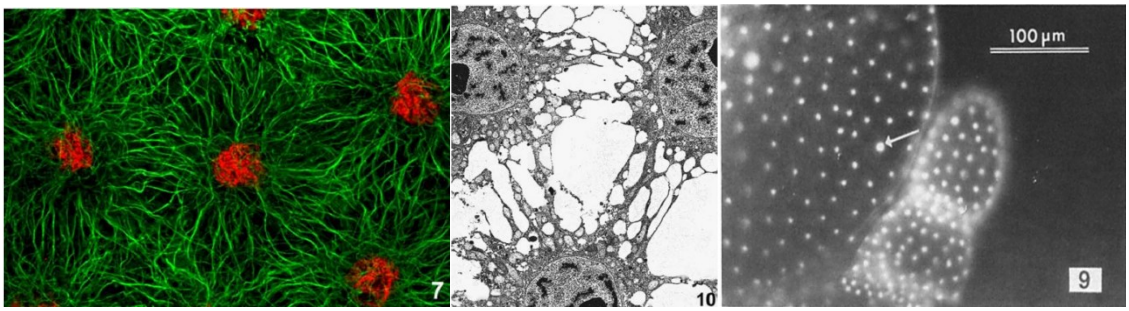

Figure 1.9: Plant endosperm is a syncytia with nucleo-cytoplasmic domains. (**Left)** Radial microtubules emanating from nuclear envelopes replace the irregular network of earlier stages and organize the cytoplasm into NCDs, which are regularly spaced in a hexagonal pattern; Bar=10µm. (**Centre)**TEM showing details of NCD organization. Nuclei appear to be in early prophase and are centrally positioned in a dense cytoplasm containing numerous plastids and mitochondria. Although the NCDs comprise distinct units within the common cytoplasm, there is no sharp line of demarcation;Bar= 6.7µm. Reproduced from (Brown and Lemmon, 2008). (**Right)** The arrow indicates a diploid nucleus. Most of the other nuclei are haploid.Notice the greater area of surrounding cytoplasm associated with the diploid nucleus. Reproduced from (Goff and Coleman, 1987).

Investigating the functional importance of NCDs, the formation of 3 distinct mitotic domains within the shared cytoplasm of the endosperm syncytium was observed. Each domain was characterized by its unique spindle orientation and the arrangement of microtubules in the NCD (Brown et al., 2003). Further characteristization of these

domains revealed that each mitotic domain had a distinct accumulation of cyclin B1;1. What is remarkable is the fact that these different domains are formed in the absence of canonical cell boundaries which delineate nuclei (Boisnard-Lorig et al., 2001). These NCD were also found to scale with the ploidy of the nuclei (Figure 1.9 Right) (Goff and Coleman, 1987; Pickett-Heaps et al., 1999).

Though the concept of NCD is well established in the endosperm, the known functional role of microtubules is limited to defining the future cell walls. No direct evidence is available on the role of microtubules in an NCD in confining/compartmentalizing the nuclear products near a nucleus.

1.2.3 The muscle cell shows “myo-nuclear domains” of restricted diffusion

In the field of muscle biology, the concept of myo-nuclear domain has been proposed. Nuclei are thought to serve a myo-nuclear domain which represents a volume of cytoplasm. Nuclear products appear to move little and are highly constrained in skeletal muscles.Further, proteins tend to remain in the vicinity of the nuclei from which they originated (Hall and Ralston, 1989; Kinsey et al., 2011).

This idea of myo-nuclear domains was tested using heterokaryons, by fusing mouse muscle cells with human non-muscle cells. Upon staining for human isoform of sarcomeric myosin heavy chain, it was to be most frequently localized to human nuclei producing it (Figure 1.10 Left). This finding was not specific to muscle-fibroblast, but also to other experiments using keratinocytes and hepatocytes.

It might be possible that this proximal localization may be a transient effect, seen only during the initial days of fusion. But upon monitoring the heterokaryons for longer duration, it was found that this localization remains over several days (Figure 1.10 Right) (Pavlath et al., 1989). This was later verified by injected plasmid DNA encoding β-galactosidase which integrated randomly into some nuclei, creating a mosaic cell (Ono et al., 1994).

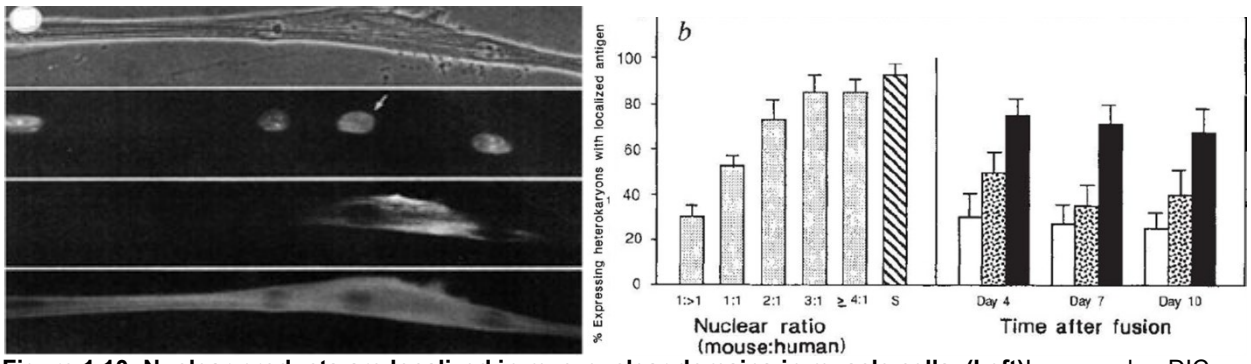

Figure 1.10: Nuclear products are localized in myo-nuclear domains in muscle cells. (Left) Image order: DIC, Hoescht staining, Human myosin staining, all myosin isoforms staining. The arrow shows the location of the human nuclei. Heterokaryon after 4 days of fusion. (**Right)** The localized distribution of myosin is correlated with an increased proportion of muscle nuclei (left) and is constant over time (right).Reproduced from (Pavlath et al., 1989)

Syncytial muscle cells also have different area with specialized functions, like the myo-tendenous junction (MTJ, the connection between the muscle fibre and the tendons) and the neuro-muscular junction (NMJ, the region where the neurons innervate the muscle fibre). Interestingly, nuclei present near the MTJ are clustered together and increase the production of myosin heavy chain upon stretching.The nuclei at the NMJ are tightly clustered, are larger and rounder than other nuclei of the muscle cell (Couteaux and Pécot-Dechavassine, 1973). Some proteins, like Syne-1, are also selectively associated with the NMJ nuclei (Apel et al., 2000), some, like acetyl-choline esterase are produced exclusively or preferentially by these nuclei (Brenner et al., 1990; Fontaine, 1989; Jasmin et al., 1993; Moscoso et al., 1995) and some others, like transcripts of actin and myosin,are seldom found near the NMJ nuclei (Moscoso et al., 1995). It was found that while nuclei producing housekeeping gene transcripts were found throughout the myofiber, nuclei producing muscle-specific transcripts were clustered together, suggesting some form of division of labour (Newlands et al., 1998).

The scaling relationship between the nuclear size, myonuclear domain size, ploidy of the nuclei and the overall muscle fibre size has also been established. It has been observed that muscle nuclei collectively establish a global scaling with respect to the syncytial muscle cell. Larger cells on average, have more nuclei. Larger nuclei also seem to “cater to” a larger area of the cytoplasm, though this correlation is not as strong as that with the nuclear scaling with the overall cell size. Moreover, nuclei near the

neuro-muscular junction have a higher nuclear size, ploidy and synthetic activity than those away from the NMJ (Moffatt and Cohen-Fix, 2019; Windner et al., 2019). Nuclei belonging to the same muscle cell show differential nuclear import rates. This difference varies during differentiation (Cutler et al., 2018).

These data suggest that syncytial muscle nuclei behave independently in terms of synthetic activity, scaling relationship and the variety of transcripts that are produced by them. Cytoplasmic domains and compartmentalization seem to be inherent properties emergent in this system.

1.2.4 Nuclei in the syncytial hyphae of the fungus *A.gossypii* maintain asynchronous divisions

A.gossypii is a fungus containing multiple nuclei in a single hypha. It provides an interesting opportunity to study how each nuclei behaves in this syncytium in terms of division times, cytoplasmic homogeneity etc, and what can bring about these properties. It was found that nuclei in a single hypha divide asynchronously despite sharing a common cytoplasm. Neighbouring nuclei can be present in different cell cycle phases and cyclins were found to diffuse freely between nuclei (Gladfelter et al., 2006). Neighboring nuclei were observed to repel each other to create space and mark their own “cytoplasmic territories”. Microtubules were found to be important in repulsion and territory demarcation. Sister nuclei remarkably retain similar division cycle times, even though they might be separated spatially, suggesting an inheritance of the cytoplasmic territory (Figure 1.11) (Anderson et al., 2013).

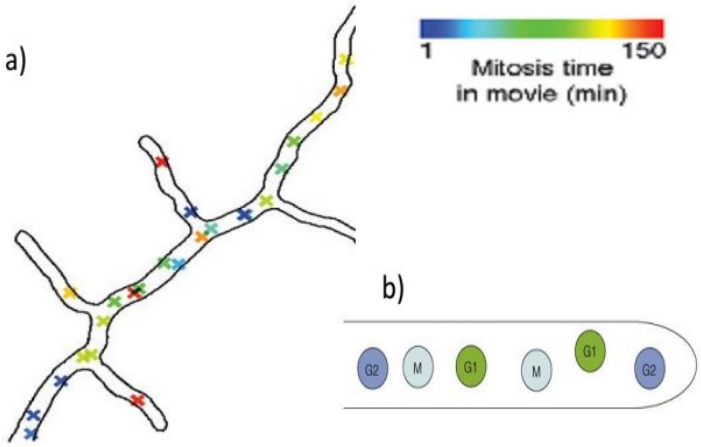

Figure 1.11: Asynchronous cell cycle in adjacent nuclei suggests compartmentalization in the fungal syncytium. a). Plot of mitosis locations throughout the cell. Each mitosis is indicated as an ‘‘x.’’ The color of the ‘‘x’’ corresponds to the time point of mitosis. **b).**Scheme summarizing the *A.gossypii* nuclear division cycle in which nuclei in hyphae are all cycling independently and direct neighbors are in different cell cycle stages. Modified from (Anderson et al., 2013).

Molecularly, how could this come about? It was found that cyclin degradation could take place in an insulated manner near a particular nucleus, though sharing a common cytoplasm (Hungerbuehler et al., 2007). Using a mutant strain of the fungi, which led to clustered nuclei, it was observed that even though the spacing between the nuclei was perturbed, yet their cell cycle independently. It is remarkable that in spite of a very thin layer of insulating cytoplasm between adjacent nuclei, the cyclin mRNA were clustered near the nucleus they were produced from (Dundon et al., 2016).

The heterogeneity in division cycles in brought about by differential accumulation of a specific G1 transcript. Since the number of copies of the transcript near a particular nucleus is different, each nucleus experiences a different concentration of the cyclin, leading to a heterogeneity. This differential accumulation is mediated by polyQ-dependent behavior of an RNA-binding protein (Lee et al., 2013).

These observations suggest that syncytial nuclei in fungi behave independently in terms of their molecular constituents, cell cycle and the variety of transcripts that they accumulate.

1.3 Model system: *Drosophila* early embryo is a syncytial cell with graded cytoplasmic components

In the following sections, I will discuss the development of *Drosophila* early embryo until cellularization, changes in cyto-architecture as cell cycle progresses, discuss about yolk & its dynamics, and highlight studies about cytoplasm & compartmentalization in the early embryo syncytium.

1.3.1 The early development of the *Drosophila* embryo

Post fertilization of the fly egg, a rapid sequence of mitotic nuclear cleavage divisions without cytokinesis, take place in the early embryo. 9 nuclear division cycles take place deep within the embryo during the pre-blastoderm stage. Nuclei along with centrosomes migrate to the cortex in nuclear cycle (NC) 10 to form the syncytial blastoderm followed by nuclear division cycles 11-14, that occur just beneath the cortex in the syncytial blastoderm embryo (Foe and Alberts, 1983; Foe,Odell and Edgar, 1993; Karr, 1986; Sullivan and Theurkauf, 1995; Warn, 1986). The interphase of cycle 14 is followed by the formation of a multiple cells (~6000 cells) at once,wherein each nucleus near the embryo surface becomes a complete cell, by the process of forming complete cells due to membrane growth and extension (Mazumdar and Mazumdar, 2002). Apart from the nucleus, the early embryo also contains a maternally loaded large supply of membrane bound compartments called yolk-particles/platelets/granules. These form the bulk of the cytoplasm, are present in the central elliptical portion of the embryo and get compressed deeper into the centre of the embryo as syncytial blastoderm stages take place (Foe,Odell and Edgar, 1993).

Each interphase nucleus of the syncytial blastoderm embryo is surrounded by apical centrosomes and a microtubule array in an inverted basket conformation. Astral microtubules reach out from the centrosomes towards the cortex and overlap with the astral microtubules originating from neighbouring nuclei (Cao et al., 2010). F-actin is present in caps above the nuclei and centrosomes. Lipid droplets and yolk are enriched at the bottom of the basket (Kuhn et al., 2015; Mavrakis et al., 2009b; Schmidt and Grosshans, 2018; Welte, 2015). During interphase, nuclei have a nascent plasma membrane between the adjacent nuclei. During the transition from interphase to metaphase, the microtubule and the actin cytoskeleton remodel during prophase and metaphase of the syncytial division cycle. The centrosomes move laterally during prophase and give rise to spindles during metaphase. Actin is enriched along the cortex at the extending plasma membrane furrows (Foe,Odell and Edgar, 1993). The short furrows present in interphase between adjacent nuclei extend deeper between spindles in metaphase and form the pseudocleavage membranes (or so called “metaphase

furrows") which separate adjacent spindles from interacting with each other (Figure 1.12) (Sherlekar and Rikhy, 2016).

The last 4 divisions, nuclear cycles 10 to 13, which are also amenable to fluorescence based microscopic observation, provide an opportunity to probe cytoplasmic compartmentalization.

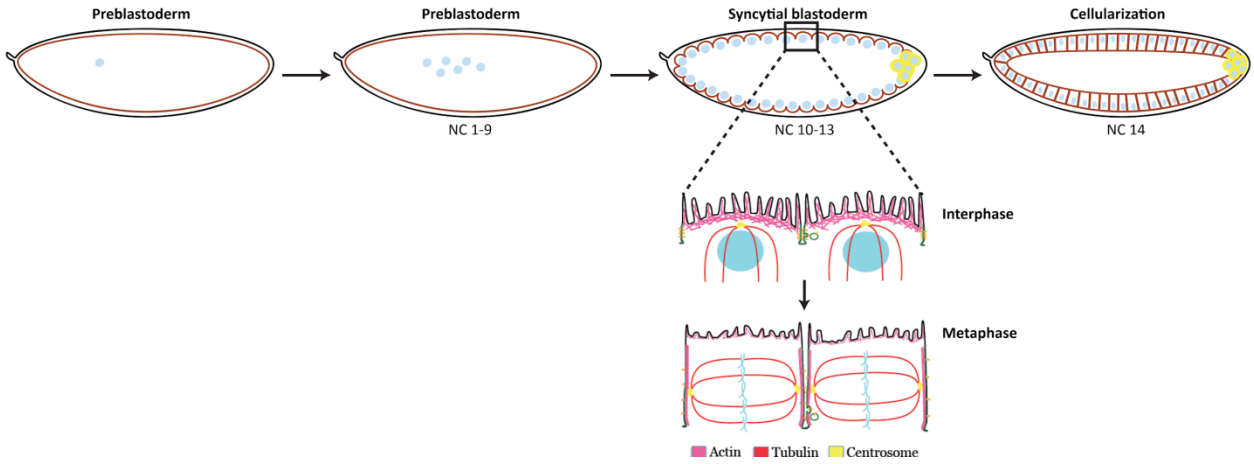

Figure 1.12: Development of the *Drosophila* early embryo until cellularization.
The blue dot represents the fertilized nuclei which undergo 9 rounds of divisions deep within the embryo. During nuclear cycle 10, the nuclei arrive near the embryo surface (cortex) and undergo three more rounds of division (NC10-13) until finally forming complete cells in cellularization (NC14). The zoomed in illustration shows two interphase nuclei and two metaphase spindles imaged in sagittal format. The apical arrangement of actin interphase and on the pseudo-cleavage furrows in metaphase can be seen.Inverted basket arrangement of microtubules in interphase and formation of spindle in metaphase can be seen.

1.3.2 Yolk as a separate compartment excluding the cytoplasm.

Yolk is the major internal food supply for most eggs. Since the development post fertilization takes place outside the mother, nutritionally dense material is deposited maternally in the egg. It is later metabolized and used for providing nutrients to the embryo until it develops to the extent of searching for food on its own.

In the *Drosophila* embryo, yolk is composed of three phosphoglycoliproteins, yolk protein 1 (YP1,46kDa), yolk protein 2 (YP2,45kDa) and yolk protein 3 (YP3, 44kDa), collectively known as vitellogenins in their precursor form (DiMario and Mahowald, 1987; Tsuruhara et al., 1990). These three proteins are deposited in the fly embryo in the form of membrane bound spherical granules (Yolk granules, YGs or platelets). The yolk proteins are derived from the maternal serum protein called Vitellogenins (Vgs),

which are synthesized by the fat body and the ovarian follicle cells of adult females These proteins are taken up by the oocyte via receptor mediated clathrin dependent endocytosis, using receptors called Vittelogenic receptors (VgRs). The oocyte receptor is called Yolkless, which returns to the oocyte plasma membrane through recycling tubular structures. The Yolkless protein is present in all endocytic structures except the yolk granules (DiMario and Mahowald, 1987; Schonbaum et al., 2000).There are several mutants of Yolkless reported which perturb its localization or expression and hence alter both the uptake of YPs and the general morphology of the endocytic compartments in the oocyte (DiMario and Mahowald, 1987; Sommer et al., 2005).

The yolk proteins have a leader sequence which is co-translationally cleaved before their secretion from the tissues in which they are synthesized (Butterworth, 1999). Upon endocytosis, initially, they accumulate in vesiculo-tubular structures (early endosomes), which coalesce into primary yolk bodies (analogous to late endosomes). In contrast to the route taken usually to degradation by lysosomes, the yolk granules are not degraded immediately but stored in latent form for degradation upon developmentally triggered cues.The mature yolk granule can be said to be a modified lysosome which has reduced hydrolytic activity (Fagotto, 1995; Schonbaum et al., 2000).

These YGs are modified lysosomes containing hydrolases required for yolk metabolism. The hydrolyzation of yolk begins at a specific developmental time, much later than the time of their formation and deposition in the egg. The latency in yolk degradation is regulated by pH and enzymatic latency. Developmentallyregulated acidification during embryogenesis triggers yolk degradation by exposing protein cleavage sites and activating proteases which lead to yolk cleavage (Fagotto, 1995). Each polypeptide (YP1,2,3) corresponds to a single copy gene (yp1,2,3) located on the X chromosome and is highly conserved (Bownes et al., 2002; Wahli, 1988). Juvenile hormone and 20-hydroxy-ecdysone regulate the expression of these genes.

Interestingly, using high levels of 20-hydroxy-ecdysone, males can be induced to express the yolk protein genes (Bownes M, 1983). The synthesis of the vitellogenin at two sites (fat and ovaries) as well as the duplication of the yolk protein gene into three

represents a means of producing sufficient gene product to ensure the rapid progression of egg development (Bownes et al., 1991).

The shape of the YGs is spherical and their movement in the early embryo has been noticed, albeit not in great detail. It is known that the yolk particles in the pre-blastoderm embryo are near the cortex, while they move more towards the centre progressively as the nuclear cycles progress in the syncytial blastoderm. In these stages the compaction of the yolk particles correlates with the formation of a yolk free cytoplasm near the cortex (Bownes M, 1983; Foe,Odell and Edgar, 1993). It has been observed that mutants of YP3 (specifically, YP3S1) package into abnormally shaped yolk particles (Butterworth, 1999).

Lipid droplets which closely follow yolk distribution, show three phases of mobility. Phase I (corresponding to syncytial blastoderm,~45 min) where the droplets are present in peripheral distribution; phase II (beginning of cycle 14 until the end of cellularization, ~55min) where droplets show basal accumulation; and phase III (corresponding to gastrulation ~20min)which shows apical redistribution of the lipid droplets (Figure 1.13) (Welte et al., 1998).

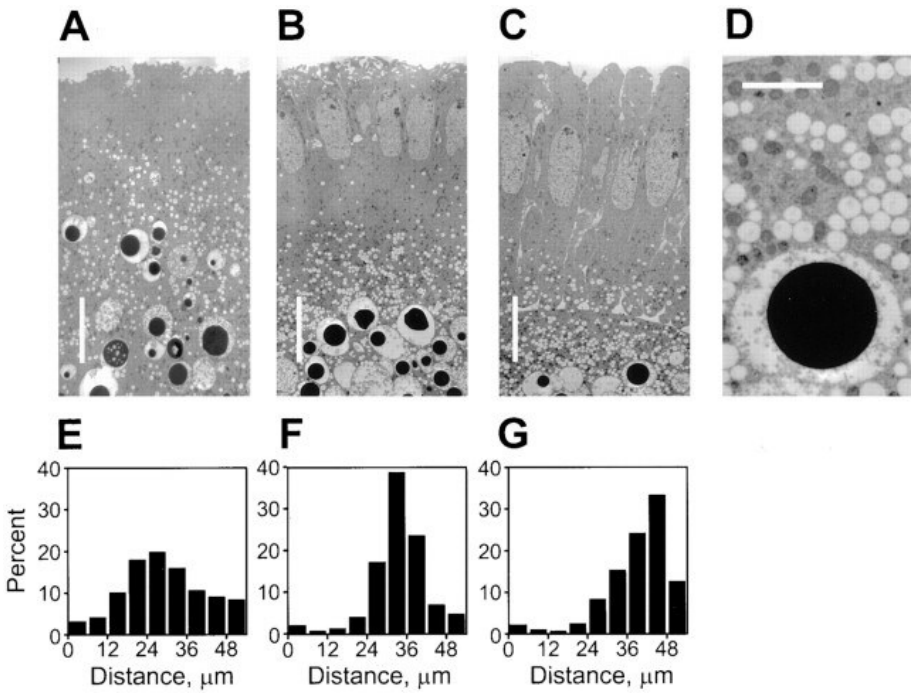

Figure 1.13: Clearing of Yolk and Lipid Droplets from the cortical cytoplasm.

Electron micrographs of wild-type embryos from cycle 12 (**A)**, cycle 14 early cellularization (**B)**, and cycle 14 cellular blastoderm (**C)**. Orientation: apical, top; basal, bottom (scale bar, 10 μm). Lipid droplets appear as small transparent circles. Yolk particles are black circles. (**D)** A high magnification view (scale bar, 2.5 μm) shows one yolk vesicle (large sphere with dark inclusion), abundant lipid droplets (transparent spheres), and mitochondria (smaller, dark vesicles). (**E–G)** For each embryo, the graph below shows the percentage of droplets in various zones along the apical–basal axis. Distance represents the distance from the cortex to the centre of the embryo. Reproduced and modified from (Welte et al., 1998).

Recently, it has been shown that separation of cytoplasm from the yolk in zebrafish embryos relies on a cell cycle dependent bulk actin polymerization wave which travels in the oocyte from the animal to the vegetal pole. This wave pulls the ooplasm apically while pushing the yolk granules vegetally (Shamipour et al., 2019). Our interest with the yolk granules in the early *Drosophila* embryo syncytium lies in finding out how cytoplasm is separated as a separate phase from the yolk and how yolk movement is coordinated towards the centre of the embryo.

The syncytial nature of the early embryo,provides a unique opportunity to study the functional impact of restriction of diffusion and compartmentalization. In the next few sections, we explore how this is so and what is known about these aspects in the early embryo syncytium.

1.3.3 What is known about the cytoplasm in the early embryo?

Diffusion in the early embryo is known to be diffusive though there is contribution by the stirring and contractions of the embryo that take place during mitosis and axial expansion. Further the viscosity of the embryo has been measured using two independent methods and shows quite varied results (Gregor et al., 2005; Wessel et al., 2015).

In order to test the diffusion rates of inert probes of various sizes in the early *Drosophila* embryo, fluorescent probes of different sizes were microinjected and the dynamics of spreading were observed using live imaging (Gregor et al., 2005). These movies of spread of these injected probes provided concentration versus time profiles at various locations in the embryo. If the motion of these probes was indeed diffusive, then their concentration profiles could be fit by a single parameter, the diffusion constant, irrespective of the size of the probe.The experimental observations suggest this to be

the case as the data fit the Stokes-Einstein equation well. The effective cytoplasmic viscosity was found to be 4.2cP, four times that of water. It was also found that the random stirring of the cytoplasm due to mitosis and other events, contributed to a fraction of the diffusion coefficient, which was molecular weight and radius independent (parameter b in Figure1.14c). This accounted for≈25% of the total diffusion coefficient for a molecule of size 55kDa (Gregor et al., 2005).

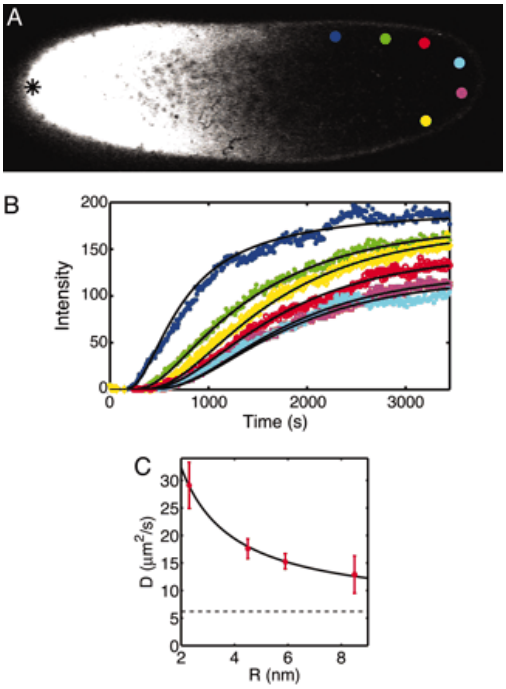

Figure 1.14: Diffusion of inert molecules in the *Drosophila* embryo. (*A*) Two-photon image of a wild-type *D. melanogaster* embryo 8 min after injection of fluorescently labeled dextran molecules at the midplane of the embryo. The tip of the glass micropipette used for the injection is located at the anterior pole (black asterisk on the left side of the image). Colored discs show areas where fluorescence intensity was analyzed. **(*B*)** Changes in the fluorescence intensity with time for the six color-corresponding discs in *A*, extracted from a time series of images taken with a frame rate of 8 s. Solid lines represent the time courses computed from the best fit of a numerical 3D diffusion model. Note that 18 curves (6 per focal plane) are fit by the solutions of the same diffusion equation, with only a single free parameter, the diffusion constant *D*. **(*C*)** Diffusion coefficients of dextran molecules of different hydrodynamic radii (red dots). The solid line represents diffusion coefficients expected from the modified Stokes–Einstein relation (10), $D = k_B T/(6\pi\eta R) + b$, with a viscosity $\eta = 4.1 \pm 0.4$ cP and $b = 6.2 \pm 1.0$ μm2/s; dashed line is at the value of *b*. Reproduced from (Gregor et al., 2005).

For the *Drosophila* early embryo syncytium, the term “cyto-architecture” refers to microtubules and actin only, since there are no intermediate filaments during this stage (Wessel et al. 2015). It also refers to the dense Golgi and ER networks, which are present from pre-blastoderm stages (Frescas et al. 2006) and may result in restricting diffusion.

Another study focused on finding the viscosity and shear moduli in the embryo at various locations and nuclear cycles (Wessel et al., 2015). Micron sized beads were injected in the embryo and their motion was tracked using a high speed camera using a technique called microrheology. The fluctuation in the positions of these micron-sized particles was then related to the viscoelastic properties of the medium surrounding them.

It was found that embryo’s interior is a highly viscous medium. A region corresponding to ~35 μm thickness near the surface of the embryo, called the cortex, has different mechanical properties than the rest of the embryo. This illustrates that cytoskeletal structures are concentrated in small sub-volumes and are diluted in the rest of the embryo. This region corresponds to the nuclear layer along with the inverted basket arrangement of microtubules and the actin caps.

Dissecting the properties within this subvolume, it was found that mechanical properties are homogeneous between the cortical nuclear layer and the central yolk. Viscosity in this region corresponds to ~1000 times higher than that of water.In the cortical nuclear layer, the shear moduli (which represents a measure of hardness or stiffness) is higher due to higher density of cytoskeletal filaments, namely microtubules. Upon perturbation of cytoskeleton dynamics using drugs, it was found that microtubules rather than actin filaments contribute to the viscoelasticity of the cortex (Wessel et al., 2015).

1.3.4 What is known about compartmentalization in the *Drosophila* early embryo syncytium?

Each nucleus during NC10-13 is associated with its own set of centrosomes, organelles and various other cellular components. It has been postulated that each nucleus has a region of influence over its surrounding volume, which in the absence of plasma

membrane boundaries have been termed as “pseudo-cells” or “nucleo-cytoplasmic regions/domains” or “energids” (Foe and Alberts, 1983). Each nucleo-cytoplasmic domain in the blastoderm embryo is associated with organelles such as the endoplasmic reticulum, Golgi complex and mitochondria (Chowdhary et al., 2017; Frescas et al., 2006; Mavrakis et al., 2009a). Experiments to study the compartmentalization of ER/Golgi in the early embryo found that protein products destined for the plasma membrane trafficked in a polarized and local fashion rather than randomly in the embryo, suggesting that each nucleus can modulate the composition of the plasma membrane associated with and above it (Figure 1.15) (Frescas et al., 2006).

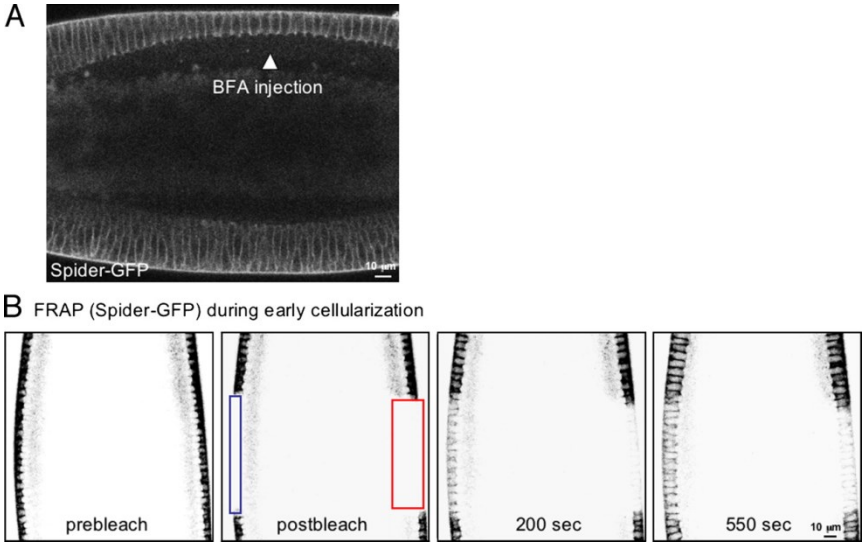

Figure 1.15: Evidence that plasma membrane–bound material originates from localized secretory units around individual nuclei. (A) Injection of BFA (arrowhead) in embryos expressing a plasma membrane marker (Spider-GFP; see Materials and methods) resulted in a dramatic slowdown of membrane invagination at the injection site, suggesting that BFA-induced impairment of secretory units at the injection site is not compensated for by adjacent secretory units. **(B)** Side view FRAP of a Spider-GFP–expressing embryo during early cellularization. ROIs encompassing plasma membrane–bound Spider-GFP (blue box) or both plasma membrane–bound and intracellular Spider-GFP pools (red box) were simultaneously photobleached, and fluorescence recovery was monitored. Spider-GFP fluorescence on the plasma membrane recovered very little in the case where the intracellular Spider-GFP pool was depleted (red box), indicating that secretion is taking place in a localized manner and not randomly through an extensive secretory system. The images shown were inverted. Reproduced from (Frescas et al., 2006).

Experiments using FLIP and photo-conversion of molecules present in the plasma membranes associated with each nucleus found that molecules diffused within each

energid but do not cross boundaries to exchange between PM regions above adjacent nuclei (Figure 1.16) (Mavrakis et al., 2009a).

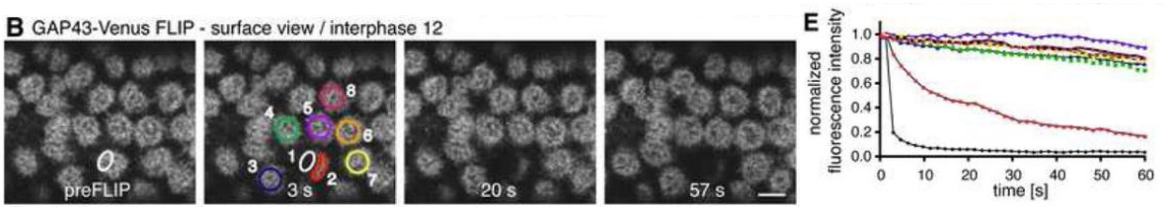

Figure 1.16: Diffusion of proteins in the PM is compartmentalized around individual interphase syncytial nuclei. An ROI (white outlined ROI in B, represented by black curve in E) was repeatedly photobleached, and fluorescence from distant areas was monitored. B and E show FLIP of GAP43 in the syncytial blastoderm, suggesting that while the ROI 2 loses intensity when 1 is photobleached, other ROIs do not lose any intensity, and are hence isolated. Reproduced from (Mavrakis et al., 2009a).

Further, experiments using photo-activation of mitochondrially localized PA-GFP showed that mitochondria are not shared between adjacent energids. Moreover, they are immobile in the lateral plane and do not mix even well within a single energid (Figure 1.17) (Chowdhary et al., 2017).

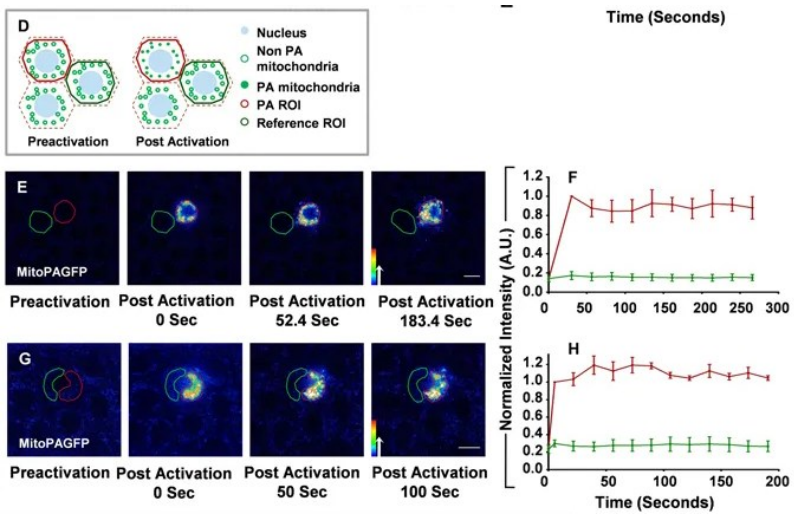

Figure 1.17: Mitochondria are immobile in the lateral plane in the syncytial *Drosophila* embryo and do not cross over to adjacent energids. (D–H) Photoactivated mitochondria are restricted in syncytial cells. Non-photoactivated and photoactivated mitochondria are represented as hollow and filled green circles respectively in a schematic of the photoactivation experiment **(D)**. Mitochondrially localized-PAGFP (Mito-PAGFP) is activated in one syncytial cell (red), fluorescence is monitored in neighbouring cells (green), which shows no gain in fluorescence in the given time **(E)** in interphase of NC12. Normalized mean fluorescence intensity of activated (red) and neighbouring (green) syncytial cell is plotted with respect to time **(F)**. Mito-PAGFP is activated in a part of syncytial cell (red) and

neighbouring region (green) from the same cell is monitored for fluorescence intensity changes **(G)**. Neighbouring region does not have an increase in fluorescence. Normalized mean fluorescence intensity of activated (red) and neighbouring (green) region is plotted against time **(H)**. Reproduced from (Chowdhary et al., 2017).

It is also known that many mRNA molecules are found in a specific localization pattern in the syncytial embryo, emphasizing a major role for mRNA localization and prevention of free mixing along with maintenance of their localization. Further, these localized mRNA can lead to production of localized cellular machineries, like cytoskeletal remodelling proteins, which can locally modulate milieus near individual nuclei (Lécuyer et al., 2007).

Another compartmentalization feature that emerges in the syncytial cycles is the compaction of yolk and separation of the cytoplasmic constituents near the cortex of the embryo. For example, it has been shown that the early embryo protein Bicoid is present near the embryo surface and not in the bulk of the embryo. In hypoxic embryos, Bicoid was found to spread cortically and not via the embryo bulk, most of which contains yolk (Figure 1.18) (Cai et al., 2017). Also, such characterization has been reported by using micrographs of the first studies on the early embryo (Foe and Alberts, 1983). It has been noted that during interphase of cycle 10-12, the depth of the yolk free cytoplasm near the cortex increases slowly and then reaches about 25µm deep in cycle 13, finally becoming almost 40µm deep during cycle 14 (Foe,Odell and Edgar, 1993). Although such reports have been in literature for a long time, a detailed characterization of the same is still elusive.

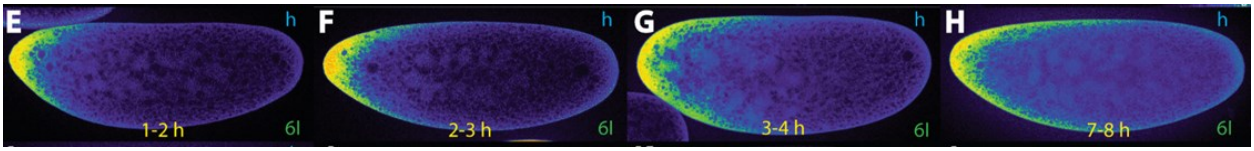

Figure 1.18: Cortical movement of Bicoid in hypoxic embryos. Pictures represent midsagittal confocal planes of embryos oriented with their dorsal side up and anterior to the left. Relative intensities of the crude confocal pictures were converted to a color scale with values of 0–255 (8-bit) **(E-I)** Relative Bcd intensities of nc 6 embryos in hypoxic *bcd*$^{+5+8}$ (mutants over producing Bicoid) embryos and collected at different time intervals after hypoxia treatment: **(E)** 1–2 h, **(F)** 2–3 h, **(G)** 3–4 h, **(H)** 7–8 h, **(I)** 17–18 h. Note the movement of the Bcd protein in the “sleeping” embryos along the cortex.Reproduced from (Cai et al., 2017)

1.4 Morphogens as representative molecules for studying cytoplasm

We will take a digression now and discuss about morphogens, their properties and how they allow us to study the diffusion in a special context. We will then discuss about morphogens in the early *Drosophila* embryo, what is known about them and how they allow us to study cytoplasmic compartmentalization in a specialized context.

1.4.1 Morphogens are molecules providing positional information

Mutli-cellular organism face the challenge to direct and organize varied cells by providing positional information. In a field of uniform cells, how is a cell directed to it's appropriate fate based on it position with respect to the tissue? Further, how is the number or proportion of cells directed to a particular fate maintained? One mechanism by which this is achieved is that of morphogen gradients.

Morphogens are long range signalling molecules, acting over a few or more cell diameter ranges and inducing a concentration dependent response in the cells over which they act. Cells exposed to high concentrations of morphogen adopt a different fate than others exposed to a lower concentration. Alan Turing coined the term "Morphogen" as early as 1952 (Turing, 1952). Graded morphogen distribution thus patterns the tissue into distinct cell types which are arranged as a function of their distance from the morphogen source (Rogers and Schier, 2011).

The current understanding of morphogens has evolved from varied concepts of cell biology, namely, induction, gradients, threshold and diffusion. Induction refers to the fact that cells can be induced to take up specific fate, based on various cues. Gradients referred to the fact that external cues can be used to induce the cell fate in a tissue and provide positional information. Threshold refers to the fact that the action of a gradient is concentration dependent and cells take up fates dependent on whether the concentration sensed by them is above or below a particular threshold. Finally, diffusion refers to the mechanism by which molecules are distributed in a graded fashion, thus forming gradients.

The influential “French Flag model” coined by Wolpert synthesized these concepts and illustrated how these gradients could function (Wolpert, 1969). In this model, the morphogen is secreted from a source and diffuses across a field. The thresholds are decided by the distance and concentration which ultimately divides the whole flag into three distinct cell fates, represented by the three colours.

Francis Crick proposed a model of morphogen formation, “the source sink model” where morphogen molecules could be produced from “source cells”, diffuse across the tissue and would be degraded by “sink” cells at the far end of the tissue. The process of diffusion and destruction ensured the maintenance of stable concentration of the gradient, which can then be interpreted (Figure 1.19) (Crick, 1970).

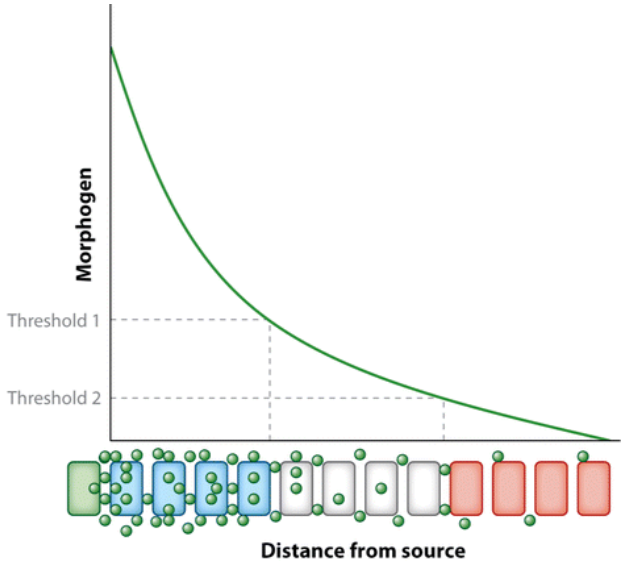

Figure 1.19: The French flag model. Morphogen is secreted from a source cell(green) and forms a concentration gradient within the tissue. Cells exposed to morphogen concentrations above threshold 1 exhibit a distinct response (blue). Cells exposed to intermediate morphogen concentrations (between thresholds 1 and 2) exhibit the “white” response, whereas cells exposed to levels below threshold 2 exhibit the “red” response. In this way, a concentration gradient of a single, diffusing substance could give rise to multiple cell fates and assign positional values to cells. Reproduced from (Rogers and Schier, 2011).

The first morphogen to be discovered was the Bicoid morphogen system in the early *Drosophila* embryo, which established a clear link between graded molecular concentration and positional information (Driever and Nüsslein-Volhard, 1988a). High levels of Bicoid are required for anterior fate specification, while lower levels for the more posterior domains (Driever and Nüsslein-Volhard, 1988b; Struhl et al., 1989).

Lowering the Bicoid signal at the source led to loss of anterior specification and anterior shifting of the posterior domains. After Bicoid, the Dorsal protein,involved in the dorso-ventral patterning of the early embryo was discovered (Roth et al., 1989).These molecules were present in the early *Drosophila* embryo syncytium.

The first extracellular morphogen to be discovered was Transforming growth factor Beta (TGFβ). Many other morphogens have been discovered since then. Dpp in the *Drosophila* wing disc, Sonic-hedgehog in the vertebrate neural tube,Nodal/Lefty morphogen system in the , FGF8 is a secreted protein in the chick presomitic mesoderm that binds to a receptor and activates a signaling cascade that patterns a field of cells (Dubrulle and Pourquié, 2004).

There are a variety of morphogens which have been studied in detail and which pattern tissues over a variety of scales and ranges. For example in the wing disc, morphogens like Dpp and Wnt which pattern the wing (Entchev et al., 2000; Teleman and Cohen, 2000). Nodal (Gritsman et al., 2000) and FGF8 (Yu et al., 2009) can act over longer distances in zebrafish embryos.

The formation of a morphogen gradient currently agreed to involve three steps: Synthesis from a source, diffusion over a given volume and degradation.This paradigm morphogen gradient formation is called the Synthesis-Difusion-Degradation or the SDD model (Wolpert, 1969). Variations and modifications to this model are also present, for example, the morphogen in question can be synthesized from a point or a spread source, its diffusion may take place in a confined or free environment or over a tissue which is expanding at a given rate, and the degradation rates might be variable over time, or immobilization, endocytosis or binding might be a way to remove the said morphogen (Müller et al., 2013). The distance (measured as the length scale) over which a morphogen diffuses is a function of its diffusion and degradation rates.

Morphogens also act in various different conditions and their formation also takes place in different scenarios. For example,Bicoid in the syncytial *Drosophila* blastoderm embryo and VegT in the *Xenopus* embryo are transcription factors that enter the nucleus and directly regulate gene expression (Gregor et al., 2007; Zhang et al., 1998). These proteins originate from RNA gradients in their corresponding embryos.The protein gradients are formed across cells in case of VegT and FGF8 in *Xenopus* and

chick embryogenesis, whereas the protein gradient is formed across nucleo-cytoplasmic domains in the case of Bicoid in the syncytial *Drosophila* embryo (Christian, 2012).

There are various means by which morphogen diffusion is seen to be modified. For example, low-affinity interactions with heparan sulfate proteoglycans (HSPGs), which are present extracellularly can bind diffusing morphogens and increase their local concentration, thereby promoting morphogen interaction with the morphogen receptors. Cells lacking functional HSPGs lead to loss of extracellular Dpp, while HSPG mutant cells exhibit attenuated Dpp responses.

In summary, the presence of intracellular morphogen molecules, like VegT, Bicoid and Dorsal, provide an opportunity to study cytoplasmic properties, by using these as a paradigm to test cytoplasmic restriction and compartmentalization.

1.4.2 Morphogens in the early *Drosophila* embryo

The Bicoid and Dorsal morphogens spread across the antero-posterior and dorso-ventral axis respectively to form gradients in the syncytial *Drosophila* embryo. These provide excellent opportunities to study cytoplasmic diffusion, dynamics and restriction, being present in the syncytial embryo and being mostly cytoplasmic.

The protein Dorsal patterns the Dorso-ventral axis of the embryo by entering the nuclei in interphase in the ventral side (Figure 1.20). The graded distribution of Dorsal leads to the formation of the three germ layers during gastrulation by switching on specific genes as per Dorsal concentration. Dorsal enters the nucleus on the ventral side by local activation of the Toll receptor. Dorsal is partially constrained to each energid and Dorsal gradient formation involves restricted diffusion (DeLotto et al., 2007). Dorsal restriction could be contributed by its presence in the nuclei in interphase and by pseudocleavage furrow formation in metaphase (Daniels et al., 2012; DeLotto et al., 2007; Kanodia et al., 2009).It was observed that during gradient formation, Dorsal shuttles between the syncytial nucleus and their shared cytoplasm.

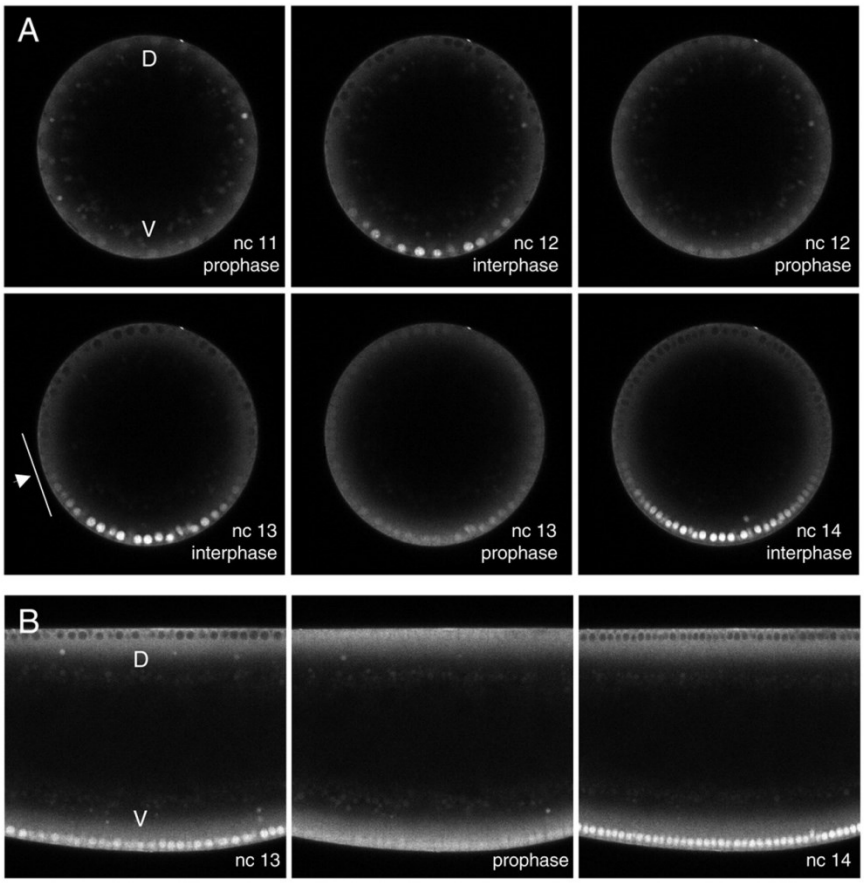

Figure 1.20: Breakdown during mitosis and reformation of the Dorsal gradient during interphase. (A) Cross-sectional views of a live *Drosophila* embryo, showing the distribution of Dorsal-GFP from nuclear cycles 11 to 14; orientation is ventral: down, dorsal up. **(B)** Sagittal views, showing interphase nuclear cycle 13, mitosis (prophase) and interphase nuclear cycle 14; the orientation in all panels is ventral: down, dorsal up. Reproduced from (DeLotto et al., 2007).

To further test how freely does the protein move and if Dorsal moves between the regions surrounding one nuclei and the next, i.e, if it is compartmentalized, Fluorescence Loss In Photobleaching (FLIP) was performed on Dorsal-GFP. Dorsal-GFP contained in one nuclei (and its associated cytoplasm) was bleached and the rate of fluorescence loss in the nearby nuclei was monitored. The results suggested that the nuclear fluorescence was reduced only modestly in the adjacent nuclei suggesting that the cytoplasm surrounding individual nuclei may be partially compartmentalized with respect to Dorsal (Figure 1.21) (DeLotto et al., 2007).

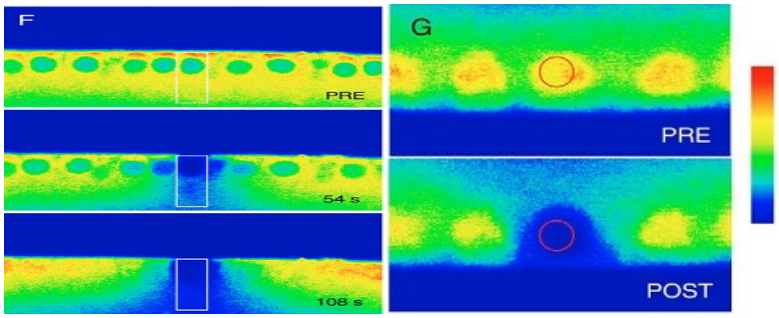

Figure 1.21: Compartmentalization of Dorsal-GFP detected using FLIP. (F) A false color image of a FLIP of peripheral and deep cytoplasm on the dorsal side (bleach box in white), indicating that Dorsal is partially constrained in its mobility near the plasma membrane surface but is more freely diffusing in the lower, deep cytoplasm. Relative linear intensities are indicated by the color bar at the left. **(G)** Dorsal is partially constrained in its diffusion to the part of the cytoplasm between the nucleus and the plasma membrane. A 5 second FRAP of nucleus (bleach box in red) transiently reduces fluorescence preferentially in the blue zone. In subsequent images (data not shown), cytoplasmic fluorescence is recovered with delayed kinetics by flow from the deep cytoplasm. Reproduced from (DeLotto et al., 2007).

Further, the diffusion of Dorsal is now known to be assisted by a reverse cytoplasmic gradient of its binding partner protein Cactus, which facilitates the diffusion of Dorsal in the DV direction. This was tested by modulating the diffusion of Dorsal, by using dimerizing GFP constructs. Further it has also been shown that Dorsal binds differently within each nucleus in DV axis and therefore shows a gradient of diffusivity as well (Asafen et al., 2018).These experiments with Dorsal suggest that the previously simplified diffusion of Dorsal is in fact effective diffusion composed of various components.

The Bicoid morphogen gradient is a classic, well-studied model for diffusion based morphogens (Figure 1.22). The maternally positioned *bicoid (bcd*) mRNA is restricted at the anterior pole of the embryo. The Bicoid protein is produced during oogenesis and embryogenesis diffuses across the embryo forming a characteristic exponentially decaying gradient (Ali-Murthy and Kornberg, 2016; Porcher and Dostatni, 2010). The synthesis, diffusion and degradation (SDD) model is a prevalent model for explaining Bicoid gradient formation (Bergmann et al., 2007; Durrieu et al., 2018; Houchmandzadeh et al., 2002; Lander et al., 2002). However the characteristic Bicoid gradient shape could also be produced by the pre-existing mRNA gradient (Spirov et al., 2009).

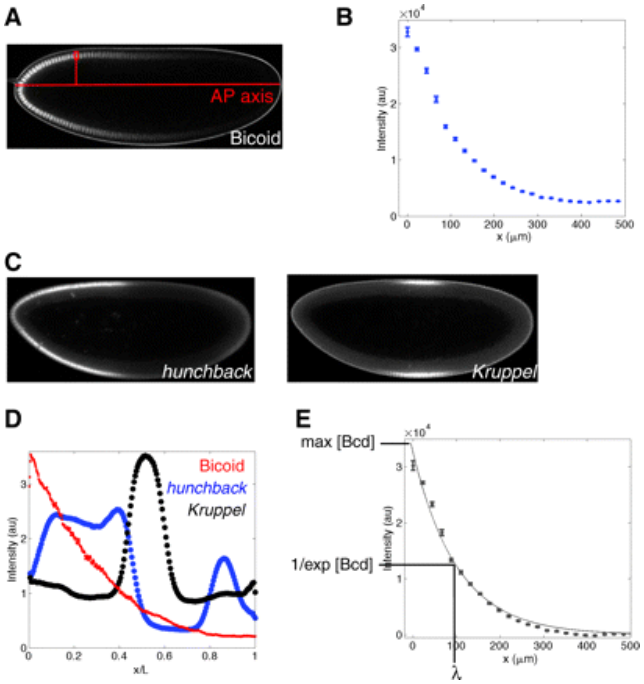

Figure 1.22: Bicoid forms a nuclear concentration gradient along the anterior-posterior axis of the *Drosophila* embryo. The Bicoid nuclear concentration gradient provides the *Drosophila* embryo with positional information. **(A)** The Bicoid gradient in cycle 14, visualised by confocal microscopy of a living embryo expressing Venus-Bicoid. Anterior is to the left. The gradient is quantified by sliding a box (red) along the nucleocytoplasmic area and computing the mean pixel intensity within the box. The intensity value is then projected onto the AP axis (red). **(B)** Quantitative information obtained from the embryo in A. The fluorescence intensity (which is proportional to Bicoid concentration) is shown as a function of egg length (x). **(C)** Expression of the Bicoid target genes *hunchback* and *Kruppel* in cycle 14. Anterior is to the left. **(D)** Graph showing the concentration of Bicoid protein (positional information in red) and expression of the target genes *hunchback* and *Kruppel* (blue and black, respectively). x/L is the relative position along the AP axis. **(E)** The length constant, λ, of the Bicoid gradient is obtained by fitting an exponential (red) to the Bicoid intensity profile and computing the position at which the concentration has dropped to 1/exp of the maximal value at the anterior (at *x*=0). au, arbitrary units.Reproduced from (Grimm et al., 2010).

Does Bicoid bind to any cytoarchitectural components? Is Bicoid diffusion in fact effective diffusion? Differential binding to nuclei along the AP axis is also known form Bicoid and has a role in gradient interpretation (Mir et al., 2017), though whether this contributes to differential spreading/gradient formation as well is not well studied. Bicoid also is seen to interact with actin structures (Lucchetta et al., 2008a), yet this is also not rigorously tested. Bicoid mutants which do not enter the nucleus seem to form gradient shapes which are like wild type (Grimm and Wieschaus, 2010), suggesting that the shuttling within nuclear compartments is not a factor in the gradient formation. Models exists which suggest that considering Bicoid or any morphogen, in the early embryo to

be forming in a field of compartments, with an inter and intra compartment diffusion rate, could recapitulate the actual dynamics of the gradient formation to a better extent (Kavousanakis et al., 2010).This compartment initially suggested to be the nucleus for Bicoid, might in fact be a nucleo-cytoplasmic regions in the early embryo.

1.5 Objectives of this project and predictions

This chapter has helped in highlighting our current understanding of cytoplasmic organization and diffusion in the early *Drosophila* syncytial embryo.The impact of restriction of diffusion, its functional context and how compartmentalization comes about in this system have not yet been explored. More insights into these areas will enable a greater understanding into macro scale organization and significance of diffusion/compartmentalization in cellular systems.Based on this, this thesis addresses the following questions about cytoplasm and its organization in the early embryo.

Objective 1: Characterization of cytoplasmic distribution, its dynamics across developmental time along with yolk compaction.
Questions addressed through Objective 1 (Chapter 3):
How is the cytoplasm in the early embryo distributed? How does this distribution change over time? To what extent can individual energids exchange cytoplasm and on what factors does this exchange depend? How is yolk movement correlated with cytoplasmic distribution?

Objective 2: Understanding the impact of cytoarchitecture in cytoplasmic diffusion
Questions addressed through Objective 2 (Chapter 4):
Does binding to the cyto-architecture restrict diffusion? What components of the cytoarchitecture mediate this restriction?

Objective 3: Understanding the impact of cytoarchitecture in cytoplasmic diffusion by creating ectopic gradients and using Bicoid as a test paradigm.
Questions addressed through Objective 3 (Chapter 5, 6):

Does binding to the cyto-architecture restrict diffusion and can we check this over developmental time? What components of the cytoarchitecture mediate this restriction? How does this restriction apply to morphogens present in the early embryo, like Bicoid?

Chapter 2: Methods and Materials

2.1 *Drosophila* stocks and genetics

Fly stocks were raised on standard cornmeal agar at 25°C. All lines requiring a Gal4 induction were expressed using maternally expressed *nanos*-Gal4 or *mat*-Gal4 (Fig 2.1). Embryos laid by F1 flies containing desired genetic combination carried the maternally derived phenotype. Stocks obtained from the Bloomington *Drosophila* Stock Center (NIH P40OD018537) were used in this study.Following is a list of the fly stocks used:

Fly Stock	**Source**
Gal4 lines	
nanos-gal4	Bloomington Stock #4937
mat-gal4-vp16; *mat-gal4-vp16* (mat-gal4)	Girish Ratnaparkhi, IISER Pune, India
RNAi stocks	
ralA RNAi	Bloomington Stock #34375
eb1 RNAi	Bloomington Stock #36599
Overexpression lines	
UASp-RhoGEF2	Bloomington Stock #9386
Tagged transgenic lines	
mRFP-Actin	Bloomington Stock #24777
mCherry-alpha-TubulinA1B (mCherry-Tubulin)	Bloomington Stock #25774

PA-GFP-alpha-Tubulin 84B (PA-GFP-Tubulin)	Bloomington Stock #32076
PA-GFP	Gerald M. Rubin (Janelia Research Campus, VA, USA)
6x-mCherry	Bloomington Stock #52268
UASp-mRFP	Richa Rikhy
Dynamin-GFP	Richa Rikhy
Histone-mRFP	Bloomington Stock # 23651
Bicoid-Venus	Eric Wieschaus and Thomas Gregor (Princeton, PA, USA)
BicoidΔK50-57-Venus	Eric Wieschaus and Thomas Gregor (Princeton, PA, USA)
GFP expressed under ubiquitin promoter (*ubi*-GFP)	Bloomington Stock #1681
Lipid droplet marker (LD-2.6-GFP)	Michael Welte, (University of Rochester, Rochester, USA)
Lifeact-GFP	Bloomington Stock # 58718
UASp-GFPS65C-alpha Tub 84B (Tubulin-GFP)	Bloomington Stock #7373
Lines created as a part of this thesis	
UASp-PH-PLC-CFP-bcd-3'UTR	
UASp-5XGFP	
UASp-8XGFP	
UASp-5XGFP-3'UTR	
UASp-8XGFP-3'UTR	

UASp-mRFP-3'UTR	
Recombinant lines	
nanos-Gal4>mRFP (RFP-nanos)	Richa Rikhy

Table 2.1 List of fly stocks used in this study

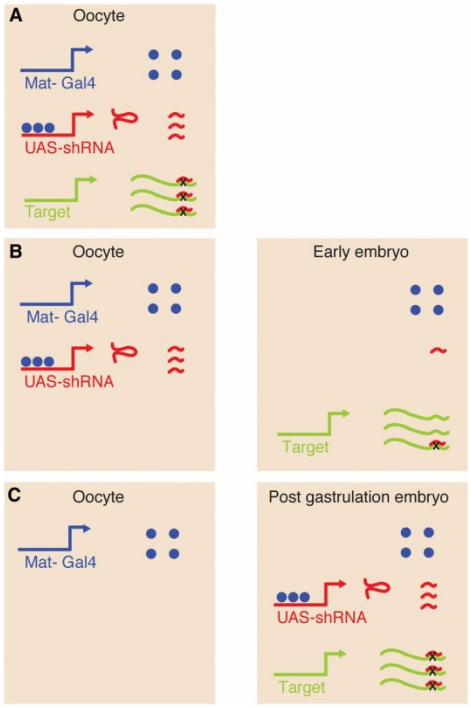

Figure 2.1: Knockdown of genes in the embryos using maternally expressed Gal4. Gal4 is expressed in the oocytes leading to production of UAS-shRNA that binds to and depletes maternally expressing target transcripts in the oocyte itself **(A)**. Zygotic transcripts are depleted by maternally expressed UAS-shRNA dumped in the embryos **(B)**. Adapted from (Staller et al., 2013).

2.2 Embryonic lethality estimation

3 hours old embryos were collected from cages containing 3% sucrose agar supplemented with yeast. On fresh 3% sucrose agar plates, the embryos were aligned in 10 × 10 array (or a smaller one based on number of embryos obtained) and incubated at the temperature in which the fly cage was kept. After 24 and 48 hrs of incubation, the number of unhatched embryos was counted and represented as a percentage.

2.3 Immunostaining

F1 flies of desired genotype were added to embryo collection cages containing yeast paste supplemented, 3% sucrose-agar plates. 1.5 hr old (for 25°C) or 1 hr old (for 28°C) embryos were obtained for syncytial or cellularization stages. Embryos were then washed,dechorionated with 4 percent bleach for 1 min, fixed using 1:1 heptane and 4% paraformaldehyde (PFA) in phosphate buffered saline (PBS - , 137 mM NaCl, 2.7 mM KCl, 10 mM Na2HPO4 and 1.8 mM KH2PO4) for 20 mins and devitellinized by shaking in 1:1 Heptate: Methanol or hand devitellinized immersed in PBS using insulin needles. Hand-devitellinization was used for staining with F-actin label, phalloidin.The embryos were then washed thrice with PBS-T (Triton X-100, 0.3%), blocked using 2% bovine serum albumin (BSA) and incubated with primary antibodies diluted in BSA overnight at 4°C. Fluorescently labelled secondary antibodies diluted in PBST (1:1000) were added after washing excess primary antibody and incubated in dark conditions at room temperature for 45 mins, followed by 3 washes with PBST. Nuclear stain Hoechst 33342 (1:1000) was added in the second wash. The embryos were mounted on slides using Slowfade Gold (Life Technologies). The samples were imaged using Plan-Apochromat 25x/0.8 Oil Immersion or Plan-Neofluar 40x/1.30 Oil objective on confocal laser scanning microscope (Zeiss, LSM 710 or 780 or Leica sp8). Z stacks with an interval of 1.1 µm were imaged. The primary antibodies and fluorescently tagged compound used are listed below.

Antibody/Probe name	**Source**	**Host Species**	**(Ab) Dilution/ Concentration**
Scrib	Kenneth Prehoda, University of Oregon, OR, USA	Rabbit	1:2000
Bicoid	SantaCruz	Rabbit	1:500
Tubulin	Sigma Aldrich	Mouse	1:1000
Anti-GFP	Molecular Probes	Chicken	1:1000
Hoechst 33342	Molecular Probes	NA	1:1000
Phalloidin	Molecular Probes	NA	1:100

Table 2.2 List of antibodies and fluorescent probes

2.4 Live imaging

1.5 hr old embryos were collected from embryo collection cage and dechorionated using 4% bleach for 1 min and washed. Embryos were mounted in 2 chambered cover glass dishes (LabTek, Germany) in PBS and imaged live at on confocal laser scanning microscope (Zeiss LSM 710/780). Positions for embryos were set with midsagittal plane and then imaged over time. Incase of Z-stacks, the interval was set at 1.1µm.

2.5 Transgenic flies

5X and 8XGFP containing plasmids were obtained from Marcus Nalaskowski (University Medical Center Hamburg-Eppendorf). The GFP multimer DNA were sub-cloned using restriction sites for NotI and AgeI into the UASp plasmid. mRFP (RFP) was inserted into UASp construct at the Kpn1 and Not1 restriction site using primers GGGGTACCATGGCCTCCTCCGAGGAC and ATTTGCGGCCGCTTAGGCGCCGGTGGAGTG. PH-PLC-CFP was cloned in pUASP previously using the primers CGGGGTACCATGGACTCGGGCCGGGACTTCC and ATAAGAATGCGGCCGCTTTACTTGTACAGCTCGTCCATGC (Mavrakis et al., 2009a) and cut using KpnI and NotI and inserted into UASp. The *bcd* gene containing plasmid with the 3'UTR was a kind gift from Elizabeth Gavis (Princeton, PA, USA). The *bcd*-3'UTR was PCR amplified using primers CATGGCGGCCGCTGGACGAGAGGCGTGTT or CATGTCTAGATGGACGAGAGGCGTGTT and CACTTCTAGAGGACGGAAATATGGGCTA primers and cut using NotI and/or XbaI and inserted in the UASp constructs containing 5X-GFP (5XGFP), 8x-GFP (8XGFP), mRFP(RFP) and PH-PLC-CFP obtained as described above. All constructs were confirmed by sequencing. Injection of UASp plasmids into *Drosophila* embryos and selection of transgenic animals was done by the NCBS transgenic injection facility, Bangalore, India.

2.6 FRAP, FLIP and Photoactivation

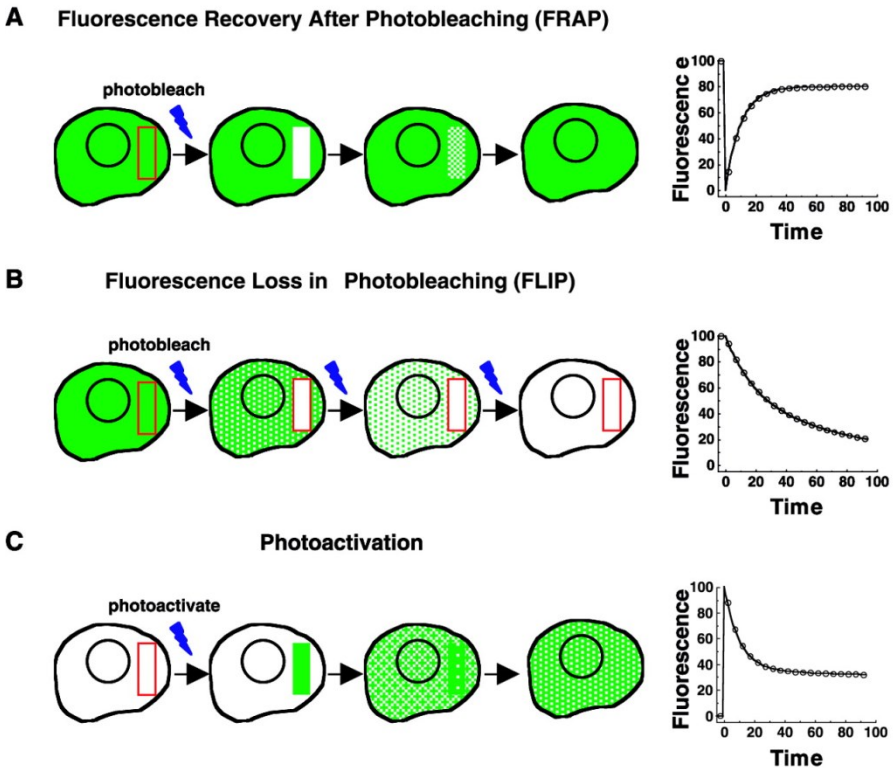

Figure 2.2: Kinetic microscopy techniques: FRAP, FLIP and Photoactivation. **(A)** In FRAP, a region of the cell (indicated in red) is selectively and intensely irradiated to photobleach fluorescent molecules. The recovery of fluorescent molecules into that region is assessed quantitatively to determine diffusion coefficients and mobile fractions. **(B)** In FLIP, a region of the cell (indicated in red) is repeatedly photobleached. Movement of fluorescent molecules into the region being photobleached results in loss of fluorescence from areas outside the box and can be used to access the boundaries for a protein's diffusional movement within a cell. **(C)** In photoactivation, selective irradiation of region (indicated in red) leads to the molecules in this region becoming fluorescent. These molecules can then be monitored as they move out of this region and throughout the cell. Reproduced from (Lippincott-Schwartz and Patterson, 2003).

2.7 Photobleaching

Photobleaching (Fluorescence Recovery After Photobleaching: FRAP or Fluorescence Loss in Photobleaching FLIP) on embryos expressing fluorescent probes was performed using the corresponding laser at 100% and 30 iterations at a selected region of interest (ROI) oil immersion objective on confocal laser scanning microscope (Zeiss LSM 710/780). Detailed specification of ROI sizes and other details are given in the corresponding chapters. Three pre-bleach images were acquired for both FLIP and

FRAP as inherent controls. For FRAP, fluorescent intensities in the FRAP ROI and Total ROI of the whole imaging field (excluding out of embryo regions) were monitored and measured using Zeiss bleaching module installed to Zen Black 10.1 software.

The data processing for FRAP involved the following steps as described in (Goldman et al., 2006):

1. Acquiring data from the Zen Black
2. Normalizing each data point in the ROI and Total to their respective average of pre-bleach data points

$$ROI\ (normalized, t) = \frac{ROI\ (t)}{ROI\ (pre - bleach\ average)}$$

$$Total\ (normalized, t) = \frac{Total\ (t)}{Total\ (pre - bleach\ average)}$$

3. Normalizing ROI intensity with the normalized Total intensity at the respective time point

$$ROI\ (final, t) = \frac{ROI\ (normalized, t)}{Total\ (normalized, t)}$$

4. The time points of the initial three pre-bleach images were subtracted to set t=0 at the first post bleach image.
5. Plotting and fitting the data in Graphpad Prism 5.0.

The Yguerabide equation was used for fitting and extracting t_{half} values (Yguerabide et al., 1982).

$$Y = \frac{F\ (0) + F\ (i) \times \left(\frac{X}{t\ (half)}\right)}{1 + \left(\frac{X}{t\ (half)}\right)}$$

where, Y is the intensity, F (0) is the initial intensity, F (i) is the intensity at the final time point, X is the time, t (half) is the value to be fit representing the half time of recovery. This equation assumes, a) the laser beam has a Gaussian profile, (b) recovery involves a single diffusion coefficient, and (c) there is no membrane flow. Since probes used were cytoplasmic, not on the membrane and showed curves which looked like single exponential fits (hence having single diffusion coefficient), we used this equation.

2.8 Image analysis of Photoactivation gradients/anteriorly expressed ectopic gradients/Bicoid gradient

Segmented lines of 10 or 20μm width were drawn across the cortex from the anterior to the posterior or centre to anterior/posterior of the embryo on the dorsal and the ventral side (Figure 2.3). Line profile measurements, containing embryo length vs intensity values were obtained using ImageJ. For XZ analysis, similar segmented lines were drawn for a distance of 90μm from the place of activation, in XY or XZ directions. The process was multiplexed using ImageJ macros. A MATLAB script was used to process the generated files. The following operations were performed using the script:

1. Rescaling the embryo length from 0 to 1 in the antero-posterior direction by division by the maximum X value (X_{max}).
2. Subtracting the minimum intensity (Y_{min}) value.
3. Rescales the value with the maximum intensity value (Y_{max}).
4. Smoothening the intensity values using sliding window averaging.
5. After excluding the first ~30μm (start at x=39.48μm in Figure 2.1), the raw data was fit using the equation (Houchmandzadeh et al., 2005):

$$a \times e^{\frac{-x}{\lambda}} + b$$

Certain steps were skipped, on a case to case basis, as they did not lead to any increase in robustness of fit or change in length scale values.

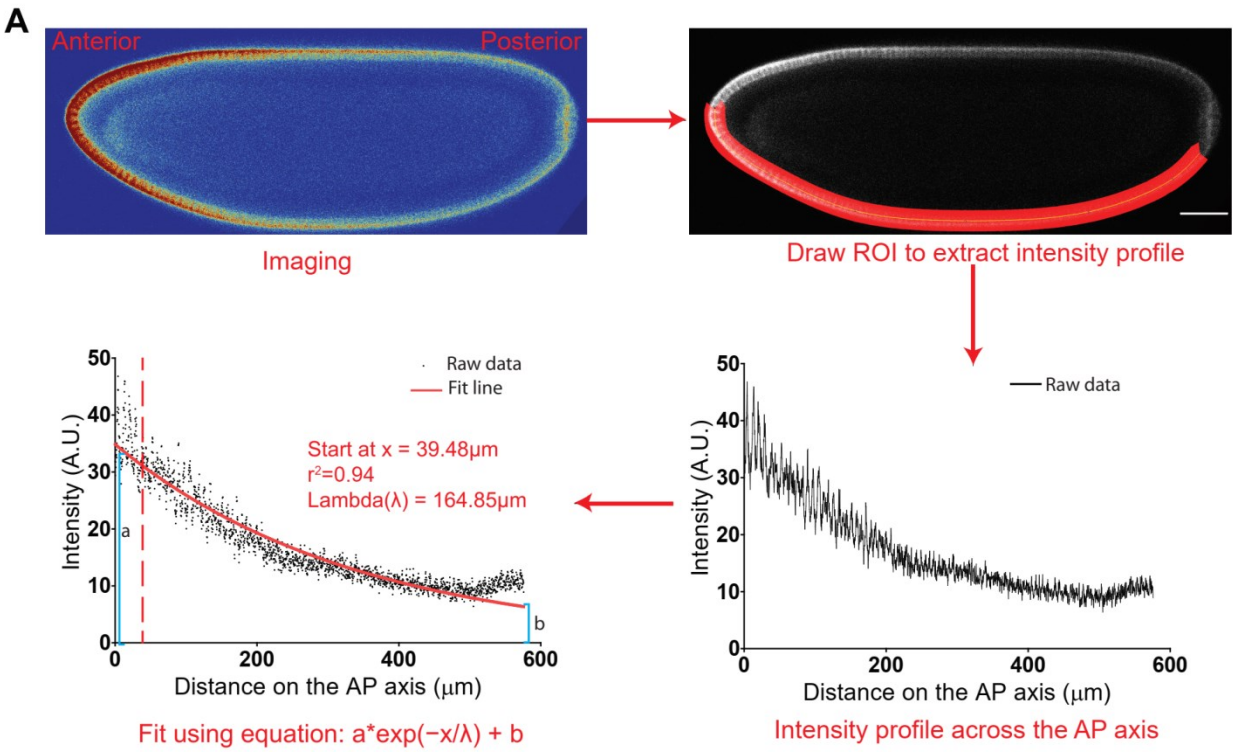

Figure 2.3: Analysis of gradient profiles.

(A). Imaging of anteriorly localized PH-PLC gradient, followed by drawing ROI to extract intensity profile. The intensity profile was then fit using the equation given (Houchmandzadeh et al., 2005). Value 'a' represents the amplitude, while 'b' is the offset from zero or the background value. 'λ' (lambda or length scale) is the characteristic length scale at which the gradient reaches 1/e of its initial value. Normalization with maximum intensity value does not change the fit. Scale bar= 50µm.

Chapter 3: Cytoplasmic distribution and dynamics in the early *Drosophila* syncytial embryo

Chapter 3 summary: *In this chapter, we have characterized the distribution of cytoplasm in the early embryo in general. We have also looked at the dynamics of exchange of cytoplasm across neighbouring energids and test if binding to cytoskeleton restricts that exchange. Further we have analysed the distribution of yolk particles and their distribution.*

3.1 Introduction

Studies involving characterization of the cytoplasm in the early embryo have shed light on its various aspects including the distribution and redistribution of cytoplasm, diffusion and dynamics as well as the movement of yolk.

How does the cytoplasm of the early embryo change in its organization over developmental time? From early studies on this area, we know that cytoplasm (as characterized by being yolk free region) is sparsely present in near the embryo cortex in pre-blastoderm cycles and further becomes enriched near the surface as the nuclear cycles progress. During interphase of cycle 10-12, the depth of this yolk free cytoplasm is reported to increase slowly and then it about 25μm deep in cycle 13, finally becoming almost 40μm deep during cycle 14 (Foe,Odell and Edgar, 1993). Does this correspond to yolk movement towards the centre of the embryo and what are the depths to which cytoplasm or cytoplasmic molecules are present? These are yet uncharacterized cytoplasmic properties in the early *Drosophila* embryo (Figure 3.1A:1).

Further, in terms of the dynamics of the cytoplasm, fluorescent dextran of various sizes when injected in the cytoplasm of the syncytial blastoderm embryo have been used to estimate the rate of cytoplasmic diffusion in the embryo and found an effective cytoplasmic viscosity of 4.2 cP, four times higher than water (Gregor et al., 2005). Micro-rheology based measurements of cytoplasmic viscosity have found that cytoplasmic viscosity is ~1000 times higher than that of water in the region between nuclei and yolk of the syncytial *Drosophila* embryo. How does local diffusion change due to architecture? (Figure 3.1A: 2). Is there any local heterogeneity in the cytoplasmic

distribution in each syncytial cell? (Figure 3.1A: 5). In addition, it was found that microtubules, but not actin contribute to the observed viscosity (Wessel et al., 2015). We also know that ER, golgi, plasma membrane and mitochondria are compartmentalized to each of the energids (Chowdhary et al., 2017; Frescas et al., 2006; Mavrakis et al., 2009a). It is an obvious extension to probe the extent to which cytoplasm is shared between the energids (Figure 3.1A: 3,4).

Apart from the cytoplasm, another major component of the early embryo is the yolk, which comprises around 20 percent of the early embryo protein content. It is composed of three yolk proteins, yp1 (46kda), yp2 (45kda), yp3 (44kda) (Bownes et al., 1983), which form yolk granules and their catabolism provides nutrition to the developing egg (Bownes et al., 2002; Kuhn et al., 2015). Yolk platelets are membrane-bound compartments formed by the dense aggregation of the yolk proteins. They are formed majorly in the ovaries and the fat-body of the fly, secreted into the hemolymph and then endocytosed into the developing oocyte (Kuhn et al., 2015).

As the embryo develops, lipid droplets and yolk take distinctive positions in the apical basal axis of each syncytial cell. The distribution of yolk granules has not yet been studied. Interestingly, the mobility, rate and distribution of yolk granules has not been studied in detail. What causes yolk granules to move towards the centre of the embryo and what are the dynamics of the process? These areas remain yet unexplored (Figure 3.1A:6).

In this chapter, I will summarize our results on the study of the early embryo cytoplasm. We have used maternally deposited mRFP as a readout for the cytoplasm as it is not known to interact with many components (Verkman, 1999). We use mRFP and other fluorescently tagged endogenous proteins, to characterize the distribution of the cytoplasm in the embryo. We use FRAP and FLIP of mRFP to study the dynamics of cytoplasm across energids and its compartmentalization and restriction. Furthermore, we have characterized the dynamics of yolk as it gets compacted towards the centre of the embryo.

3.2 Special notes on Materials and Methods

Imaging

512 pixel X 512 pixel images were acquired after that with a scan speed of 1.56 seconds per frame.Mean line averaging of 2 was used. The gain and laser power were adjusted to be cover the dynamic range of each fluorescent tag and care was taken to not reach 255 on the 8 bit scale. Pinhole was kept open at 90µm.

FRAP experiments

For mRFP FRAPs at various Z-positions, the ROI size used was 4.62µm^2, for FRAP in RFP vs RFP in 8XGFP was 54.13µm^2.the laser line used for bleaching and imaging was 561nm. Bleaching was performed at 100 percent laser power and imaging was performed at a lower power using the same laser. Iterations were kept at 30, which corresponds to a bleaching time of 3.72 seconds.

FLIP experiments

For FRAPs at various Z-positions, the ROI size used was 3.38µm^2 and the laser line used for bleaching and imaging was 561nm for mRFP, 488nm for Tubulin-GFP. Bleaching was performed at 100 percent laser power and imaging was performed at a lower power using the same laser. Iterations were kept at 30, which corresponds to a bleaching time of 0.489 seconds.

FLIP analysis

For FLIP analysis, at least 4 analysis ROIs were drawn equidistant from the FLIP ROI. For this a concentric circle was drawn around the FLIP ROI and analysis ROIs were drawn touching this circle, hence making them equidistant. Fluorescent intensities in the FLIP ROI and analysis ROIs were monitored and measured using Zeiss bleaching module installed to Zen Black 10.1 software.
The data processing for FLIP involved the following steps as described in (Goldman et al., 2006):

1. Acquiring data from the Zen Black
2. Normalizing each data point in the FLIP ROI and analysis ROI to their respective average of pre-bleach data points

$$FLIP\ ROI\ (normalized, t) = \frac{FLIP\ ROI\ (t)}{FLIP\ ROI\ (pre - bleach\ average)}$$

$$Analysis\ ROI\ (normalized, t) = \frac{Analysis\ ROI\ (t)}{Analysis\ ROI\ (pre - bleach\ average)}$$

3. The time points of the initial three pre-bleach images were subtracted to set t=0 at the first post bleach image.
4. Plotting and fitting the data in Graphpad Prism 5.0.

Binding and Restriction analysis of mRFP and Lifeact-GFP

For finding how much do surrounding energids deplete in fluorescence, FLIP experiments (with ROI size 30μm^2) were performed using 561nm laser for mRFP and 488nm laser for Lifeact-GFP. The above analysis of normalizing FLIP data was performed. To find the extent of restriction the following analysis was performed on the data obtained after the above analysis.

The minimum fluorescence intensities of the ROI were subtracted from 1, which represented the extent of depletion from the beginning of the experiment. To normalize between experiments and tags, this number is then divided by the extent of depletion of the FLIP ROI.

$$Surrounding\ depletion = \frac{1 - min\ (ROI)}{1 - min\ (FLIP\ ROI)}$$

3.3 Results

3.3.1 Cortical enrichment of the cytoplasm across syncytial division cycles in the *Drosophila* embryo

The syncytial *Drosophila* blastoderm embryo has a characteristic arrangement of

microtubules around each nucleus. Microtubules emanate from the apical centrioles and spread vertically covering the nuclei in an inverted basket like arrangement (Karr, 1986; Sullivan and Theurkauf, 1995). In order to test the extent of spread of molecules in the cytoplasm we imaged embryos expressing mRFP under the control of the *nanos* promoter in the sagittal imaging format (Figure 3.1A). mRFP, like GFP is expected to be present primarily in the cytoplasm and is not known to interact with any cytoplasmic components (Verkman, 1999). We compared the expression of cytoplasmic mRFP to fluorescently labelled tubulin as it would partition into the cytoplasm and also incorporate into the microtubule cytoskeleton. For this we imaged live embryos expressing fluorescently tagged alpha-Tubulin (UASp-mCherry-Tubulin) (Rusan and Peifer, 2007) with *mat*-Gal4-*vp16* (*mat*-Gal4). We found that cytoplasmic mRFP was enriched cortically and accumulated inside the cortical nuclei (Figure 3.1B).

Accumulation of mRFP occurs passively inside the nucleus as a result of its small size which allows it to pass through the nuclear pore complex (Ruiwen Wang, 2007). The fluorescence intensity of cytoplasmic mRFP progressively increased near the cortex as syncytial division cycles progressed but remained above the yolk filled region (Figure 3.1B). mCherry-Tubulin was enriched on apical centrioles, in microtubules spreading vertically from the cortex and in the cytoplasm in the syncytial division cycles (Figure 3.1B). mCherry-Tubulin also showed progressive accumulation of fluorescence signal near the cortex as the syncytial cycles progressed (Figure 3.1B, Movie Mov3.S1).

We further imaged *mat*-Gal4-*vp16* (*mat*-Gal4) driven Dynamin-GFP and 6x-mCherry (6 molecules of mCherry in tandem), and also Histone-mRFP driven under Histone 2A variant promoter, in the similar sagittal imaging format (Figure 3.1A). All transgenes showed similar enrichment near the cortex and the enrichment progressed in depth as the cycles progressed (Figure 3.1B). Lipid-droplets show an enrichment away from the cortex and seem to mark the extent of the microtubule network as the cycles progress, similar to previously reported results (Welte, 2015).We can represent this enrichment in the form of a kymograph to visually observe the gradual enrichment and expansion of the cytoplasm near the cortex. We draw a line from outside the embryo towards the centre and extract the kymograph as shown in an intensity graded

scale (Figure 3.1C). It is interesting to note a gradual cytoplasmic enrichment near the cortex and the expansion of this zone. It is also worth noting that during metaphase stages, the cytoplasm seems to retract somewhat towards the cortex, only to start expanding again later (arrows in Dynamin-GFP).

The intensity profiles from the cortical region to the centre of the embryo have also been quantified (Figure 3.2).In general, we observe a shift of the peak intensity position towards the right side to deeper sections in general, in the mRFP, mCherry-Tubulin, 6x-mCherry and Dynamin-GFP as the cycles progress (Figure 3.2A,B,D,E). This implies that there is an increase in the depth of the region, over which the cytoplasm localises beneath the cortex across the syncytial cycles. Lipid droplets peak over at greater depths and the peaks extend to increased depths as the syncytial cycles progress marking the gradual movement of lipid droplets towards the embryo centre (Figure 3.2C, Movie Mov3.S2) .

It is also worth noting that when the profiles of these different markers were plotted together (Figure 3.2F,G), they fall around the same range of depth (0-~40μm), for both interphase (Figure 3.2F) and metaphase (Figure 3.2G). Further, the lipid droplet profile shows the enrichment of lipid droplets between 20 to ~40μm, in both interphase and metaphase (Figure 3.2F,G). This seems to mark the lower end of the cortical cytoplasmic region and corresponds to a region where the concentration of cytoplasmic molecules drops.

Thus cytoplasm is concentrated near the cortex to 30~40μm and further enriched during the progression of the nuclear cycles. In addition, cytoplasmic components, were present in a separate cortical layer of cytoplasm on top of and distinct from the inner yolk-filled region of the embryo.

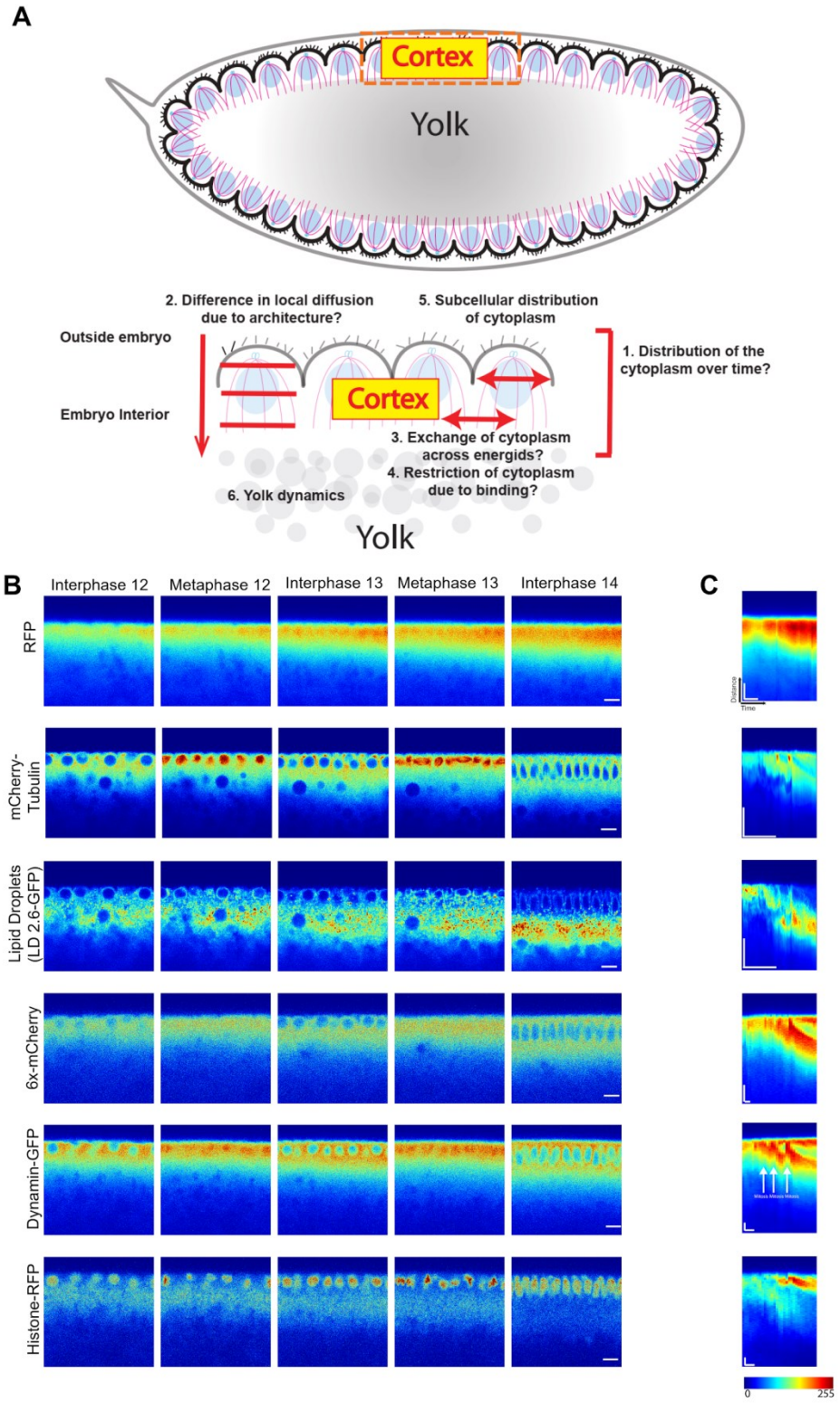

Figure 3.1: Organization of cytoplasm across nuclear cycles.

(A). Questions regarding distribution and dynamics of cytoplasm addressed in this study.

(B). Characterization of cortical spread of mRFP, mCherry-Tubulin, Lipid Droplets (marked using LD 2.6-GFP), 6x-mCherry, Dynamin and Histone-mRFP in the syncytial division cycles. Images are shown from interphase and metaphase of different cycles (NC11,12,13,14) of embryos carrying the transgenes (similar trends were observed for n=3 movies) Scale bar= 10µm.

(C). Kymographs show cortical enrichment of fluorescent signal for all transgenes, except Lipid Droplets, which show enrichment in the opposite direction over time. Scale bar=10µm, 600s. Dynamin-GFP and Histone mRFP, Scale bar=5µm,600s.

The images are shown in a 16 color intensity rainbow where blue represents the lowest intensity and red represents the highest intensity.

3.3.2 FRAP reveals no apical to basal difference in local diffusivity within an energid

Since the cytoplasm was seen to be enriched at the cortex, we asked if mobility of the cytoplasmic molecules will be more in regions closer to the cortex and if we can observe an increase in the molecular crowding in the cytoplasm.The arrangement of actin and microtubule network in a characteristic manner around each nucleus during the syncytial stages, led us to hypothesize that the local mobility of proteins may be different at varied position in the XZ location, namely above the nuclei and in the nuclear plane. To test the same, we performed Fluorescence Recovery After Photobleaching (FRAP) at these three locations during interphase and fit the recovery curves to extract t_{half} values.

Before the experiment, as standardization, in order to normalize FRAP data, we conducted theoretical studies on simulated FRAP data. We generated a simulated data set which can be fit using Yguerabide empirical equation (Yguerabide et al., 1982) for extracting t_{half} values and immobile fractions. Using this data,we first checked if the goodness of fit changes depending on the normalization and which values relevant to FRAP analysis are affected by this (Figure 3.3A). We found that normalization does not change the t_{half} extracted after fit (Figure 3.3B), while the immobile fraction changes considerably (Figure 3.3C). Further, as expected, the FRAP curve fitting is sensitive to the number of time points which are fit (Figure 3.3D). While number of time points which are used for fitting, doesn't change the immobile fraction (Figure 3.3E) but the extracted t_{half} values vary slightly (Figure 3.3F). In conclusion, we suggest that the number of

points fit for any experiment and control should be similar, to extract data which are comparable to each other.

We performed FRAP in the embryo using maternally expressed mRFP under the *nanos* promoter at various different Z positions, namely above, in the plane of and below the nuclear plane (Figure 3.4A). We found that contrary to expectation, the t_{half} values (which represents a quantification for local mobility and diffusivity), do not change between the three locations (Figure 3.4B,C).

These experiments are based on the assumption that any crowding in the local environment would be reflected in changes in the t_{half} values in FRAP. To further test if mRFP slows down in a crowded environment and if this shows in t_{half} values, we performed similar FRAP of mRFP in an embryo overexpressing 8XGFP (Figure 3.4D). We expected the 8XGFP to provide considerable hindrance to local diffusion due to crowding and steric hindrance. We found no significant difference between the t_{half} values for FRAP of mRFP in control and in 8XGFP background (Figure 3.4E,F). This can either mean that the concentration of 8XGFP is not sufficient for reducing the mobility or we are unable to detect a change during FRAP analysis.

Another interesting observation is the increase in the variation of t_{half} values observed when FRAP was performed below the nucleus (Figure 3.4C) or in the 8XGFP background (Figure 3.4F). This might occur due to heterogeneity in the local environment, leading to variable observations. Another probable reason might be thatregions below the nucleus (for Figure 3.4C) and pre-blastoderm (for Figure 3.4F) have access to a large pool of fluorescent molecules. As a result of this, the extent to which bleaching of fluorescence can be performed can be variable, leading to such results.

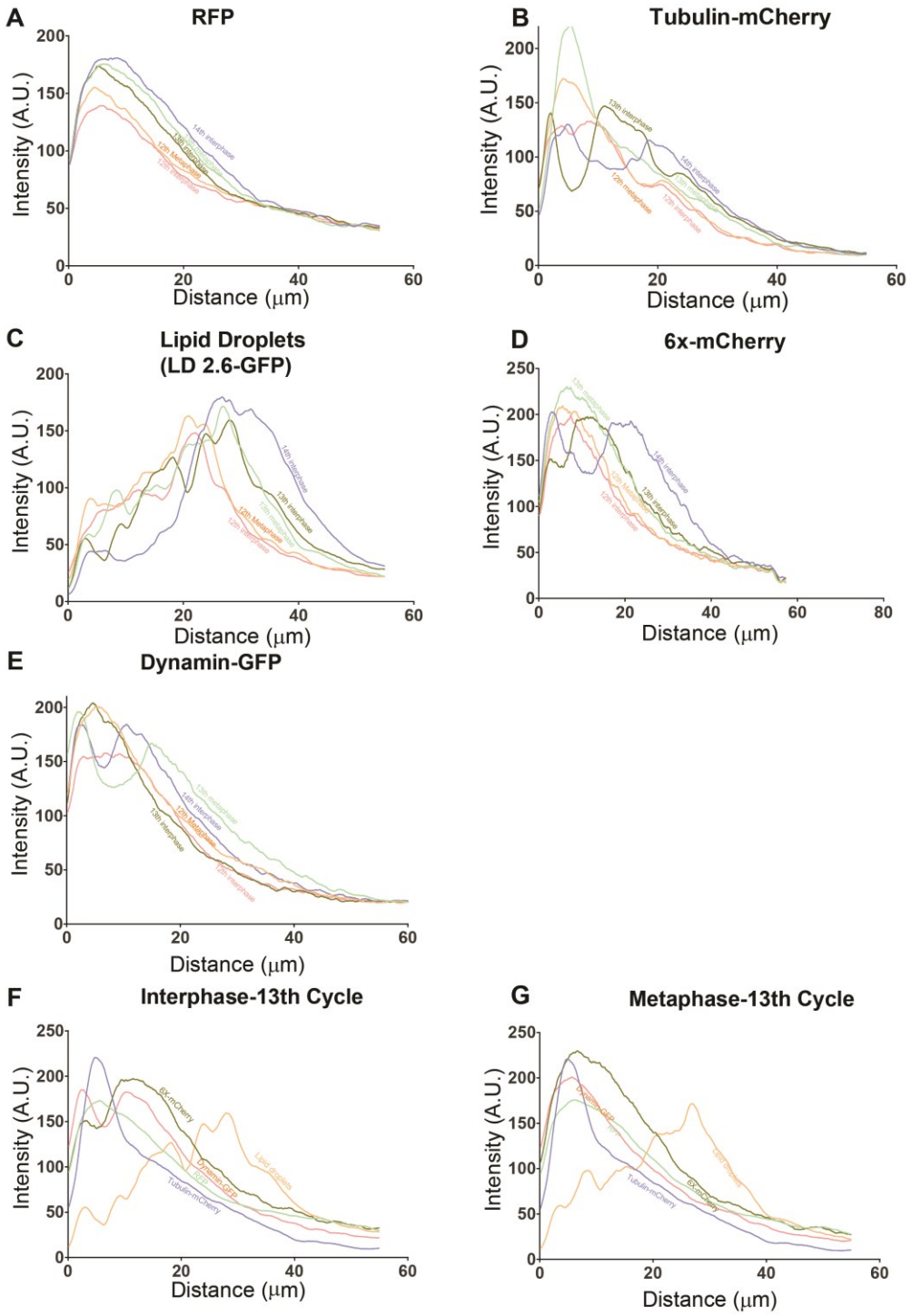

Figure 3.2: Quantification ofXZ intensity profiles across nuclear cycles

(A-E). Quantification of cortical enrichment of fluorescent signal for nuclear cycles 12th to 14th interphase. Graph shows intensity profile for all the transgenes obtained from a line drawn from the cortical region towards the centre of the embryo. Distance represents the distance from the cortex to the centre of the embryo.

(F,G). Comparative graph of intensity profiles across all transgenes in Interphase (F) and Metaphase (G) of Cycle 13th. Note that all profiles are similar except for Lipid Droplets, which enriches away from the cortex.

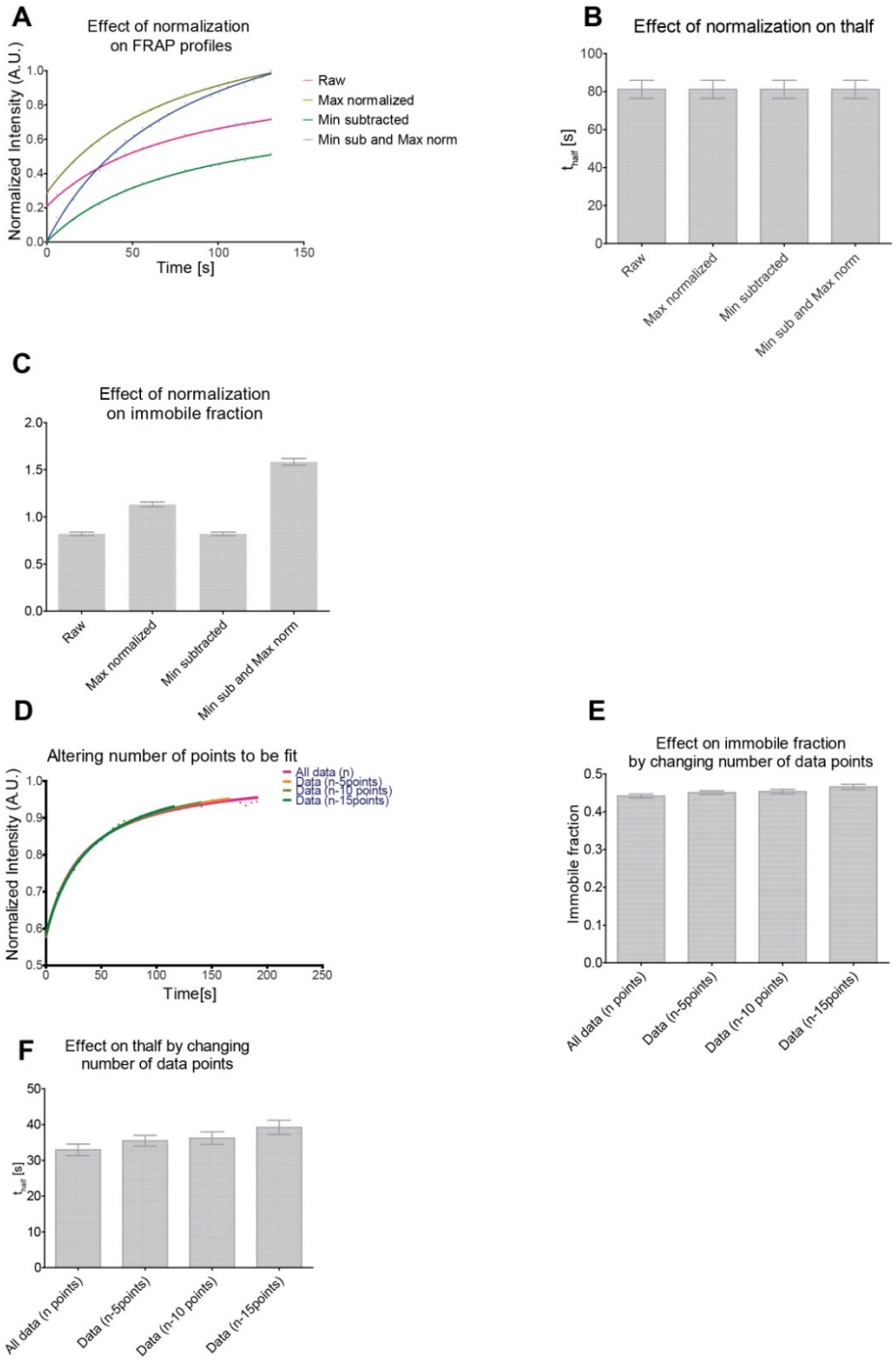

Figure 3.3: Standardization of FRAP analysis using simulated curves

(A)- (C). Effect of normalization on FRAP curves and their analysis. FRAP curves were normalized to the maximum intensity or minimum intensity was subtracted from each data point, or both these operations were performed

together **(A)**. None of the normalizations change t_{half} values calculated post fitting **(B)**, while the calculated immobile fraction values change drastically **(C)**.

(D)- (F). Effect of changing the number of time points analysed on FRAP analysis. The same FRAP data was analysed using n, n-5, n-10 and n-15 data points **(D)**. The immobile fraction does not seem to change much **(E)** while the t_{half} considerably changes **(F)**.

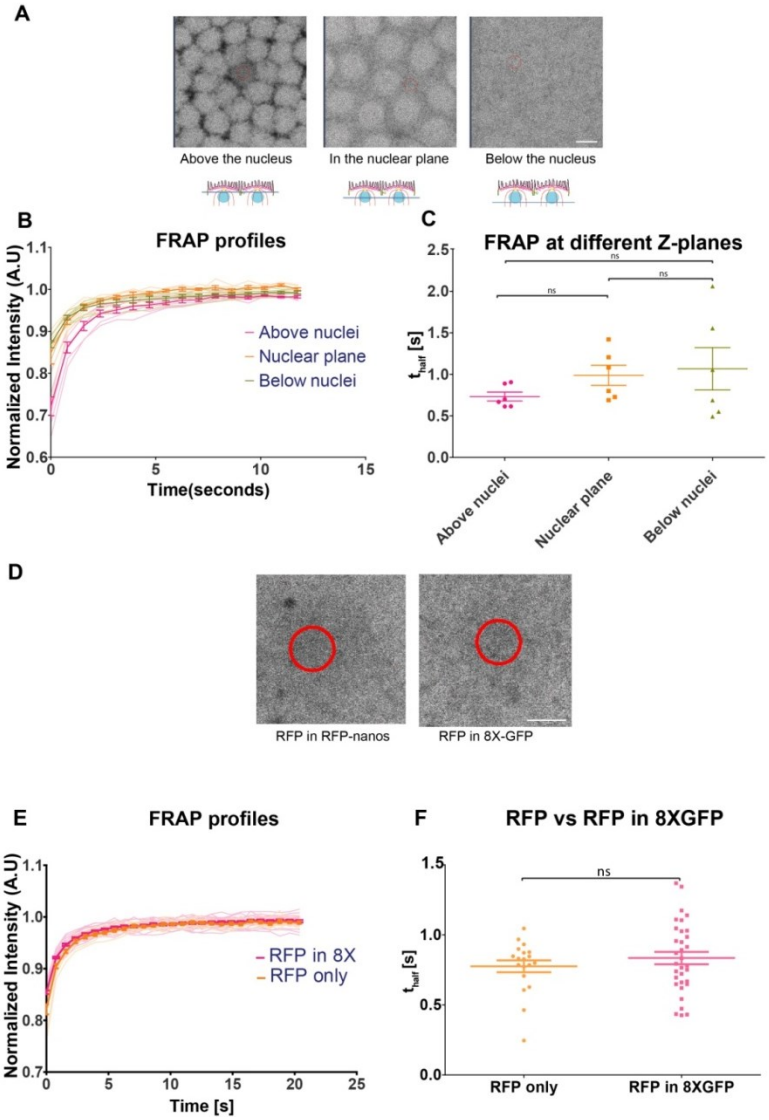

Figure 3.4: FRAP of maternally expressed mRFP under various conditions

(A)- (C). FRAP of mRFP was performed at various Z-planes (depths) from the cortex during interphase. Representative images for FRAP in mRFP are shown for each depth of NC13 (**A)** and the resultant FRAP curves were analysed **(B)**. The t_{half} values were extracted and compared. The graph shows t_{half} derived from different FRAP experiments which suggest no difference in mobility **(C)** (One-way ANOVA (F (3) = 1.105, p = .3566), Tukey's multiple comparison test). Scale bar= 10µm, n=6 experiments in 3 embryos.

(D)- (F). FRAP of mRFP was performed in control or 8XGFP background. Representative images for FRAP in both are shown as performed in pre-blastoderm **(D)** and the resultant curves were analysed **(E)**. The t_{half} values were

extracted and compared. The graph shows t_{half} derived from different FRAP experiments which suggest no difference in mobility **(F)** (Two tailed Mann-Whitney non-parametric test with p value=0.62) . Scale bar= 10μm, n=33 experiments in 4 embryos for mRFP in 8XGFP and 19 experiments in 4 embryos for mRFP in control embryos.The images are shown in a 16 color intensity rainbow where blue represents the lowest intensity and red represents the highest intensity.

3.3.3 Cytoplasmic dynamics using FLIP reveal apical restriction of cytoplasmic diffusion

While FRAP is informative about the local diffusivity of a protein in an environment, Fluorescence Loss in Photobleaching (FLIP) can be used to gather information on the extent of diffusion of proteins across energids. We wanted to test the extent to which cytoplasm is shared between adjacent energids.

We designed an assay where a region of interest (ROI) in an embryo expressing a fluorescent molecule is photobleached with a high intensity laser continuously to remove the fluorescence in the region. Freely diffusing molecules from within the same energid or the neighboring energid will exchange with the ROI and an estimate of the rate of depletion of fluorescence at various locations can be used to assess extent of exchange between neighboring energids. The analysis is done post imaging as follows: we mark multiple regions within and outside an energid equi-distant in XY direction, and analyse the loss of fluorescence in these regions vis-a-vis the region where FLIP was performed.If there is any restriction between the FLIP region and the analysed ROIs, they would show differential rate of fluorescence loss, whereas if there is no restriction in diffusion across energids, then all ROIs would decay at the same rate (Figure 3.5A)..

We tested this experimental schema using mRFP expressed maternally using *nanos*-Gal4 at different Z positions and cell cycle phases (Figure 3.5B). During interphase, we performed this experiment either above the nuclear region, where the presence of individual energids is already somewhat visible or in the nuclear plane (Figure 3.5C,Movie Mov3.S3). We find that the fluorescence exchanges faster within an energid as compared with ROIs marked in a neighbouring energid for both the nuclear cycles, 12th and 13th (Figure 3.5 C,D,E).

On the other hand, we found that when FLIP is performed in the nuclear plane, regions all throughout deplete at similar rates, showing almost no restriction in diffusion

for both the nuclear cycles, 12th and 13th (Figure 3.5 C,F,G,Movie Mov3.S4). When similar analysis was performed during metaphase where the furrows separate adjacent spindles, by drawing an ROI at a planes above or along the spindle (Figure 3.6A), we observe clear presence of restriction of diffusion between neighbouring energids for both the nuclear cycles 12th and 13th (Figure 3.6B).

Similar analysis were performed for interphase using Tubulin-GFP for both nuclear cycles 12th and 13th, above (Figure 3.7A,B) and in the plane of the nuclei (Figure 3.7C,D), which showed similar restriction as seen using mRFP, thus verifying our results. The results are summarized in (Figure 3.7E) showing apical, but not basal restricted diffusion in interphase between energids. In metaphase, cytoplasmic diffusion is highly restricted between adjacent energids.

In summary our FLIP experiments on freely diffusing cytoplasmic probes showed that there is greater restriction above each nucleus in interphase and even at greater depths in metaphase.

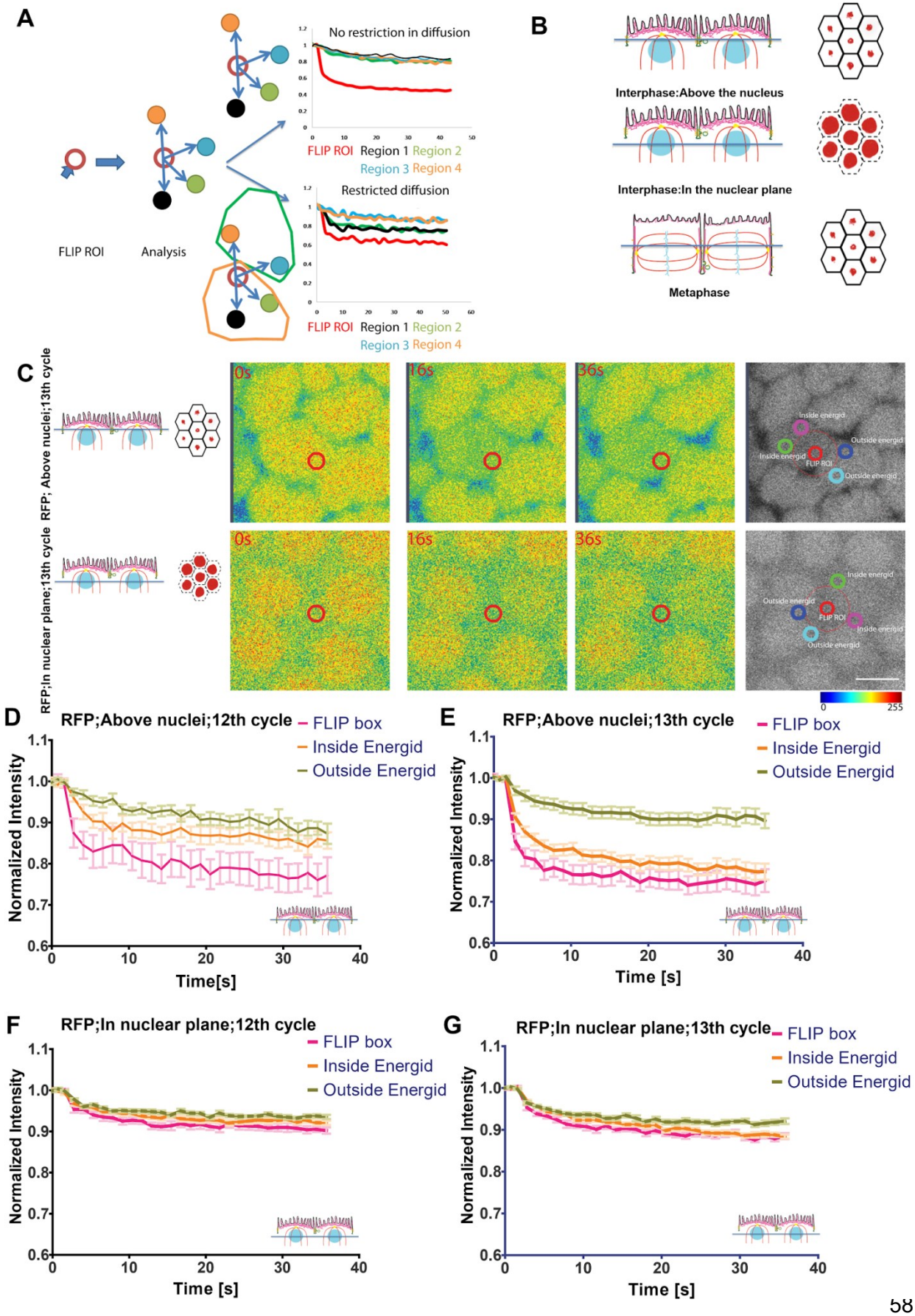
A
No restriction in diffusion
FLIP ROI Region 1 Region 2
Region 3 Region 4
Restricted diffusion
FLIP ROI Region 1 Region 2
Region 3 Region 4
FLIP ROI
Analysis
B
Interphase:Above the nucleus
Interphase:In the nuclear plane
Metaphase
C
RFP; Above nuclei;13th cycle
RFP;In nuclear plane;13th cycle
0s
16s
36s
Inside energid
Outside energid
FLIP ROI
0
255
D
RFP;Above nuclei;12th cycle
FLIP box
Inside Energid
Outside Energid
Normalized Intensity
Time[s]
E
RFP;Above nuclei;13th cycle
FLIP box
Inside Energid
Outside Energid
Normalized Intensity
Time [s]
F
RFP;In nuclear plane;12th cycle
FLIP box
Inside Energid
Outside Energid
Normalized Intensity
Time [s]
G
RFP;In nuclear plane;13th cycle
FLIP box
Inside Energid
Outside Energid
Normalized Intensity
Time [s]

Figure 3.5: FLIP of mRFP suggests restricted diffusion above but not in the plane of the nucleus

(A)- (B).Schematic of the FLIP protocol. A ROI is marked and bleached continuously while imaging embryos carrying fluorescently labelled proteins in cross sectional imaging format. Analysis of the FLIP experiment allows testing of restriction in diffusion **(A)**. The experiments were performed either above or in the plane of the nucleus during interphase or in any plane during metaphase **(B)**.

(C). Representative time-lapse images for FLIP using mRFP are shown for pre bleach, bleach and post-bleach of NC13 Interphase above and in the plane of the nucleus.The ROIs for analysis were drawn equidistant from the FLIP ROI inside or outside the energid as shown in the last panel.Scale bar=10µm.

(D)- (E). Analysis of FLIP of mRFP above the nucleus in cycle 12th **(D)** and 13th Interphase **(E).** The results suggest restricted diffusion across an energid for a free probe like mRFP above the nucleus. n=5 experiments in 4 embryos for NC12 and 12,4 for NC13.

(F)- (G). Analysis of FLIP of mRFP in the nuclear plane in cycle 12th **(F)** and 13th Interphase **(G).** The results suggest free diffusion across an energid for a free probe like mRFP in the plane of the nuclei. n=10 experiments in 4 embryos for NC12 and 12,3 for NC13.

The images are shown in a 16 color intensity rainbow where blue represents the lowest intensity and red represents the highest intensity.

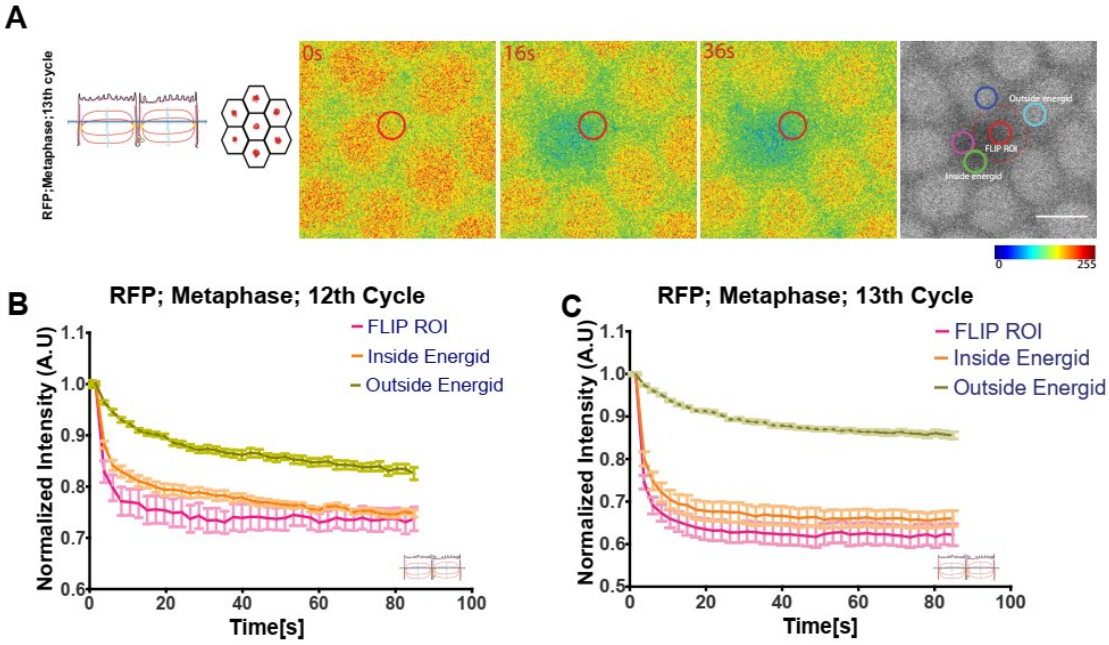

Figure 3.6 FLIP of mRFP during metaphase suggests restricted diffusion

(A)- (C). Representative time-lapse images for FLIP using mRFP are shown for pre bleach, bleach and post-bleach of NC13 Metaphase**(A)**. The ROIs for analysis were drawn equidistant from the FLIP ROI inside or outside the energid as shown in the last panel. Scale bar=10µm.

Analysis of FLIP of mRFP in cycle 12th **(B)** and 13th Metaphase **(C)**. The results suggest restricted diffusion across an energid for a free probe like mRFP in metaphase, possibly due to presence of cytokinetic furrows. n=5 experiments in 4 embryos for NC 12 and 7,4 for NC13.

The images are shown in a 16 color intensity rainbow where blue represents the lowest intensity and red represents the highest intensity.

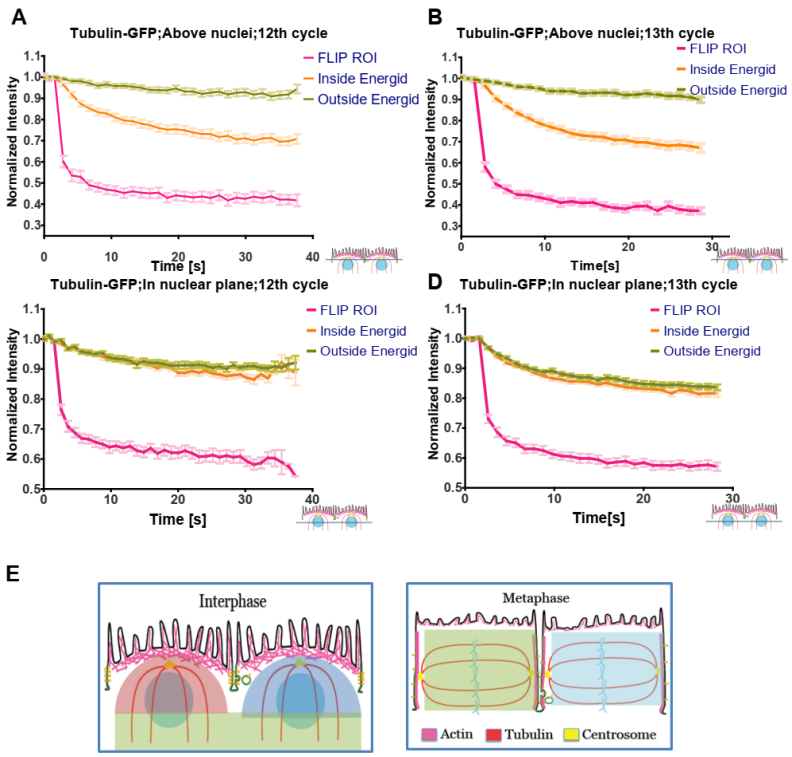

Figure 3.7: FLIP of Tubulin-GFP suggests restricted diffusion above but not in the plane of the nucleus

(A)-(B). Analysis of FLIP of Tubulin above the nucleus in cycle 12th **(A)** and 13th Interphase **(B)**. The results suggest restricted diffusion across an energid for Tubulin-GFP above the nucleus. n=11 experiments in 3 embryos for NC 12 and 13,3 for NC 13.

(C)-(D). Analysis of FLIP of Tubulin in the nuclear plane in cycle 12th**(C)** and 13th Interphase **(D)**. The results suggest free diffusion across an energid for Tubulin-GFP in the plane of the nuclei. n=6 experiments in 2 embryos for NC12 and 16,2 for NC13.

(E). Summary schematic: In interphase, apically but not basally, diffusion is restricted. In metaphase, diffusion is highly restricted between adjacent energids.

The images are shown in a 16 color intensity rainbow where blue represents the lowest intensity and red represents the highest intensity.

3.3.4 Testing restriction of diffusion due to binding with cytoarchitectural components: Lifeact-GFP vs mRFP

Does binding to any components near a particular energid restrict the exchange of the molecule across energids? In order to test this idea, we needed two probes which were of similar size, to normalize for the difference in diffusion due to size. Lifeact is a 17 amino-acid probe which binds to F-actin (Riedl et al., 2008) and thus is likely to remain

in an energid due to the abundance of F-actin in all energids. Lifeact-GFP (~29kDa) can be compared with mRFP (~27kDa) alone which provides us with a way to test this idea, without changing the size of the probes drastically.

For testing this, used a FLIP based assay. We performed FLIP in a particular energid above the nuclei and measured the loss in fluorescence in surrounding energids, which are equidistant to the FLIP ROI (Figure 3.8A,B).We calculated a quantitative measure for the fluorescence loss in surrounding energid, normalized to the extent of fluorescence loss in the FLIP ROI (Figure 3.8C,D).The greater this number, the greater the extent of exchange between energids, after normalizing extent of bleaching. When the loss of fluorescence in the surrounding energids was monitored, we observed that the mRFP depleted much more than Lifeact-GFP after normalizing to the extent to which it is bleached (Figure 3.8E). This suggests that Lifeact-GFP is more restricted near a particular energid by the virtue of its binding to the components of the energid, namely actin in this case.

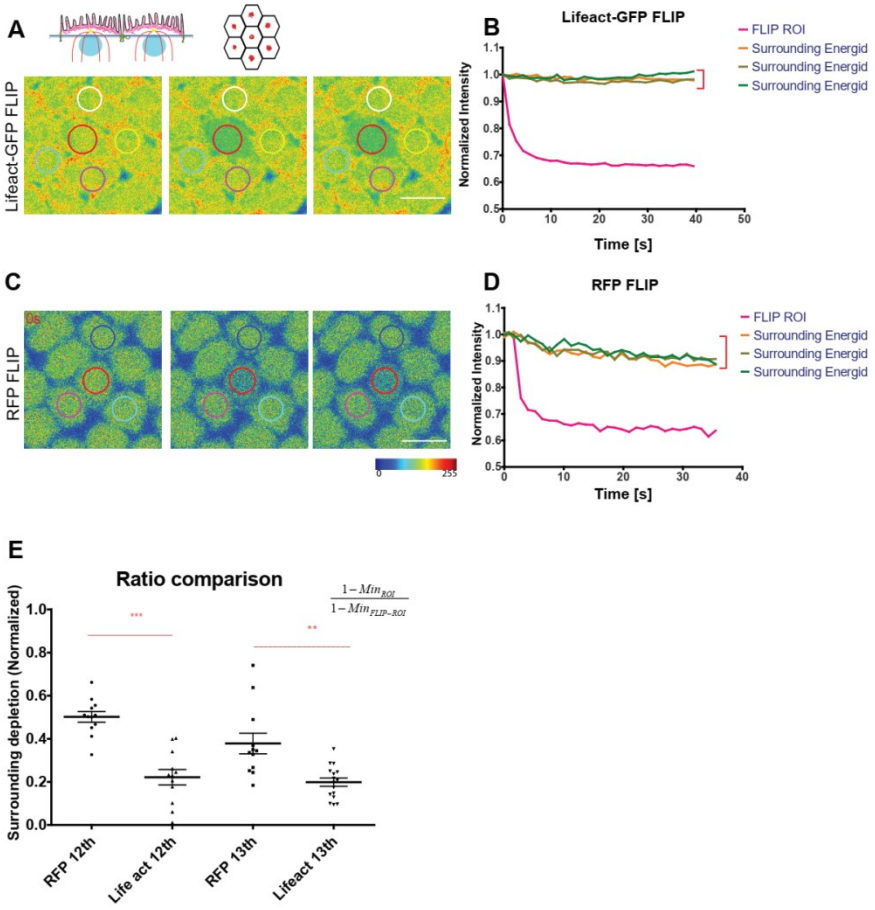

Figure 3.8: Restriction of diffusion due to binding to cytoskeleton

(A), (C): Representative time-lapse images for FLIP using Lifeact-GFP **(A)** and mRFP **(C)** are shown for pre bleach, bleach and post-bleach of NC13 above of the nucleus in interphase.Scale=10μm.

(B), (D):Analysis of FLIP of Lifeact-GFP **(B)** and mRFP **(D)** above the nucleus in 13th Interphase.Note that for similar levels of bleaching, the extent to which the neighbouring energid loses fluorescence (shown in red bracket) is variable between the two probes.

(E): Normalized analysis of loss of fluorescence between Lifeact-GFP and mRFP. The Y-axis is the ratio of loss of fluorescence in neighbouring energid (fluorescence intensity difference between t=0 and t=30s), to the FLIP ROI. Note that neighbouring energids lose mRFP fluorescence to a greater extent than Lifeact-GFP, suggesting that binding restricts diffusion.n=12 experiments in 1 embryo.

The images are shown in a 16 color intensity rainbow where blue represents the lowest intensity and red represents the highest intensity.

3.3.5 mRFP is enriched in nuclei during interphase and spindle region during metaphase

Since the nuclear region changes its shape and structure between interphase and metaphase, it was interesting to assess the difference in mRFP localization between these two phases. Across a nuclear cycle, we notice that, mRFP becomes partially enriched in the nucleus during interphase and in the spindle region during metaphase (Figure 3.9A,B).For interphase, we characterized this better using intensity graded scales and quantified the same by drawing line profiles over the nuclear region and non nuclear region (Figure 3.9C).We find that on the intensity profile over the nuclear region shows a higher intensity corresponding to greater concentration of the mRFP in the nucleus during interphase (Figure 3.9C).This might be due to the pore size of the nuclear-pore complexes which can delay the exit of mRFP from the nucleus. It is also interesting to note that both 5XGFP (probably due to size, not shown) and Tubulin-GFP (not shown) do not enter the nucleus.

During metaphase, mRFP is seen to be enriched in the spindle region to a slightly greater extent than in the surrounding cytoplasm, as seen using intensity graded scale (Figure 3.9B).We find that on the intensity profile over the spindle region shows a slightly higher intensity corresponding to greater concentration of the mRFP in the spindle region (Figure 3.9D). This can be due to the presence of megator/chromator network which has been reported earlier. Spindle enrichment has also been seen earlier as reported (Maddox and Ladouceur, 2015; Schweizer et al., 2015; Yao et al., 2012;

Yao et al., 2018). Overall, it is interesting in itself to find local enrichment of a small, ectopic probe in the nucleus and spindle regions, due to cellular processes.

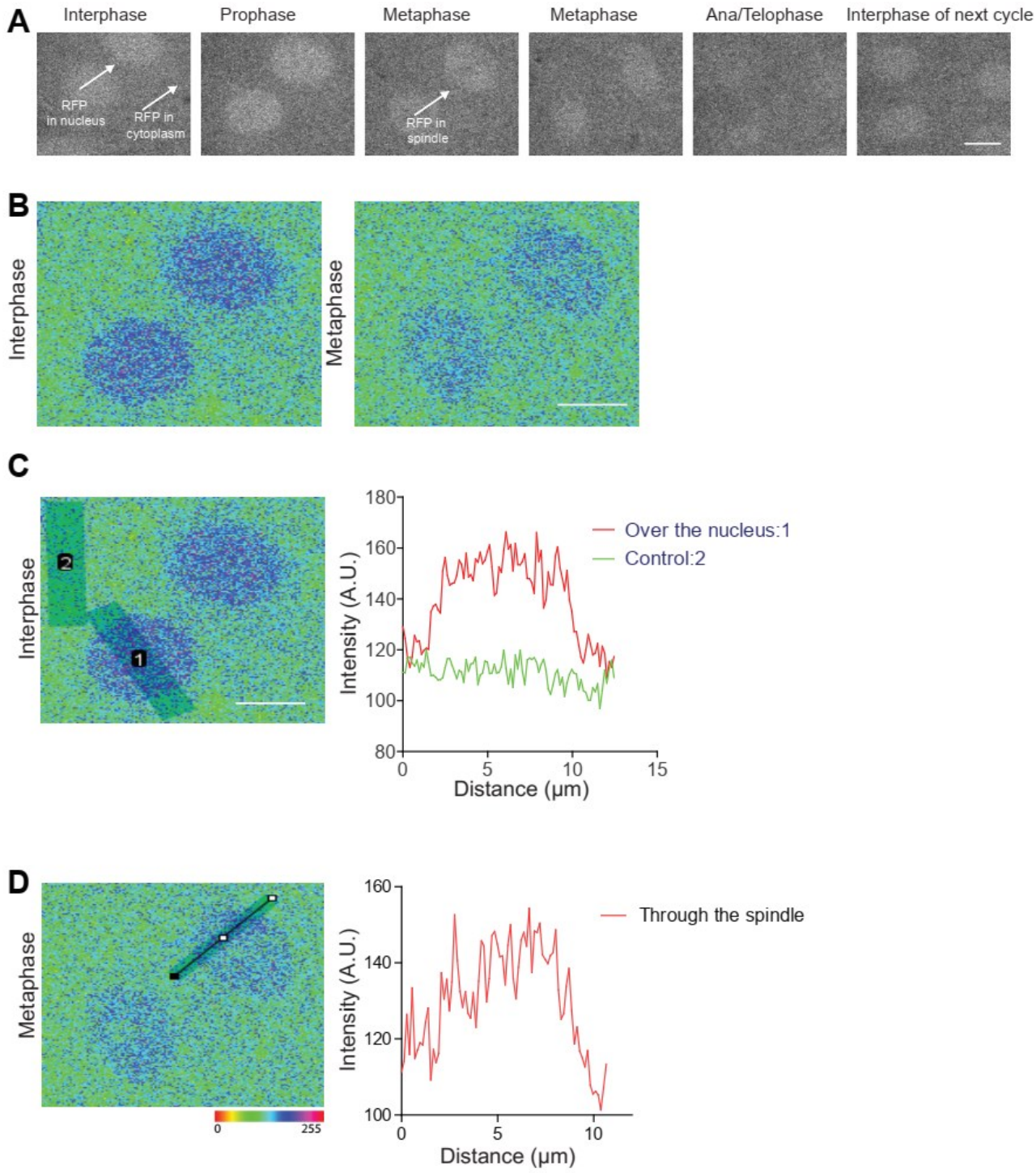

Figure 3.9: mRFP enrichment in nuclear regions and spindle

(A) Representative time-lapse images from XY movies of mRFP are shown for NC13 Interphase to Metaphase and then to the next interphase.Notice the enrichment of signal in some areas of the image.
(B) Representative intensity graded image of interphase of NC 13 of an embryo expressing mRFP in interphase and metaphase **(B)**.Notice the change in the color in the nuclear and the spindle region. Scale bar=10μm.
(C) Interphase:Graph showing the change in intensity profile when lines are drawn across a nucleus and control region as shown and their intensity measured.Scale bar=10μm.
(D) Metaphase:Graph showing the change in intensity profile when lines are drawn across a nucleus and control region as shown and their intensity measured.Scale bar=10μm.
The images are shown in a 16 color intensity rainbow where blue represents the lowest intensity and red represents the highest intensity.

3.3.6 Characterizing Yolk dynamics across and within nuclear cycles reveals cell cycle dependent differences in yolk movement

(In collaboration with Mithun Mitra, Amitabha Nandi and Bivash Kaity,IIT Mumbai)

The separation of yolk into interior regions from the cytoplasm present cortically is an opportunity to monitor the dynamics and motion of individual yolk particles and how they gradually move towards the centre of the embryo. These particles which appear opaque under 561nm laser, when imaged along with mRFP and these live movies allow for an analysis of the dynamics of the cytoplasm and yolk with respect to each other (Figure 3.10A).

We imaged embryos containing maternally expressed mRFP under *nanos*-Gal4 across the syncytial division cycles. We imaged embryos in 4 dimensions i.e. in a cross sectional format (XYZ) and upto a depth of 33μm. This allowed us to track and analyze cytoplasmic and yolk movement across developmental time (Figure 3.10B,Movie Mov3.S5). We observed a gradual movement of yolk to deeper Z-sections (deeper into the embryo) as the nuclear cycles progress. This was estimated by thresholding to quantify and track yolk particles using algorithms developed by our collaborators Mithun Mitra, Amitabha Nandi and Bivash Kaity at IIT Mumbai. The total number of yolk particles, in each Z-slice along the depth of the embryo, seen in the first 30 Z-stacks (~33μm) is drastically different between nuclear cycle 10 and 14th (Figure 3.10C).

We further tracked the yolk particle movement across depth during the different phases ofa single nuclear cycle (Figure 3.10D). We found that while the total number of yolk particles observable near the cortex, decreased consistently in interphase and

metaphase, these particles would resurface and move upwards near the cortex during anaphase/telophase of the nuclear cycle. This is seen as a major spike in the cumulative total observable number of particles across the cycle (Figure 3.10E). This implied a correlation of the yolk movement with a sub-cellular event in the cell cycle such as microtubule network reorientation/pseudo cleavage furrow extension and retraction in anaphase.

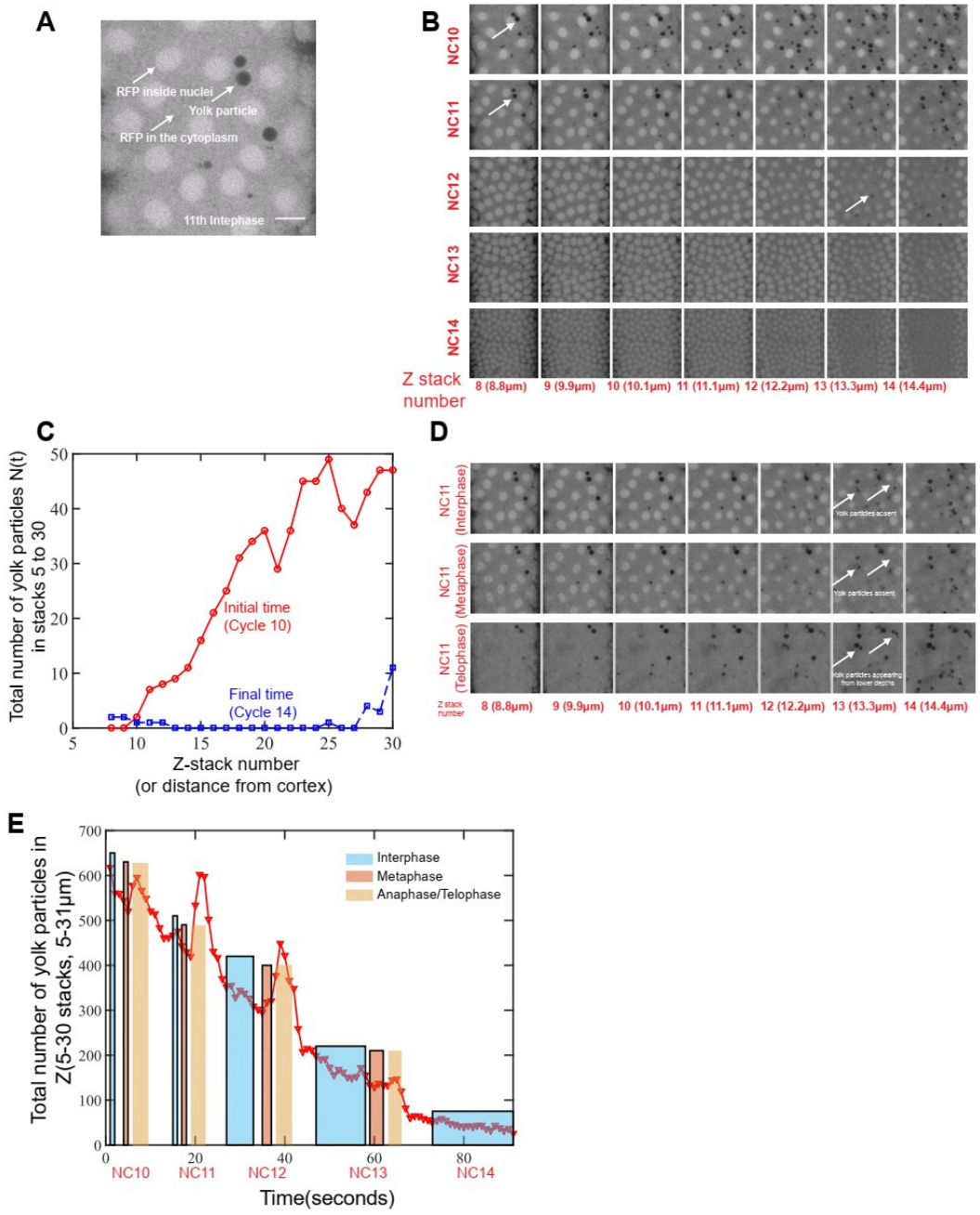

Figure 3.10: Yolk movement across and within nuclear cycles

(A): Representative image from XY movies of mRFP is shown for NC11 Interphase. Note that mRFP in cytoplasm and nuclei can be clearly made out. The black circular regions are impenetrable to mRFP and represent yolk granules.Scale bar=10μm.
(B)-(C):Representative time-lapse images from XY movies of mRFP are shown for Interphase of NC11 to NC14 (**B)**. Each column represents an optical Z-slice at the nuclear cycle, while each row is a different nuclear cycle. Graph showing the change in number of yolk particles at each Z-slice at initial time point (red) and at the final time point (blue) **(C)**.
(D)- (E):Representative time-lapse images from XY movies of mRFP are shown for one cycle (NC11) from Interphase to metaphase to telophase**(D)**. Each column represents an optical Z-slice at the nuclear cycle, while each row is a different stage of the nuclear cycle. Graph showing the change in the total number of yolk particles in the 31μm region near the cortex, across different stages of cell cycle of different nuclear cycles.

3.4 Discussion

In this chapter, I have shown results which suggest:

1. Cytoplasm is enriched in 30 to 40μm layer near the cortex of the embryo and this enrichment increases in depth as time progresses across the syncytial cycles. Lipid droplets are enriched towards base of the cytoplasm.
2. FRAP reveals similar mobility of mRFP above and below the nucleus in interphase despite differences in subcellular architecture.
3. Cytoplasmic restriction is greater above the nuclei in interphase and all along the depth in metaphase. Binding to the cytoskeleton reduces the cytoplasmic exchange between neighboring energids.
4. mRFP accumulates asymmetrically in different cortical regions and is enriched in the nuclear region in interphase and spindle region in metaphase.
5. Yolk particles move gradually deeper into the embryo and show differential movement across the cell cycle.

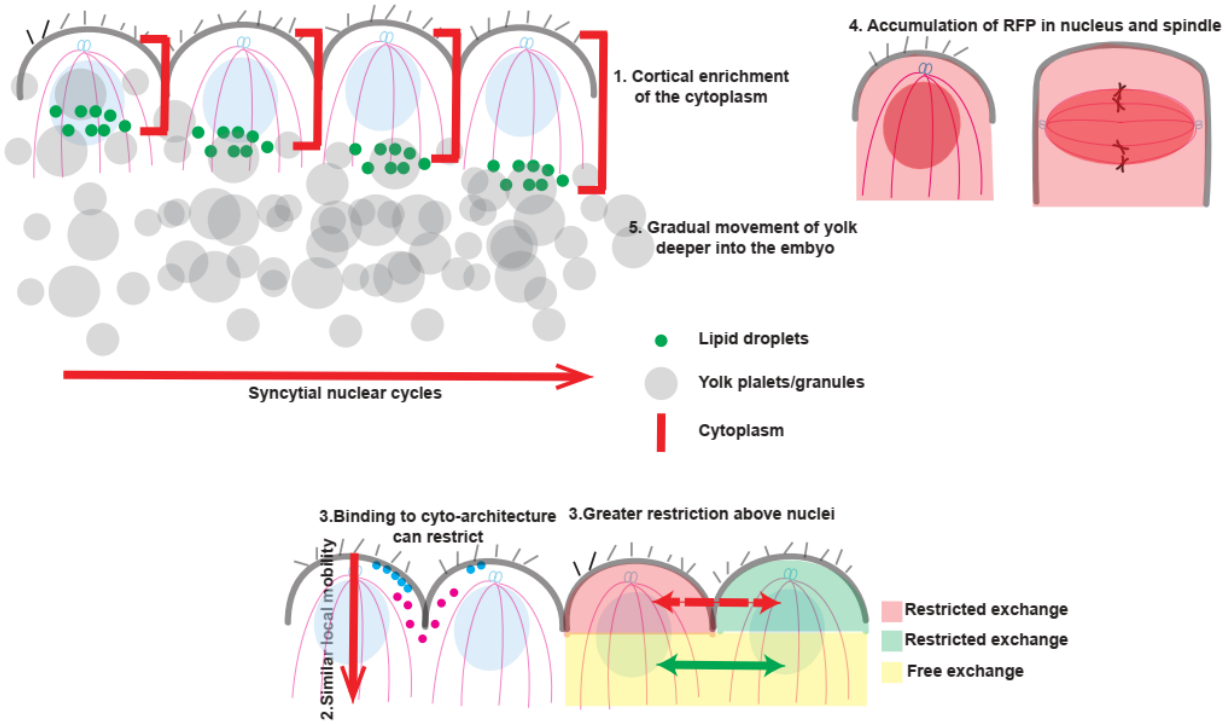

Figure 3.11: Schematic summarising observations regarding the distribution and dynamics of cytoplasm & yolk in the early *Drosophila* syncytial embryo.

Cortical enrichment of the cytoplasm maybe due to yolk compaction

The observation that cytoplasmic components are cortically enriched corroborates previously reported data. SEM images from cross sectioned *Drosophila* embryos show the presence of similar biphasic compartments (Figard et al., 2013; Turner and Mahowald, 1976). Filamentous actin and non-muscle myosin are concentrated in the 3-4 µm and 1-2 µm region of the “yolk-free” cytoplasm just beneath the plasma membrane of the embryo, respectively (Foe,Odell and Edgar, 1993). The cortical yolk-free cytoplasm increases in its depth as the syncytial cycles progress (Foe,Odell and Edgar, 1993). It is also interesting to note that most of *hunchback (hb)* transcripts accumulate above and below a nucleus and are confined in the depth till 12 to 15µm near the cortex (Figure S3A in (Little et al., 2013). Our study is a further characterization of protein mobility in these phases, and we show that the cortical cytoplasm and yolk beneath it seem to form two separate compartments. The size of the cortical cytoplasmic region as determined by the spread of cytoplasmic mRFP (and other probes) is approximately 40 µm, where the fluorescence intensity falls off sharply.

The depth of this cortical cytoplasm increases with nuclear cycles. This can either be attributed to the greater organization of the cytoskeletal elements across time or gradual compaction of yolk which “oozes” the cytoplasm near the cortex. It can even be a combination of both these processes. This observation raises further questions about how these two phases are separated and the mechanisms that contribute to maintaining their integrity.

Cortical cytoplasmic enrichment and morphogen gradients

The observation about the presence of two separate phases of cortical cytoplasm and embryo yolk provides an interesting perspective to our current understanding of morphogen gradients in the early embryo, namely, Bicoid, Dorsal and Torso. The Bicoid gradient has been extensively studied using the framework of the synthesis, diffusion and degradation (SDD) (Durrieu et al., 2018; Gregor et al., 2007; Grimm et al., 2010) and related models. However, a complete theoretical understanding of the mechanisms underlying the formation of the Bicoid gradient is still lacking. Our finding implicates a restriction of the effective volume to a small space near the cortex, in which Bicoid gradient develops and matures. Previous reports suggest Bicoid movement in the cortex and its dependence on the actin and the microtubule cytoskeleton of syncytial blastoderm embryos (Cai et al., 2017). This also raises the possibility that various cytoarchitectural components could impinge on its formation. For example, perturbations in furrows or cytoskeletal structures can change the effective concentration of morphogens in the cortical cytoplasm, leading to changes in the morphogen profiles, specifically for Bicoid. This is an idea we explore in detail in Chapter 6.

Effect of architecture on diffusion and mobility

The finding that mRFP local mobility does not change at different Z planes suggests either a difference does not exist or we are unable to detect a difference using the existing experimental design. The latter can be due to the fact that the difference in the diffusivity is too subtle to be observed using a gross method like FRAP (Stasevich et al., 2010; Trembecka et al., 2010). Similar cases of changes in diffusivity changes have

been observed in case of Bicoid where observation using FRAP led to very different results when compared with FCS (Abu-Arish et al., 2010).

In the case where the difference in mobility might exist, it is possible to predict probable outcomes,namely that diffusion is slower near the apical region as compared to other regions. This can be attributed to the denser apical microtubule network near the centrosome, causing restriction and transient trapping. Near the nuclear plane and below the same, the microtubule network might be sparse leading to faster diffusion values. A theoretical modelling study predicts similar outcomes, though it specifically considers molecules which bind to microtubules (Chen et al., 2012). The study predicts the compartmentalization of cytoplasm just due to the presence of microtubule density. Further experiments which disrupt microtubule length and dynamics, like those seen in *eb1* mutants (Chapter 4) are needed to check these hypotheses.

The experiments concluding greater inter energid restriction above the nucleus as compared to other planes, provide a contrast to this. It is worth noting that while the previous experiment measures local diffusion in an energid, this experiment is a measure of restriction in diffusion across energids. The results of the FRAP experiment pertains to the local diffusion of the molecule per se, while the FLIP is for finding restrictive boundaries.

The FLIP experiments suggest that molecules above the nuclei take a longer path to exchange with neighbouring energids in comparison to molecules in the plane or below nuclei. This is inferred from the differential rates of fluorescence loss. The restriction is maintained across nuclear cycles. It becomes pronounced in metaphase which shows strong restriction in diffusion. These restrictions in interphase could arise due to either increased inter molecular crowding above the nuclei, mediated by microtubules, or due to the presence of the nascent membrane between nuclei. A closer look at the data suggests the latter being the case, though definitive analysis still needs to be performed. Firstly, we know that the nascent interphase membrane is longer in cycle 13th than in cycle 12th. This reflects in the extent of the rate of fluorescence loss between the two cycles. In cycle 12th the difference between the within and outside energid rates is smaller as compared to cycle 13th where this difference in more pronounced. Secondly, the FRAP analysis discussed above also suggests that this

difference is less likely to be because of crowding.

Further experiments with *ralA* mutants (Holly et al., 2015) which perturb furrow lengths are needed to conclusively decipher this observation.

Transient crowding in the spindle region

We have shown that mRFP, even though being an inert molecule not known to interact with any components present in the early embryo, is found to be enriched in the spindle region during metaphase. Earlier it has been shown that the metaphase spindle is surrounded by a gel like spindle matrix, which is a form of a membrane-less macromolecular assembly, made of protein constituents like Skeletor, Megator and Chromator, which embed the microtubule-based spindle apparatus (Yao et al., 2012).

This matrix exists independently of microtubules and facilitates the accumulation of molecules in the spindle region.This is done by excluding organelles and causing a distinct molecular corwing state, or an arrangement of spindle matrix and microtubules that facilitates passive accumulation and trapping of molecules in the spindle region. Passive accumulation of Tubulin into the spindle space was observed (Maddox and Ladouceur, 2015; Schweizer et al., 2015). Later,it was shown that a number of key cell cycle proteins, such as Cycle B, Polo and Ran also co-localized with the spindle matrix (Yao et al., 2018).

Our results are a demonstration of the passive accumulation of free cytoplasmic probe mRFP in the spindle matrix and corroborates previous reports of cytoplasmic compartmentalization in this region.

Further analysis of this observation can include checking for accumulation of Bicoid, Dorsal or Torso in the spindle region, and if so does it have a functional significance. Another question to study is spindle compartmentalization by using various mutants and checking for loss of this compartmentalization. Interestingly, mRFP imaging with Eb1 mutants which show joint spindles, shows that the enrichment of mRFP within each spindle in intact (data not shown).

Yolk movement correlates with microtubule positioning

Our analysis of yolk using mRFP imaging shows that yolk granules move towards the

centre of the embryo as nuclear cycles near the cortex proceed. The movement follows a definite pattern, with yolk granules moving down during interphase and metaphase while showing an upward movement during anaphase/telophase. Recently, the role of actin comets and actin driven flows in separating the ooplasm from the yolk has been found (Shamipour et al., 2019).Yolk movement in the early *Drosophila* embryo is not well studied as yet. Early studies make note of the gradual compaction of yolk leading to move cytoplasmic volume near the embryo cortex (Foe et al., 2000; Foe,Odell and Edgar, 1993) For example, a yolk-free region is known to appear around the male pronucleus when the large sperm aster forms prior to pronuclear fusion.The yolk free cytoplasm is thought to result from the organized microtubule arrays organized by centrosomes (Karr, 1986).

Precisely what mechanisms lead to clearing of the cytoplasm is not known, though it is thought to be dependent somehow on microtubules (Ault et al., 1991; Hotani and Miyamoto, 1990). Can it be that yolk particles are carried by microtubule based motors, like Kinesin? Quite remarkably, in an unfertilized but activated egg, microtubules organize around the meiotic chromosomes in the absence of centrosomes and therefore in random orientations. Yet the region around the chromosomes becomes free of yolk, thus hinting that the yolk movement is independent of microtubule based motors (Huettner, 1923; Sonnenblick, 1941).

What causes this gradual movement of yolk? The cell cycle dependance of the yolk granule movement suggests that the microtubule basket surrounding the nuclei are involved in this phenomenon. The greater depth to which yolk are pushed as cell cycles progress, also suggests that as cell cycles progress and increase in the extent to which the microtubule basket is formed, the yolk granules are pushed down. Further the release of the microtubule based push is abrogated when the microtubule network dissolves in ana/telophase of the nuclear cycle. We do not rule out the role of actin or pseudo cleavage furrows in this phenomenon, but do not expect it to be of major significance as both are confined to the plasma membrane and are not present at depths where yolk is found.

These results present the first characterization of yolk movement in the early embryo. Further analysis will include using mutants to dissect the role of microtubules

versus actin versus the cytokinetic furrows in yolk movement. Also we suggest using injection of beads to verify if this movement is active (motor driven) or passive.

3.5 Supplementary Movies

Mov3.S1: mCherry-Tubulin: mCherry-Tubulin expressed with *mat*-Gal4 is imaged in the syncytial division cycles. Note mCherry-Tubulin incorporation into centrosome, spindle and cortical microtubules.
Mov3.S2: Lipid Droplets (LD-2.6-GFP): Lipid Droplets tagged with the LD-2.6-GFP marker expressed with *mat*-Gal4 is imaged in the syncytial division cycles. Note lipid droplets move gradually below the nuclei, towards the centre of the embryo across nuclear cycles.
Mov3.S3: FLIP of Dynamin-GFP above the nuclei. Note the discernable boundaries of the energids and rates of fluoresence depletion within and outside the energids.
Mov3.S4: FLIP of Dynamin-GFP in the nuclear plane. Note that there are no discernable boundaries of the energids and rates of fluoresence depletion near and far from the ROI are only dependent on the distance from the ROI.
Mov3.S5: Yolk movement across cycles in time and depth. Yolk can be seen as black circles in this embryo containing mRFP expressed under *nanos*-Gal4. Notice the gradual movement of yolk towards lower Z sections across cycles.
All movies (except S5) are in shown in 16 color intensity rainbow scale where Blue represents the lowest intensity and red represents the highest intensity. Scale bar=10μm or 50μm as mentioned.

Chapter 4: Photoactivation as a tool to test cytoplasmic distribution and dynamics by creating ectopic localized gradients

(In collaboration with Bipasha Dey & Swati Sharma at IISER Pune and Mithun Mitra, Amitabha Nandi & Bivash Kaity at IIT Mumbai)

Chapter 4 summary: *In this chapter, we discuss how the early embryo syncytium provides a tractable system to study reaction-diffusion systems. We use the mixing of photoactivated and non-photoactivated molecules to assess how diffusion in the early embryo takes place, in the context of the synthesis-diffusion-degradation (SDD) model.*

4.1 Introduction

Our current understanding of the *Drosophila* early embryo syncytium suggests that there exist mechanisms that limit the exchange of molecules between adjacent syncytial cells. For example, the restriction of Lifeact-GFP near energids as compared to mRFP, though having the same size, suggests that restriction due to binding or polymerization may be a way to restrict diffusion (Chapter 3).

Morphogen gradient formation in the syncytial *Drosophila* provides a paradigm to estimate properties and details of such exchanges. Morphogens are molecules generated from a source which diffuse across the embryo, forming a graded distribution or a gradient (Chapter 1). This along with various other studies (Carrell et al., 2017; Coppey et al., 2008; DeLotto et al., 2007) together imply that formation of gradients in the syncytial blastoderm cortex depends upon the interaction of morphogen molecules with other cytoplasmic components or the syncytial cyto-architecture. Thus, protein molecules diffusing from a source can be identified distinctly and tracked. This can provide a useful tool to study cytoplasmic exchange. It also provides insights on how biologically relevant gradients, like Bicoid and Dorsal may be spreading in the same context.

In this chapter, we attempted to elucidate the extent of cytoplasm exchange across nucleo-cytoplasmic domains by creating local pools of trackable fluorescent molecules. We used photoactivation in a specific region to fluorescently label and track

(thereby distinctly identify) molecules as they spread through an otherwise non-fluorescent embryo. Further, we use a comparison between cytoplasmic PA-GFP and PA-GFP-Tubulin to test the difference between molecules that are restricted due to binding/ polymerization (PA-GFP-Tubulin) versus those which are free to diffuse (PA-GFP). We find that the gradient of PA-GFP-Tubulin is more restricted as compared to PA-GFP in the antero-posterior axis. PA-GFP and PA-GFP-Tubulin have a decreased spread when generated in the middle of the embryo as compared to the anterior. We also find that both diffuse in the cortical region as compared to the yolk filled central region of the syncytial blastoderm embryo. The PA-GFP-Tubulin gradient diffuses to a greater distance in mutants showing a loss of plasma membrane furrows or disruption of the microtubule network. The PA-GFP gradient is not affected in these mutants.

4.2 Special notes on Materials and methods

We tried using *nanos*-gal4 to drive PA-GFP, but does not seem to drive the expression enough to be imaged. PA-GFP-Tubulin has been tried with *nanos*-gal4 and is suitable for imaging.

Microscopy

PA-GFP and PA-GFP-Tubulin were photoactivated using the 405 nm diode laser at 100 percent power using the bleach module on the LSM software. PA-GFP and PA-GFP-Tubulin thus produced was imaged using the 488 nm laser. ROI size was kept constant at 373μm^2. Photoactivation iterations were kept constant at 10 iterations per frame with activation being performed after every frame. The photoactivation was carried out for 0.36 s (10 iterations). 512 pixel X 512 pixel images were acquired after that with a scan speed of 1.97 seconds per frame. Mid sagittal sections were imaged. 8 bit images were acquired with mean line averaging of 2. The gain and laser power were adjusted to be cover the dynamic range of each fluorescent tag and care was taken to not reach 255 on the 8 bit scale. Pinhole was kept open at 180μm.

4.3 Results

4.3.1 Photoactivation generates a source of PA-GFP and PA-GFP-Tubulin at the anterior that forms a cortical gradient along the anterior-posterior axis

Labelled tubulin had a cytoplasmic and a microtubule bound fraction, in contrast to GFP, which had a cytoplasmic fraction in the *Drosophila* syncytial blastoderm embryo. This gave us an opportunity to assess the diffusion of these two proteins in the cytoplasm across nucleo-cytoplasmic domains. Computational simulations have predicted that binding to microtubule network and movement on motors is sufficient for partitioning the cytoplasm, in the absence of membrane boundaries in the syncytial blastoderm embryo (Chen et al., 2012). We therefore asked whether tubulin which partitions partially into microtubules could be more restricted as compared to GFP in the syncytial blastoderm embryo.

Photoactivation of cytoplasmic and cytoskeletal proteins have been used to generate a local source of protein molecules for monitoring their directional spread in axons (Gauthier-Kemper et al., 2012; Gura Sadovsky et al., 2017). In order to differentially test the spread of cytoplasmic and cytoskeletal proteins in the syncytial blastoderm embryo, we used photoactivation to create a local source of fluorescent PA-GFP or PA-GFP-Tubulin at different locations of the embryo (Figure 4.1A). Unlike morphogens such as Dorsal and Bicoid, GFP and tubulin are not differentially distributed in the syncytial embryo. PA-GFP and PA-GFP-alpha-Tubulin 84B (PA-GFP-Tubulin) were expressed individually in embryos by crossing the transgenic flies to *mat*-Gal4. A fixed area was continuously photoactivated to form fluorescent PA-GFP/PA-GFP-Tubulin, thus creating a local source of PA-GFP/PA-GFP-Tubulin at the anterior pole of the embryo (Figure 4.1B,D). PA-GFP localizes to the nuclei, shows cortical enrichment and also apical restriction (data not shown), as seen for mRFP, thus following similar distribution in an energid as reported in Chapter 3. The movies of PA-GFP photoactivation also showed the presence of a strong autofluorescent signal at the base of the cortex comprising of yolk (Movie Mov4.S3). The movies of PA-GFP-Tubulin showed an increase in fluorescence in the cytoplasm and PA-GFP-Tubulin was also incorporated in microtubules in interphase and in metaphase spindles (Movie Mov4.S4).

Both PA-GFP and PA-GFP-Tubulin increased in concentration by diffusion away from the source across the syncytial division cycles. A kymograph obtained at the source of photoactivation showed a distinct increase in amount of photoactivated molecules over time (Figure 4.1C,E).The kymograph also showed that the fluorescent signal was enriched near the cortex and did not enter the central yolk filled region of the embryo. A 30% drop in the signal was obtained between 40 to 45μm for PA-GFP and 20 to 25μm for PA-GFP-Tubulin beneath the cortex. An analysis of the directionality of spread showed that both molecules spread to a greater distance cortically along the antero-posterior axis (XY) as compared to the depth within the embryo (XZ) (Figure 4.1F,G). The cytoplasm of syncytial *Drosophila* blastoderm embryo has a biphasic distribution with cortical nucleo-cytoplasmic domains present above a barrier comprising of yolk and other unknown components (Mov4.S1,S2) (Foe and Alberts, 1983; Wessel et al., 2015). This organization possibly allows for greater spread along the cortex in the antero-posterior axis as compared to the centre.

4.3.3 Photoactivation of the cytoplasmic PA-GFP and PA-GFP-Tubulin in the middle of the *Drosophila* embryo results in a gradient with a smaller length scale as compared to the anterior activation

The syncytial *Drosophila* embryo has three domains containing distinct patterns of density of nuclei and packing (Blankenship and Wieschaus, 2001; Rupprecht et al., 2017). The domains show different speeds of furrow extension during cellularization. The anterior and posterior domain contain nuclei at a lower density as compared to the middle domain and the cells formed have a shorter plasma membrane furrows as compared to the middle domain in cellularization. This difference in architecture across the antero-posterior axis is regulated by the patterning molecules Bicoid, Nanos and Torso (Blankenship and Wieschaus, 2001). This difference in the density of nucleo-cytoplasmic domains prompted a comparison of the extent of gradient spread, when it originates in the middle of the embryo versus when it originates in the anterior domain (Figure 4.3A).

We tested if there was a difference in the kinetics of gradient formation when photoactivation was carried out in the middle (Figure 4.3) of the embryo as compared to

the anterior (Figure 4.1,4.2). For this we photoactivated PA-GFP and PA-GFP-Tubulin containing embryos in a fixed region in the middle of the embryo (Figure 4.1A,4.3A,C). Photoactivation produced a cortical gradient with a progressive increase in gradient spread across the syncytial division cycles((Figure 4.3B,D,F Movie Mov4.S5,6). The gradient of PA-GFP and PA-GFP-Tubulin spread to a greater extent in the antero-posterior axis (XY) as compared to the depth of the embryo (XZ), away from the region of photoactivation (Figure 4.3G,H)

Length scale values were extracted by fitting an exponential equation and it was found that the extent of spread for both the probes was lower than that observed when photoactivation was performed anteriorly (Figure 4.3I,K).

We further analysed if there was any difference in the gradient formation from the centre towards the anterior versus centre towards the posterior pole (Figure 4.3L,M). We found the length scales of the gradients did not differ in either direction (Figure 4.3N). These analyses show that the gradient spreads uniformly across the syncytial nucleo-cytoplasmic domains towards the anterior pole and the posterior pole of the *Drosophila* embryo, negating the presence of any cytoplasmic flows or currents. In summary, photoactivated molecules generated in middle spread to a smaller distance as compared to when they were generated at the anterior pole.

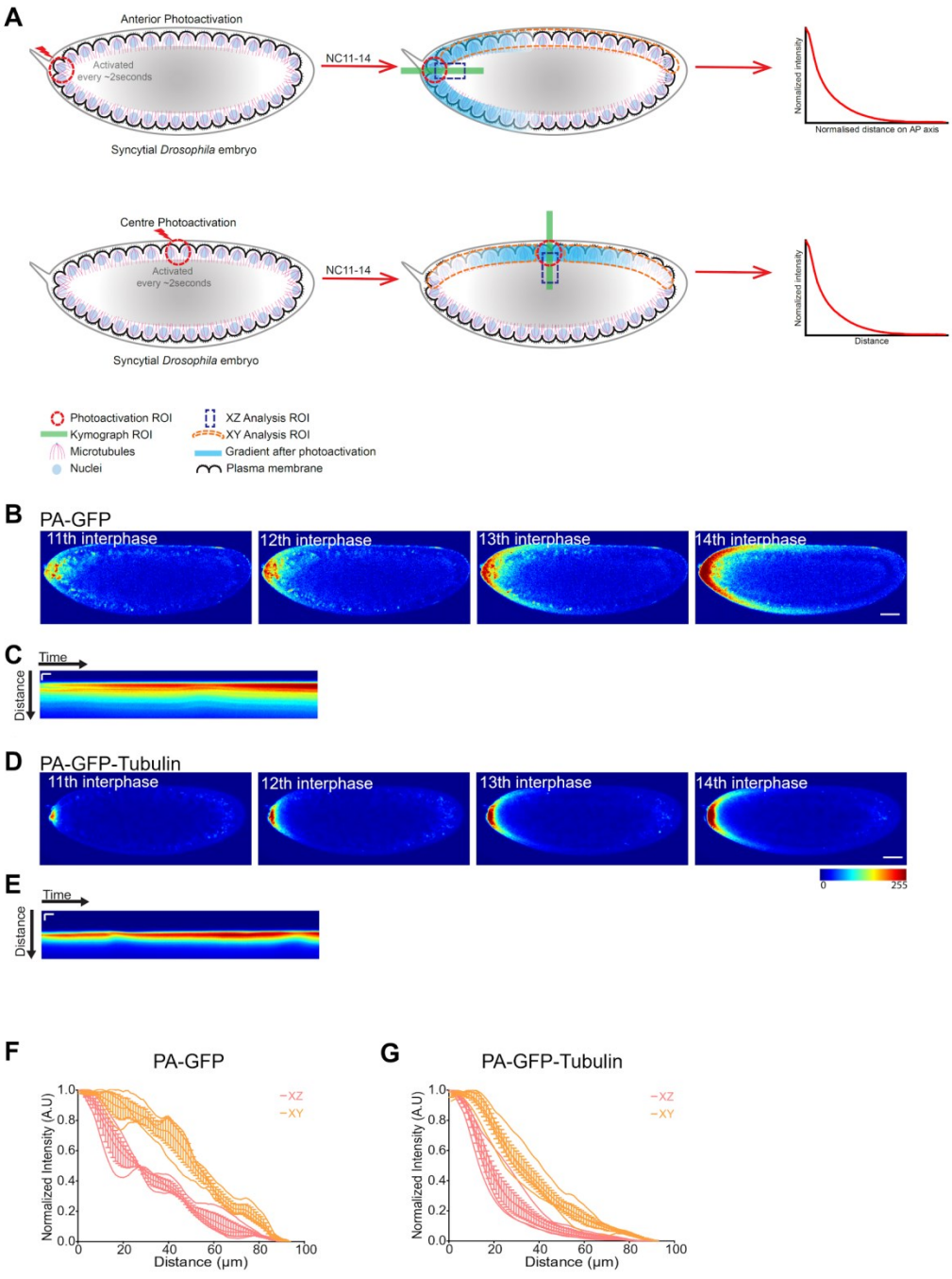

Figure 4.1:Anteriorly photoactivated PA-GFP and PA-GFP-Tubulin produces a cortical gradient

(A). The photoactivation method to create an ectopic source of PA-GFP and PA-GFP-Tubulin. Photoactivation was carried out, continuously with an interval of ~2 seconds, in a fixed area (373μm^2) in the anterior or the center of the syncytial embryo. A kymograph monitoring the increase in signal was drawn at the source (green bar). A cortical region was drawn to estimate the change in intensity in the antero-posterior axis (orange). The exponential function was fit to estimate the length scale of spread for the gradients.

(B-E). Anteriorly photoactivated PA-GFP and PA-GFP-Tubulin forms a gradient. Images for NC11,12,13,14 of embryos from expressing PA-GFP **(B)** or PA-GFP-Tubulin **(D)** are shown after photoactivation at the anterior pole. Kymograph shows increase in cortical fluorescence over time in PA-GFP **(C)** and PA-GFP-Tubulin **(E)** expressing embryo. Scale bars=50μm,60s.

(F-G). PA-GFP and PA-GFP-Tubulin spreads preferentially at the cortex. Graph quantifying the spread of photoactivated protein fluorescence in the antero-posterior XY axis vs depth or XZ direction for PA-GFP **(F)** and PA-GFP-Tubulin **(G)** with a line drawn across either XY or XZ direction from the activated region. The raw data is in a lighter color and the averaged data is in a darker color, error bars represent standard error on means (n=6 from 3 embryos for PA-GFP-Tubulin and PA-GFP each, the PA experiment in 1 embryo gave 2 estimates of spread in the AP direction from the dorsal or ventral side).

The images are shown in a 16 color intensity rainbow where Blue represents the lowest intensity and red represents the highest intensity. Scale bar= 50μm.

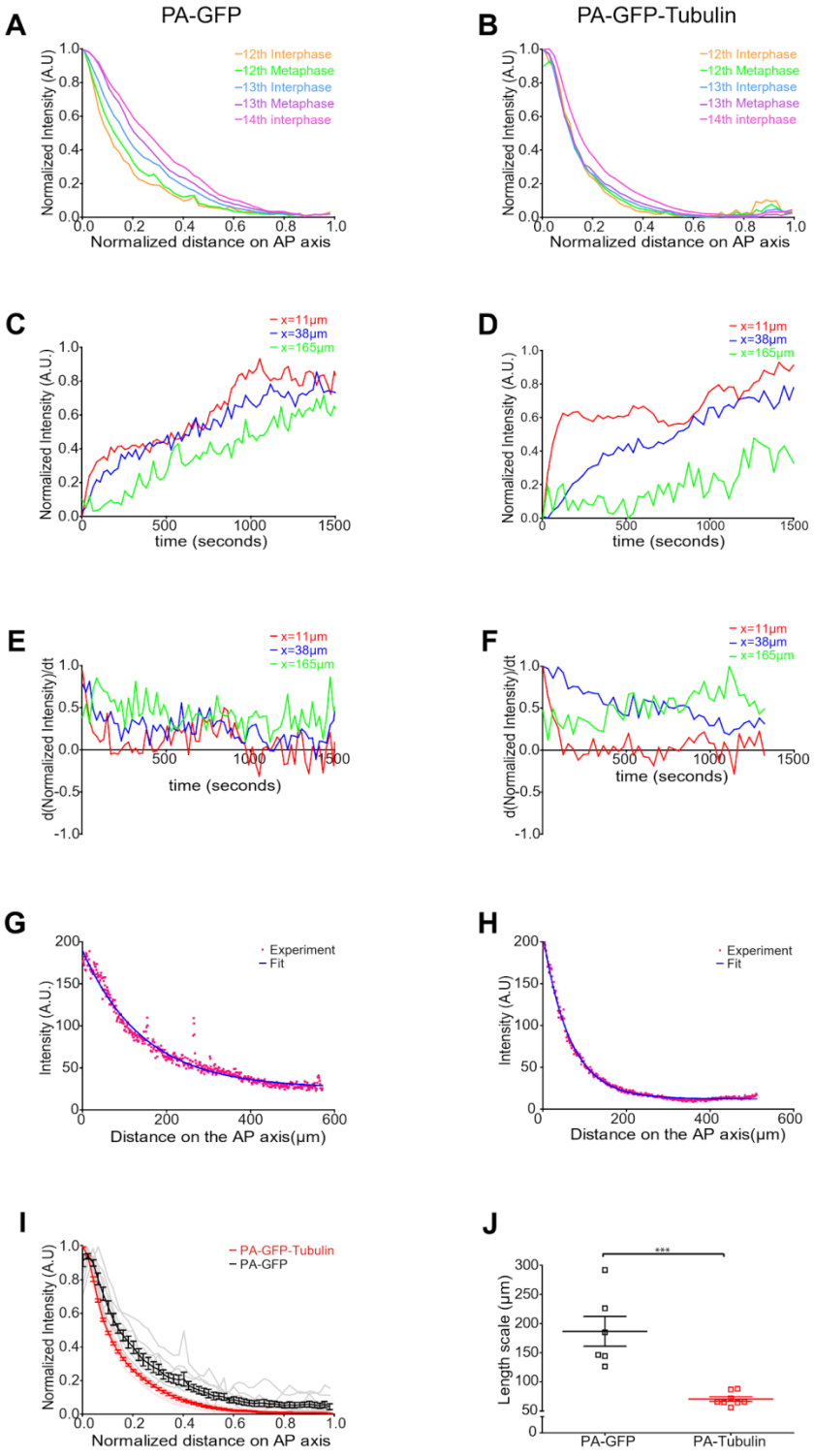

Figure 4.2: Anteriorly photoactivated PA-GFP and PA-GFP-Tubulin shows an exponential spread with PA-GFP-Tubulin being more restricted as compared to PA-GFP

(A-B). Quantification of the photoactivated signal across nuclear cycles. Graph shows intensity for PA-GFP **(A)** and PA-GFP-Tubulin **(B)** for one embryo with a line drawn across the cortical region in the syncytial nuclear cycles. Similar profiles were observed in multiple embryos (n=3 for each).
(C-D). PA-GFP and PA-GFP-Tubulin increases in concentration over time. The graph depicts an increase in PA-GFP **(C)** or PA-GFP-Tubulin **(D)** fluorescence intensity over time as measured at different locations (11, 38, 165µm from the source of photoactivation at the anterior).
(E-F). Graph shows the rate of change in concentration of photoactivated PA-GFP **(E)** and PA-GFP-Tubulin **(F)** to assess if the steady state has reached. Each plot is a derivative of the corresponding plot in C,D.
(G-H). Anteriorly photoactivated PA-GFP and PA-GFP-Tubulin shows an exponential spread. Raw experimental values (red) were fit to an exponential function (blue) for each probe.
(I). Quantification of intensity profile of photoactivated probe measured at the end of the experiment for PA-GFP and PA-GFP-Tubulin. Graph shows raw data in a lighter color and averaged data in a darker color, error bars represent standard error on means (n=3 embryos each for PA-GFP and PA-GFP-Tubulin).
(J). Scatter plot of length scales extracted after fitting an exponential decay function to the intensity profiles seen in I (n=6, 3 i.e 6 length scales extracted from 3 embryos in the AP direction on the dorsal or ventral side for PA-GFP, 8,4 for PA-GFP-Tubulin, Two tailed Mann-Whitney non-parametric test with p value=0.0007).

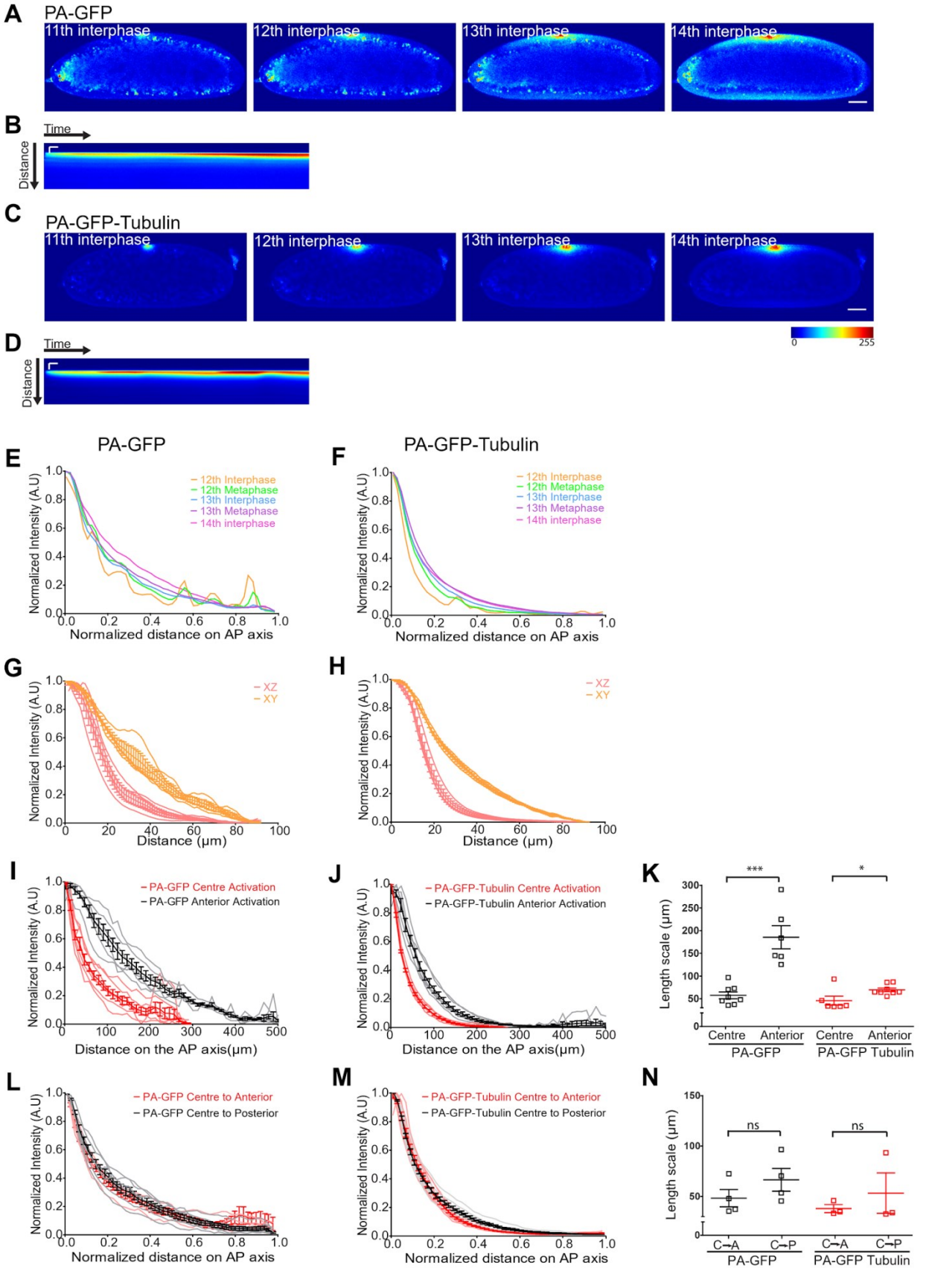
A
PA-GFP
11th interphase
12th interphase
13th interphase
14th interphase
B
Time
Distance
C
PA-GFP-Tubulin
11th interphase
12th interphase
13th interphase
14th interphase
0
255
D
Time
Distance
E
PA-GFP
12th Interphase
12th Metaphase
13th Interphase
13th Metaphase
14th interphase
Normalized Intensity (A.U)
Normalized distance on AP axis
F
PA-GFP-Tubulin
12th Interphase
12th Metaphase
13th Interphase
13th Metaphase
14th interphase
Normalized Intensity (A.U)
Normalized distance on AP axis
G
XZ
XY
Normalized Intensity (A.U)
Distance (µm)
H
XZ
XY
Normalized Intensity (A.U)
Distance (µm)
I
PA-GFP Centre Activation
PA-GFP Anterior Activation
Normalized Intensity (A.U)
Distance on the AP axis(µm)
J
PA-GFP-Tubulin Centre Activation
PA-GFP-Tubulin Anterior Activation
Normalized Intensity (A.U)
Distance on the AP axis(µm)
K
***
*
Length scale (µm)
Centre
Anterior
Centre
Anterior
PA-GFP
PA-GFP Tubulin
L
PA-GFP Centre to Anterior
PA-GFP Centre to Posterior
Normalized Intensity (A.U)
Normalized distance on AP axis
M
PA-GFP-Tubulin Centre to Anterior
PA-GFP-Tubulin Centre to Posterior
Normalized Intensity (A.U)
Normalized distance on AP axis
N
ns
ns
Length scale (µm)
C→A
C→P
C→A
C→P
PA-GFP
PA-GFP Tubulin

Figure 4.3: Photoactivation of the cytoplasmic PA-GFP and PA-GFP-Tubulin in the middle of the *Drosophila* embryo

(A-D). Monitoring spread of center photoactivated PA-GFP and PA-GFP-Tubulin. Images from NC11,12,13,14 expressing PA-GFP **(A)** or PA-GFP-Tubulin **(C)** and photoactivated at the centre of the embryo are shown.Kymograph shows increase in cortical fluorescence with time for PA-GFP **(B)** and PA-GFP-Tubulin **(D)** embryo.Scale bars=50µm, 60s.

(E-F). Quantification of evolution of photoactivated signal in syncytial nuclear cycles. The graph depicts the fluorescence intensity for PA-GFP **(E)** and PA-GFP-Tubulin **(F)** from one embryo for a line drawn from the source along the antero-posterior axis. Similar profiles were observed in multiple embryos (n=6,3 embryos for each).

(G-H). Quantification of photoactivated protein in XY vs XZ direction for PA-GFP **(G)** and PA-GFP-Tubulin **(H)**. Graph shows intensity profile of a line drawn in the XY or XZ direction from the activated region. The raw data is shown in a lighter color and the averaged data is shown in a darker color, error bars represent standard error on means (n=6,3 for PA-GFP-Tubulin and PA-GFP each).

(I-J). Graphs comparing the intensity profile obtained upon photoactivation at the anterior pole versus the centre of the embryo for PA-GFP **(I)** and PA-GFP-Tubulin **(J)** (n=3 embryos for PA-GFP and PA-GFP-Tubulin each).

(K). Scatter plot of the length scales extracted after fitting an exponential decay function to the intensity profiles seen in I,J. The values of length scales for PA-GFP and PA-GFP-Tubulin for anterior photoactivation are repeated from Figure 3J. (n=8,4 for PA-GFP center activation, 6,3 for PA-GFP activated anteriorly, 6,3 for PA-GFP-Tubulin center activation and 8,4 for PA-GFP-Tubulin anterior activation. Two tailed Mann-Whitney non-parametric test with p value=0.0007 for PA-GFP values and 0.04 for PA-GFP-Tubulin values).

(L-M). Graphs comparing the intensity profiles obtained upon photoactivation at the centre of the embryo for analysis of directionality of spread. Fluorescence intensity is obtained from a line drawn from the centre activated region towards anterior or posterior pole for PA-GFP **(I)** and PA-GFP-Tubulin **(J)**. The raw data is shown in a lighter color and the averaged data is shown in a darker color, error bars represent standard error on means (n=3 embryos for PA-GFP-Tubulin and PA-GFP each).

(N). Scatter plot of the length scales extracted after fitting an exponential decay function to the intensity profiles seen in L,M. (n=4,4 for PA-GFP center activation, center to anterior subset from K, 4,4 for PA-GFP center activation, centre to posterior subset from K, 3,3 for PA-GFP-Tubulin center activation, centre to anterior subset from K and 3,3 for PA-GFP-Tubulin center activation, centre to posterior subset from K. Two tailed Mann-Whitney non-parametric test with p value=0.34 for PA-GFP values and 1 for PA-GFP-Tubulin values).

The images are shown in a 16 color intensity rainbow where Blue represents the lowest intensity and red represents the highest intensity. Scale bar= 50µm.

4.3.4 Photoactivation of PA-GFP-Tubulin during pre-blastoderm stage/syncytial blastoderm stage leads to similar length scales of spread

To evaluate whether the presence of syncytial pseudo cells/energids has any effect on the spread of the gradient, we performed similar activation of PA-GFP-Tubulin during pre-blastoderm stages of the embryo. In these stages, nuclei are still deep in the yolk and the cytoplasm is sparsely present near the embryo cortex. The presence of yolk

granules can be seen much closer to the embryo cortex which gradually compresses and becomes compact towards the embryo centre as the syncytial cycles progress. A further discussion on this is available in Chapter 1 and 3.

We first tried activation of PA-GFP in these early pre-blastoderm stages, but due to the presence of yolk which confounded the signal and the low level of activation of PA-GFP, we were not able to fit the activation profiles well, leading to unreliable length scale values (not shown). When PA-GFP-Tubulin was activated in these pre-blastoderm stages at the anterior and centre (Figure 4.4A), we found no difference in the length scales between the corresponding pre-blastoderm and syncytium experiments (Figure 4.4B). We also tried activation at the posterior pole (Figure 4.4A) and found no difference in the length scales estimates between the anterior and posterior pole activations (Figure 4.4B). Further, this similarity sustains in the pre-blastoderm and syncytial stages as well for posterior activation (Figure 4.4B).

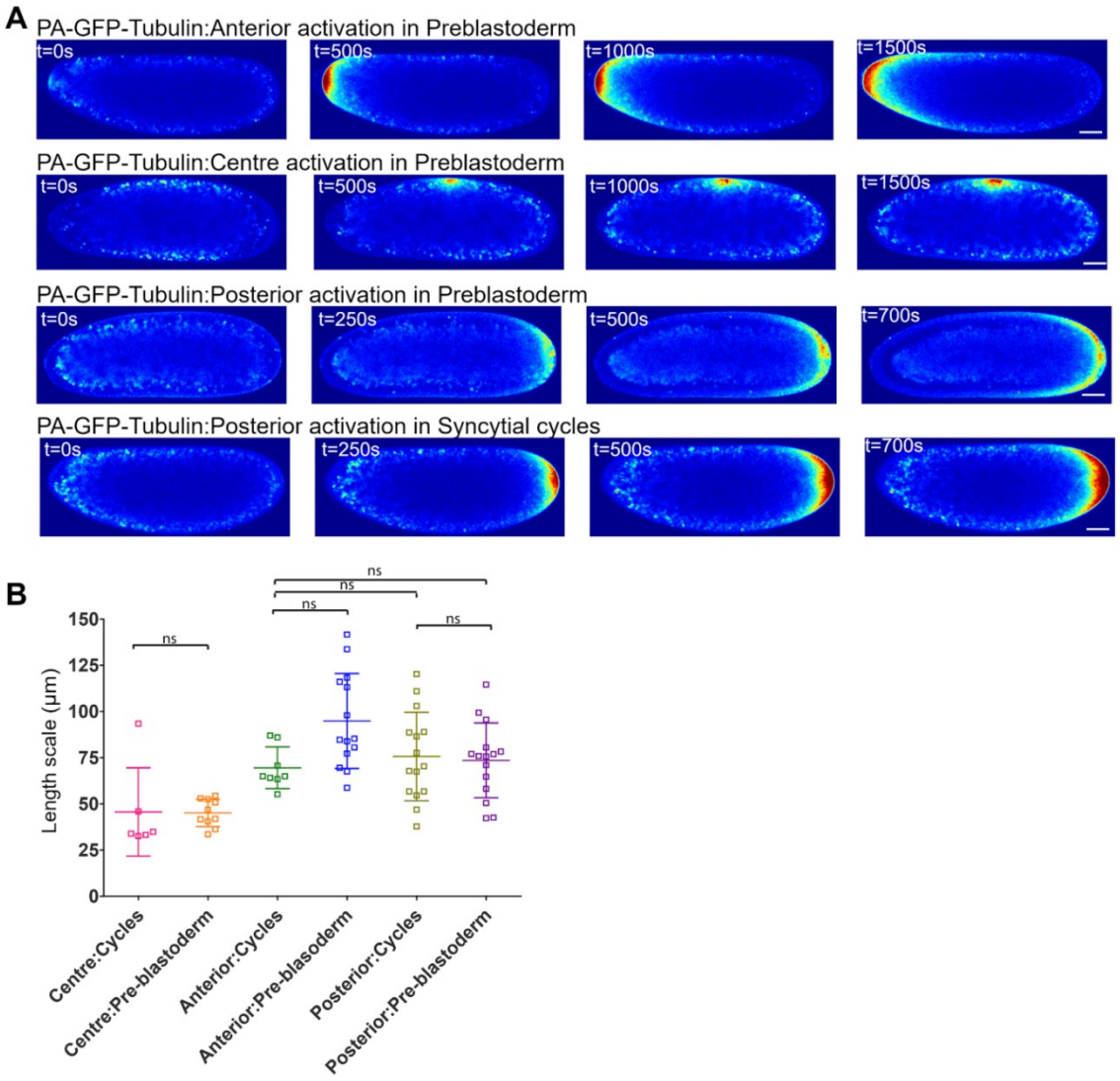

Figure 4.4: Photoactivation of the PA-GFP-Tubulin in the anterior, middle and posterior of the *Drosophila* embryo in pre-blastoderm stages and syncytial cycles.

(A). Monitoring spread of center photoactivated PA-GFP-Tubulin. Images extracted from time-lapse movies of embryos PA-GFP-Tubulin in pre-blastoderm (anterior activation)**,** pre-blastoderm (centre activation)**,**pre-blastoderm (posterior activation) and syncytial cycles (posterior activation). Scale bar=50µm.

(B). Scatter plot of the length scales extracted after fitting an exponential decay function to the intensity profiles. The values of length scales for PA-GFP-Tubulin for anterior and centre photoactivation are repeated. (6,3 for centre activation (syncytial cycles), 10,5 for center activation (pre-blastoderm stages), 8,4 for anterior activation (syncytial cycles),14,7 for anterior activation (pre-blastoderm stages), 15,8 for posterior activation (syncytial cycles),15,8 for posterior activation (pre-blastoderm stages). (One-way ANOVA (F (6) = 8.840, p<0.0001), Tukey's multiple comparison test)). The images are shown in a 16 color intensity rainbow where Blue represents the lowest intensity and red represents the highest intensity. Scale bar= 50µm.

4.3.5 In embryos containing an overexpression of RhoGEF2 which leads to a loss of pseudo cleavage furrows, length scale of the anteriorly photoactivated PA-GFP-Tubulin gradient increases

The gradients produced by PA-GFP and PA-GFP-Tubulin provided a framework to test the role of syncytial cytoarchitecture in regulating their diffusion. Each cortical nucleus in the syncytial blastoderm embryo of *Drosophila* contains a small ingression of the plasma membrane around it. Astral microtubules support ectopic furrows (Barmchi et al., 2005; Cao et al., 2008; Crest et al., 2012). The plasma membrane furrows ingress deeper in metaphase to form pseudocleavage furrows (Schmidt and Grosshans, 2018). To test the role of furrows in regulation of gradient formation across the syncytial nucleo-cytoplasmic domains, we performed photoactivation experiments in embryos defective in furrow formation. RhoGEF2 is a Rho-GTP exchange factor specifically needed for the formation of furrows in the syncytial embryo (Barmchi et al., 2005; Cao et al., 2008; Crest et al., 2012). Depletion of RhoGEF2 leads to shortened furrows and increase in RhoGEF2 is likely to increase active Myosin II and abolish furrow formation (Sherlekar and Rikhy, 2016; Zhang et al., 2018). We overexpressed RhoGEF2 by crossing flies containing *mat*-Gal4 and UASp-RhoGEF2. Embryos overexpressing RhoGEF2 showed short or missing furrows in metaphase (Figure 4.5A). The metaphase spindles did not show a significant change in these embryos as compared to controls (Figure 4.5A).

Next, we generated embryos expressing PA-GFP or PA-GFP-Tubulin along with RhoGEF2 overexpression. We performed continuous photoactivation at the anterior pole in a fixed area and followed the resultant gradient across time (Figure 4.5B,D Movie Mov4.S7,8). We found that similar to the control embryos ((Figure 4.1A)), the gradients evolved over time (Figure 4.5B-G). Further, in spite of major contractions in the embryo yolk (Movie Mov4.S7,S8), the activated fluorescent molecules remained near the cortex and did not mix with the underlying inner yolk region of the embryo (Figure 4.5H,I). This was also evident from the kymographs which showed undulations in the cortical layer of fluorescence, yet maintaining a separation from the embryo's inner yolk region (Figure 4.5C,E). The PA-GFP gradients did not change in the embryos

over-expressing RhoGEF2 (Figure 4.5J). The PA-GFP-Tubulin gradient however changed significantly (Figure 4.5K) when compared to their respective gradients in control embryos (Figure 4.1). The length scales were extracted on fitting an exponential function to the concentration profile obtained. It was found that PA-GFP-Tubulin gradient spread to a greater extent in embryos over expressing RhoGEF2 (Figure 4.5L). It is interesting to note that the length scale of PA-GFP-Tubulin in mutant embryos increased from its control value and became similar to PA-GFP. RhoGEF2 overexpression led to loss of plasma membrane furrows and loss of restriction of PA -

GFP-Tubulin gradient in the syncytial *Drosophila* embryo.

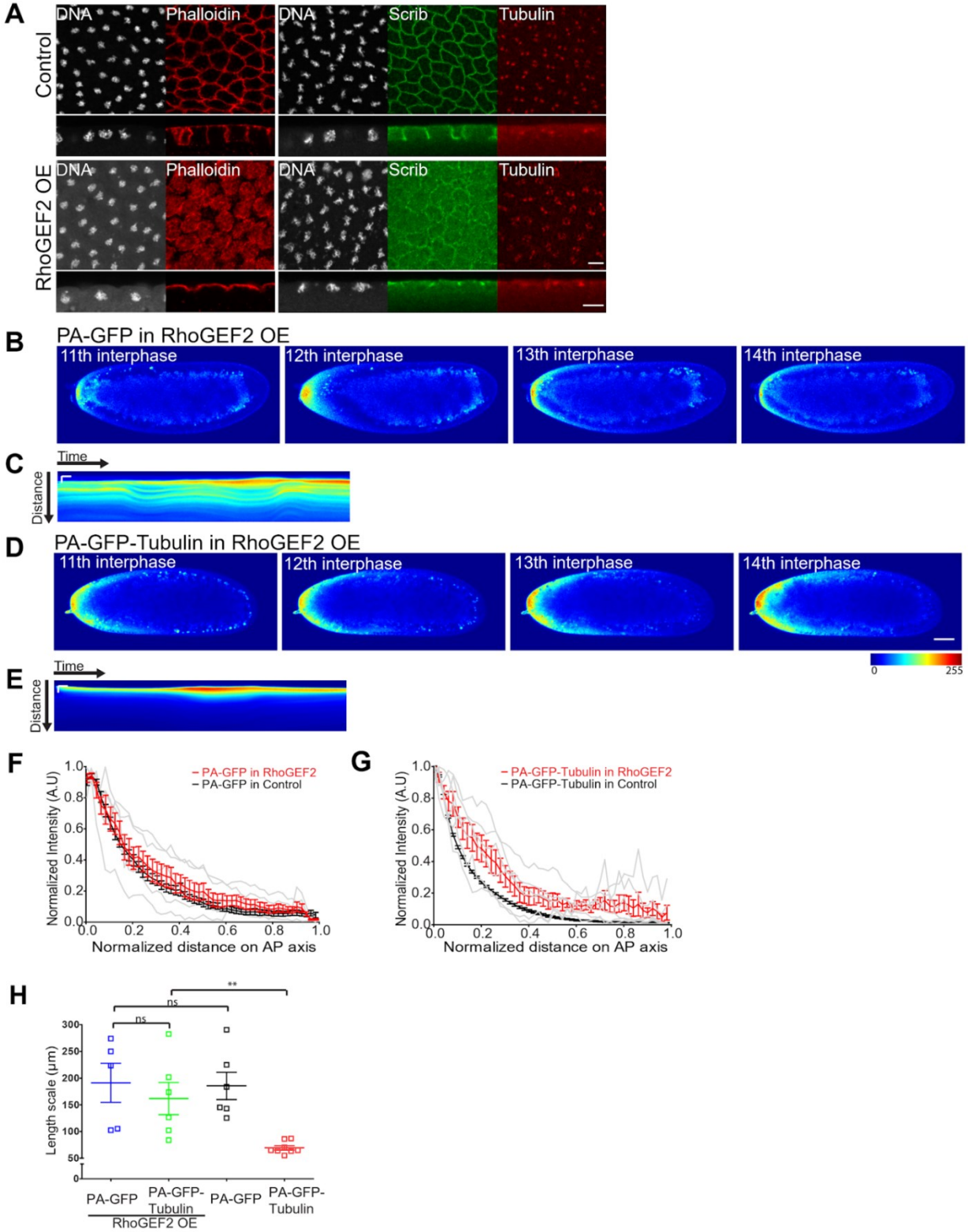

Figure 4.5:PA-GFP-Tubulin spreads to a greater extent in embryos containing RhoGEF2 overexpression

(A). Embryos overexpressing RhoGEF2 show loss of metaphase furrows: Surface and sagittal views of fixed control or RhoGEF2 overexpressing embryos, stained with Tubulin (Red), Scribbled (Green) and DNA (Grey), show loss of furrows and no significant effect on metaphase spindles (100%, n=30 embryos). Scale bar=10μm.
(B-E). Images from syncytial cycles of an embryo co-expressing RhoGEF2 along with PA-GFP **(B)** or PA-GFP-Tubulin**(D)** which has been photoactivated at the anterior pole.Kymograph for PA-GFP **(C)** and PA-GFP-Tubulin **(E)** shows increase in cortical fluorescence with time while sometimes changing the extent to which the fluorescence is confined. Scale bars=50μm, 60s.
(F-G). Quantification of intensity profile of photoactivated probe as measured at the end of the experiment for PA-GFP **(F)** and PA-GFP-Tubulin **(G)** in embryos overexpressing RhoGEF2. The raw data is shown in a lighter color and the averaged data is shown in a darker color, error bars represent standard error on means (n=3 embryos for PA-GFP-Tubulin and PA-GFP each). The graph for photoactivation of PA-GFP and PA-GFP-Tubulin in control embryos is the same as that shown in Figure 3I and is repeated here for comparison.
(H). Scatter plot of the length scales extracted after fitting an exponential decay function to the intensity profiles seen in F and G. The values of length scales for PA-GFP and PA-GFP-Tubulin for anterior photoactivation in control embryos are repeated from Figure 3J. (n=6,3 for PA-GFP in RhoGEF2-OE, 6,3 for PA-GFP-Tubulin in RhoGEF2-OE. Kruskal-Wallis nonparametric test of variance p value=0.0064, followed by Dunn's posttest at 95 percent confidence interval).

4.3.6 Anteriorly photoactivated PA-GFP-Tubulin gradient length scale increases in EB1 RNA*i* expressing embryos

Microtubules emanate from the centrosome at the apical side and spread vertically downwards in the syncytial blastoderm embryo (Kellogg et al., 1988; Sullivan and Theurkauf, 1995). EB1 is present at the growing end of microtubules and its depletion is likely to disrupt the microtubule architecture (Rogers et al., 2002). We depleted embryos of EB1 by combining *eb1* RNAi to *mat*-Gal4 to disrupt microtubule organization. The microtubule staining was reduced in embryos expressing *eb1* RNAi expressing embryos. Also the plasma membrane levels for Scribbled were lowered in interphase (Figure 4.6A) and metaphase (Figure 4.7A). Upon live imaging of *eb1* RNAi containing embryos co-expressing mcherry-Tubulin, we found mis patterned nuclei, free tubulin clusters in Interphase and aberrant or joint/multipolar spindles in metaphase (Figure 4.6B) .

We combined the *eb1* RNAi with flies expressing PA-GFP or PA-GFP-Tubulin and performed anterior photoactivation experiments in a fixed area (Figure 4.7B,D, Movie S9,10). We found that similar to the control embryos (Figure 4.1), the gradient evolved over time (Figure 4.7B-G). Similar to RhoGEF2 overexpression embryos, in

spite of major contractions in the embryo yolk, the activated fluorescent molecules remained near the cortex (Figure 4.7C,E) and did not mix with the underlying inner yolk region of the embryo. Length scales were extracted by fitting these gradients (Figure 4.7F,G) to an exponential function. We observed that the PA-GFP gradient did not change, while PA-GFP-Tubulin gradient in mutant embryos changed significantly (Figure 4.7H). The length scale analysis showed that PA-GFP-Tubulin in *eb1* mutant embryos was similar to PA-GFP. In summary, *eb1* mutant embryos showed a disrupted microtubule architecture and showed a loss of restriction of PA-GFP-Tubulin gradient in the syncytial *Drosophila* embryo.

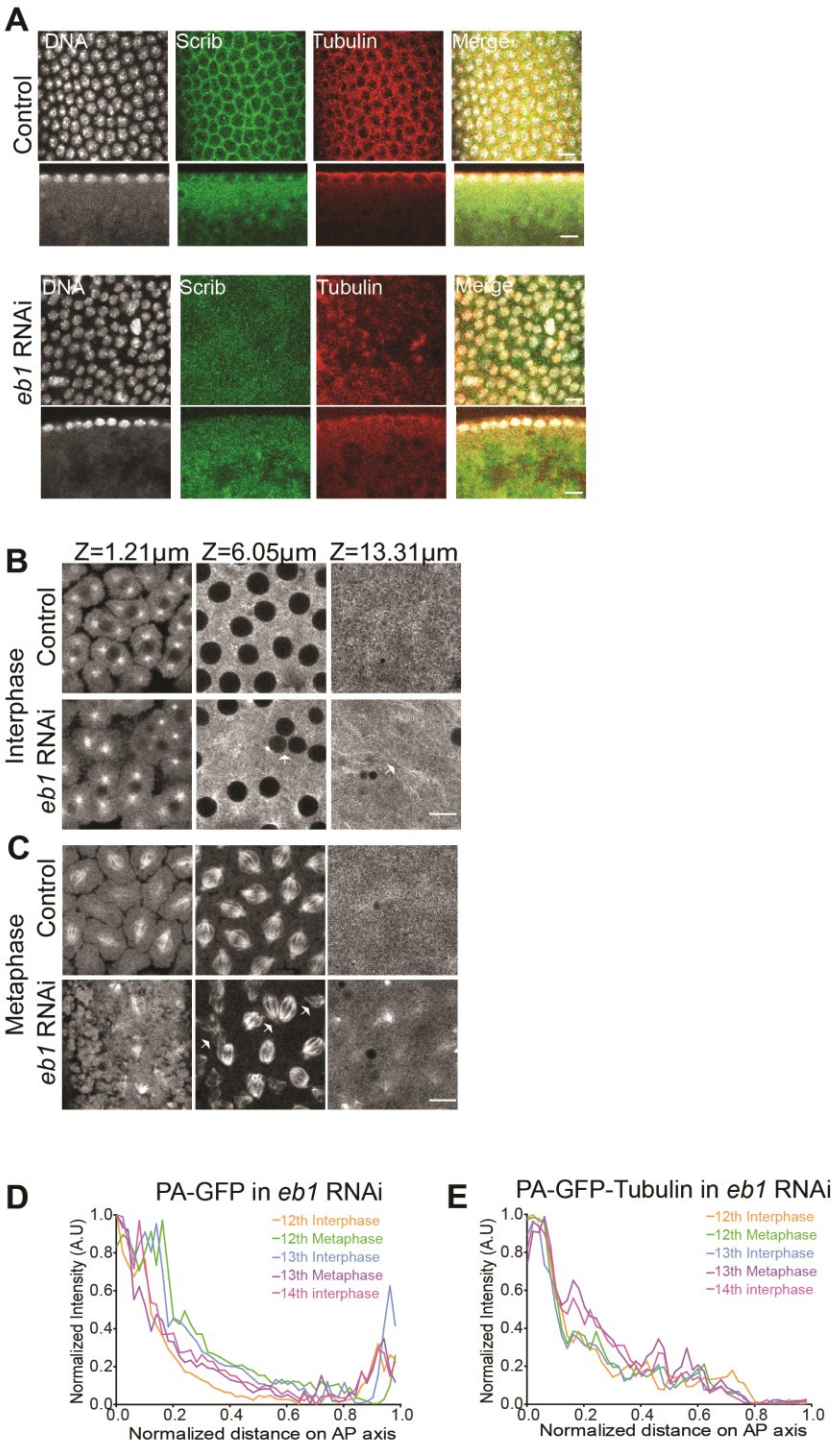

Figure 4.6: Analysis of photoactivation and morphological defects in spindles in *eb1* RNAi expressing embryos

(A).*eb1* RNAi expressing embryos show perturbed tubulin architecture: Surface and sagittal views of fixed control or *eb1* RNAi embryos in interphase, stained with Tubulin (Red), Scribbled (Green) and DNA (Grey), show lowered interphase tubulin and scrib staining (100%, n=25 embryos). Scale bar=10µm.

(B). Interphase images are shown from different Z-stacks of embryos expressing maternally expressing mCherry-Tubulin in a control or an *eb1* RNAi background (similar trends were observed for n=3 movies). Regular spacing of nuclei is disturbed and fused nuclei can be seen. Long tubulin fibres are also observed below the nuclear plane. Scale bar=10μm.
(C). Metaphase images are shown from different Z-stacks of embryos expressing maternally expressing mCherry-Tubulin in a control or an *eb1* RNAi background (similar trends were observed for n=3 movies). Weakly marked spindles (left of the image) and tripolar spindles (right of the image) can be observed in this stage. Scale bar=10μm.
(D-E). Quantification of evolution of photoactivated signal across nuclear cycles in *eb1* RNAi embryos. Graph depicts intensity change in PA-GFP **(E)** and PA-GFP-Tubulin **(F)** for one embryo. Similar profiles were observed in multiple embryos (n=3 for each).

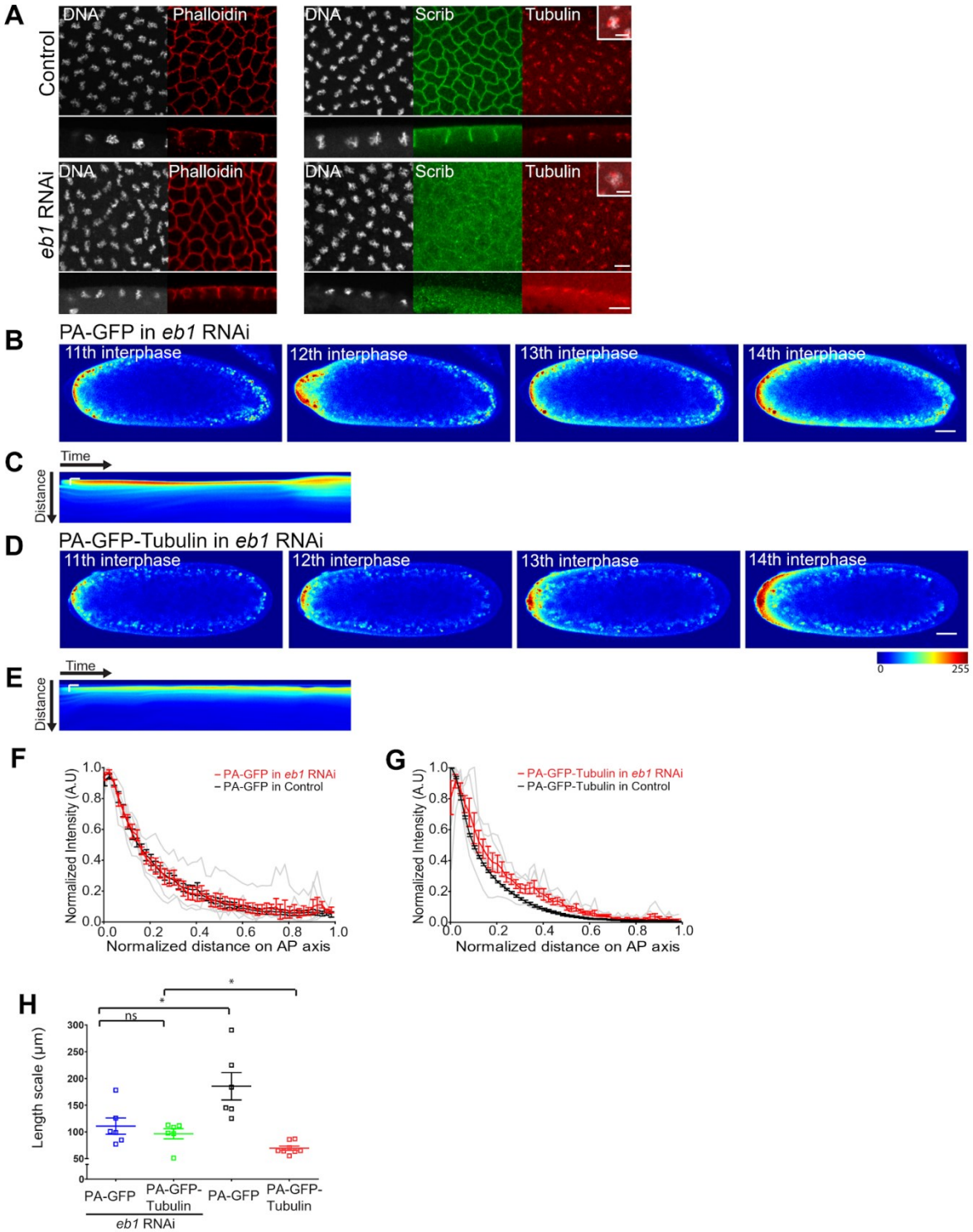

Figure 4.7:PA-GFP-Tubulin spreads to a greater extent in *eb1* mutant embryos

(A).*eb1* RNAi expressing embryos show perturbed tubulin architecture: Surface and sagittal views of fixed control or eb1 RNAi embryos, stained with Tubulin (Red), Scribbled (Green) and DNA (Grey), show perturbed spindles in metaphase (100%, n=25 embryos). Zoomed inset of spindles show loose organization in *eb1* RNAi expressing

embryos. Scale bar=10μm, inset scale bar=5μm.

(B-E).Images from syncytial cycles of an *eb1* RNAi expressing embryo co-expressing PA-GFP **(B)** or PA-GFP-Tubulin **(D)** with photoactivation at the anterior pole. Kymograph for PA-GFP (B) and PA-GFP-Tubulin **(E)** shows increase in cortical fluorescence across time while sometimes changing the extent to which the fluorescence is confined. Scale bars=50μm, 60s.

(F-G). Quantification of intensity profile of photoactivated probe as measured at the end of the experiment for PA-GFP **(F)** and PA-GFP-Tubulin **(G)** in *eb1* RNAi embryos. The raw data is shown in a lighter color and the averaged data is shown in a darker color, error bars represent standard error on means (n=3 embryos for PA-GFP-Tubulin and PA-GFP each). The graph for photoactivation of PA-GFP and PA-GFP-Tubulin in control embryos is the same as that shown in Figure 4.2I and is repeated here for comparison.

(H). Scatter plot of length scales extracted after fitting an exponential decay function to the intensity profiles seen in **(F)** and **(G)**. The values of length scales for PA-GFP and PA-GFP-Tubulin for anterior photoactivation in control embryos are repeated from Figure 4.2J. (n=6,3 embryos for PA-GFP in eb1 RNAi, 6,3 for PA-GFP-Tubulin in eb1 RNAi.Kruskal-Wallis nonparametric test of variance p-value=0.0008, followed by Dunn's post test at 95 percent confidence interval).

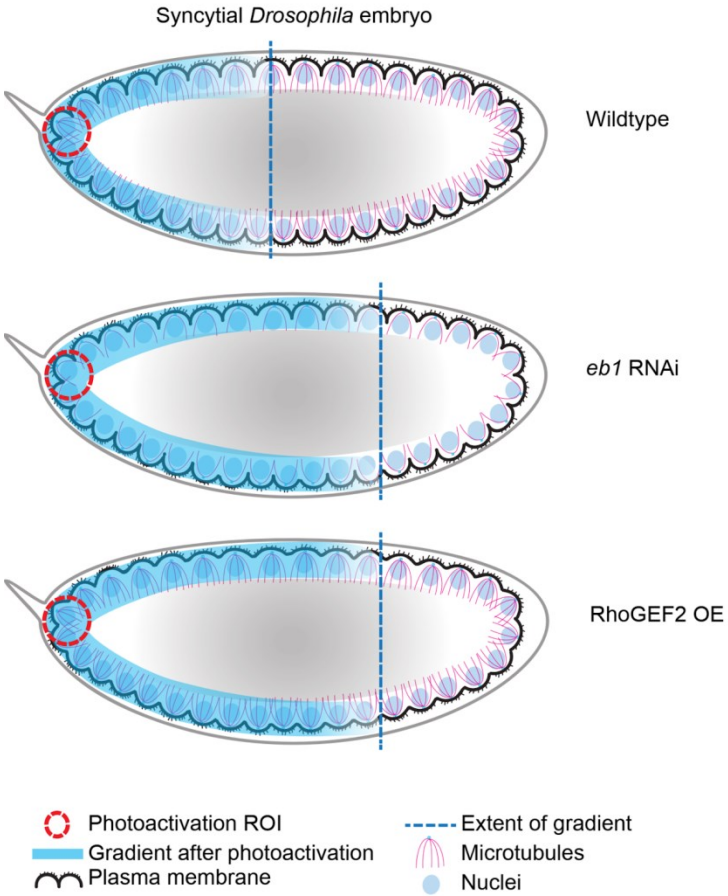

Figure 4.8: Model for regulation of spread of molecules across the nucleo-cytoplasmic domains in the syncytial *Drosophila* embryo

Photoactivated PA-GFP-Tubulin and PA-GFP spread cortically in the syncytial blastoderm embryo. RhoGEF2 overexpression caused loss of plasma membrane furrows and increased spread of the anteriorly induced PA-GFP-Tubulin. EB1 loss caused perturbation of the microtubule cytoskeleton and increased spread of the anteriorly induced PA-GFP-Tubulin.

4.4 Discussion

In this chapter, we have examined the distribution and diffusion of cytoplasmic components of the *Drosophila* syncytial blastoderm embryo. We have used photoactivation of cytoplasmic PA-GFP to analyze its distribution and diffusion across nucleo-cytoplasmic domains of the syncytial *Drosophila* embryo and further compared it to PA-GFP-Tubulin, which is present in the cytoplasm and is also incorporated in microtubules. We find that the cytoplasmic components have an increased concentration at the cortex near the nucleo-cytoplasmic domains. Photoactivation of these components shows diffusion to a greater distance in the antero-posterior axis in the cortex as compared to the depth of the embryo. Also photoactivated cytoplasmic components diffuse less when generated at the center of the embryo as compared to the anterior, a difference which exists in the pre-blastoderm embryo as well. Posterior and anterior activations lead to similar length scales for PA-GFP-Tubulin. Diffusion is constrained by interaction with the cyto-architecture components of the syncytial blastoderm embryo (Figure 4.8).

Photoactivation as a method to study regional differences in kinetics of gradient formation in the syncytial *Drosophila* embryo

The use of photoactivatable GFP molecules allows for the creation of localized ectopic gradients and enables us to follow their evolution in real time across the syncytial nuclear cycles. Photoactivation has been used previously to analyze the spread of morphogen gradients in similar contexts. Photoactivation of Dorsal-PA-GFP allowed an analysis of the extent of its spread in the dorsal versus ventral side of the syncytial blastoderm embryo. Sequestration of Dorsal by signaling components and nuclear capture on the ventral side gave a more constrained gradient as compared to the dorsal

side of the embryo (Carrell et al., 2017). In our study we used two photoactivatable proteins which are incorporated in all nucleo-cytoplasmic domains. This allows us to quantify the differences in their diffusion due to inherent differences in their association with cyto-architecture of the embryo. We found that PA-GFP and PA-GFP-Tubulin had smaller length scales when activated at the center as compared to the anterior of the syncytial blastoderm embryo. We expected that the restricted diffusion at the center of the embryo could be a result of a difference in relative crowding of nucleo-cytoplasmic domains in these two regions (Blankenship and Wieschaus, 2001; Rupprecht et al., 2017). An increase in the density of nucleocytoplasmic domains in the center could lead to greater sequestration of cytoplasmic components in general, leading to a smaller length scale. However, upon activation in the pre-blastoderm stages where no such difference in nuclear crowding is reported, we found a similar difference in length scales. Is this difference due to shape difference between the embryo centre and anterior? This may be so as a change in the embryo shape leading to a change in gradient profile has been reported for Bicoid. The protein dynamics is predicted to encounter difference in geometric shape at the conical anterior region as compared with the flatter central region of the embryo (He et al., 2010). Performing similar activation experiments in rounder embryos using *fat2* mutants (Rupprecht et al., 2017) is an approach which can help resolve this. Alternatively, though unlikely, but this could also come about due to differences in protein degradation or sequestration machinery between these two regions.

While it is true the length scales observed during pre-blastoderm and syncytial cycles are similar, which suggests that furrows do not have a significant role in restricting diffusion, the changes in length scales are an emergent property of the mutant defects. We observe that length scale changes in mutants can also be due to abnormal contractions, which take place due to change in contractility or timing of nuclear division within the embryo. Also changes in yolk compaction, which has been observed in *eb1* RNAi may be a source of restriction of diffusion.

There is no difference in the gradient spread when activation was performed during pre-blastoderm versus syncytial cycles, though these two different stages are starkly different in the organization of their cyto-architecture. This suggests that the

architecture doesn't contribute to the formation of the gradient, or that though differently organized, the pre blastoderm/syncytial architecture essentially leads to similar restriction of diffusion. The former seems less likely, as PA-GFP-Tubulin activation in RhoGEF2 overexpressing embryos, which have shorter furrows, shows an increase in gradient spread, suggesting that architecture restricts diffusion in the syncytial stages. What components can contribute to restricting diffusion in pre-blastoderm? ER and Golgi are known to form dense networks during pre-blastoderm stages (Frescas et al., 2006) and presence of yolk platelets near the cortex, may cause restricted diffusion. It would be interesting to check the gradient properties in pre-blastoderm stages in mutants which perturb these components. It can even be that our results which show increase in gradient spread in embryos with *eb1* RNAi (Figure 4.7G,H), are a combination of microtubule disruption and yolk compaction defects.

Non-membrane bound organization of cytoplasm in cells

The cytoplasm of majority of living cells can be described as an inhomogeneous, multi-phasic medium. Images of different components when drawn to scale (Goodsell, 2013) clearly convey the fact that the cytoplasm is quite contrary to the earlier picture of a freely flowing medium. The cytoplasm can be likened to a complex medium comprising of physical constraints and constraints due to binding and crowding. Fluorescent dextran of various sizes when injected into cells partitions based on their size (Luby-Phelps, 2000). This further corroborates the fact that the space available for various cytoplasmic components is constrained depending on their size. The metabolic state can also change the properties of the cytoplasm in the bacterial cell into either a glass-like or fluid-like state (Parry et al., 2014b). Cytoplasmic distribution can change depending on the ability and strength of a cytoplasmic molecule to bind to other components. A modelling based study showed that binding to negative end directed dynein motors on the mitotic spindle was sufficient to partition the cytoplasm into two halves even without the presence of any membrane bound compartments (Chen et al., 2012).

Our finding that PA-GFP-Tubulin is more restricted in its spread as compared to PA-GFP suggests that cytoplasmic components having multiple interactors are more

confined in their diffusion. For the syncytium, this property is beneficial, as components produced from a syncytial nucleus tend to remain near their parent nucleus, with no clear boundaries being present in the shared cytoplasm. This observation suggests that different components in a cell could be restricted by distinct mechanisms, some binding to microtubules, some to actin or some being sequestered in the nuclei or other organelles ultimately resulting in restricting their action in space and time. The restricted diffusion of PA-GFP-Tubulin in our study was lost on abrogation of the metaphase furrows and microtubule cytoskeleton in embryos over-expressing RhoGEF2 and *eb1* RNAi, which highlights how binding and sequestration were responsible for PA-GFP-Tubulin restriction. Loss of plasma membrane furrows could also lead to disorganization of astral microtubules (Cao et al., 2010; Crest et al., 2012) in the periphery thereby increasing the effective diffusion of PA-GFP-Tubulin.

Implications on morphogen diffusion

The observation about the presence of two separate phases of cortical cytoplasm and embryo yolk provides an interesting perspective to our current understanding of morphogen gradients in the early embryo, namely, Bicoid, Dorsal and Torso. The Bicoid gradient has been extensively studied using the framework of the synthesis, diffusion and degradation (SDD) (Durrieu et al., 2018; Gregor et al., 2007; Grimm et al., 2010) and related models. However, a complete theoretical understanding of the mechanisms underlying the formation of the Bicoid gradient is still lacking. Our finding implicates a restriction of the effective volume in which Bicoid gradient develops and matures. It also raises the possibility that various cytoarchitectural components could impinge on its formation. For example, perturbations in furrows or cytoskeletal structures can change the effective concentration of morphogens in the cortical cytoplasm, leading to changes in the morphogen profiles, specifically for Bicoid.

There have also been various studies, implicating the size and shape of the mRNA source in Bicoid gradient formation (Fahmy et al., 2014; Little et al., 2011; Spirov et al., 2009). Photoactivation allows creation of different sized sources which can produce PA-GFP/PA-GFP-Tubulin or morphogen gradients at different rates and

provides an opportunity to study the effect of the source on the gradient shape and dynamics.

The observation of distinct gradient length scales of PA-GFP-Tubulin versus PA-GFP points to another facet of morphogen gradient formation, namely decrease in the diffusivity of morphogens based on their interactions. FGF gradient is known to interact with Heparan sulfate proteoglycans which changes the effective diffusivity of the morphogen. The removal of these proteoglycans leads to an increase in the morphogen spread (Balasubramanian and Zhang, 2016). We can interpret the difference between the PA-GFP and PA-GFP-Tubulin profiles as being a consequence of increased binding of tubulin to the microtubule architecture. This leads to increase in its residence time by sequestration and thus a lower effective diffusion and consequently, a smaller length scale. It would be interesting to analyse the effect of removal of binding interactions for well-studied morphogen like Bicoid. It is notable that Dorsal gradient is known to be modulated depending on the presence or absence of a dimerizing GFP (Carrell et al., 2017).

Finally, our observation of difference in length scales between anterior versus centre photoactivation suggests a difference in cyto-architectural properties for different regions of the embryo. Our studies necessitate a systematic analysis of the impact of local architectural properties in the formation and maintenance of morphogen gradients.

4.5 Supplementary Movies

Mov4.S1: Cytoplasmic GFP: GFP expressed under the *ubi* promoter is imaged across the syncytial division cycles. Note that GFP enters the nuclei in interphase.
Mov4.S2: mCherry-Tubulin: mCherry-Tubulin expressed with *mat*-Gal4 is imaged in the syncytial division cycles. Note mCherry-Tubulin incorporation into centrosome, spindle and cortical microtubules.
Mov4.S3: PA-GFP anterior photoactivation: Region of interest at the anterior is photoactivated to create a source of PA-GFP. Note that PA-GFP enters the nuclei in interphase.

Mov4.S4: PA-GFP-Tubulin anterior photoactivation: Region of interest at the anterior is photoactivated to create a source of PA-GFP-Tubulin. Note PA-GFP-Tubulin incorporation into centrosome, spindle and cortical microtubules.
Mov4.S5: PA-GFP middle photoactivation: Region of interest in the middle of the embryo is photoactivated to create a source of PA-GFP.
Mov4.S6: PA-GFP-Tubulin middle photoactivation: Region of interest in the middle of the embryo is photoactivated to create a source of PA-GFP-Tubulin.
Mov4.S7: PA-GFP anterior photoactivation in RhoGEF2-OE embryos: Region of interest at the anterior is photoactivated to create a source of PA-GFP in RhoGEF2-OE embryos.
Mov4.S8: PA-GFP-Tubulin anterior photoactivation in RhoGEF2 mutants: Region of interest at the anterior is photoactivated to create a source of PA-GFP-Tubulin in RhoGEF2-OE embryos.
Mov4.S9: PA-GFP anterior photoactivation in *eb1* mutant embryos: Region of interest at the anterior is photoactivated to create a source of PA-GFP in *eb1* RNAi expressing embryos
Mov4.S10: PA-GFP-Tubulin anterior photoactivation in EB1 mutants: Region of interest at the anterior is photoactivated to create a source of PA-GFP-Tubulin in *eb1* RNAi expressing embryos. Note the undulations caused by yolk contractions and that the cytoplasm remains peripheral, without mixing with the embryo yolk region.
All movies are in shown in 16 color intensity rainbow scale where Blue represents the lowest intensity and red represents the highest intensity. Scale bar=10μm or 50μm as mentioned.

Chapter 5: Estimation of the role of molecular size and interaction with cyto-architecture in formation of antero-posterior gradient

Chapter 5 summary: *In this chapter, we study cytoplasmic compartmentalization by locally tethering mRNA of fluorescent probes and thereby create local protein sources of diffusion. This allows us to study how by varying molecular size or binding interactions changes the extent of spread of these molecules.*

5.1 Introduction

We introduced morphogen gradients as a way to study cytoplasmic compartmentalization and other cytoplasmic properties in the introduction (Chapter 1). In this chapter, we will focus on the AP morphogen of the embryo:Bicoid.
There are various components that can influence how any morphogen gradient forms. Morphogen gradient formation can involve hindered diffusion, contributed by tortuosity mediated and/or binding mediated hinderance (Müller et al., 2013). Tortuosity mediated hindered diffusion increases the geometric path taken by diffusing molecules and thus changing its effective diffusion, while in binding-mediated hindered diffusion morphogen molecules diffuse slowly due to binding to receptors or extra-cellular matrix components (Müller et al., 2013). In addition to binding to specific receptors, morphogen spread could be restricted due to interaction with the cyto-architecture in complete cells or nucleo-cytoplasmic domains of syncytial cells, like the *Drosophila* early embryo syncytium.

The discrete distribution of *bicoid* mRNA at the anterior of the early *Drosophila* embryo suggests that the nucleo-cytoplasmic domains maintain different cytoplasmic compositions. From various examples, we know that despite sharing a common cytoplasm, key molecules such as transcription factors, cell cycle molecules and mRNA are inhomogeneously distributed in syncytia (Cutler et al., 2018; Gladfelter, 2006; Gladfelter et al., 2006). The mechanisms that restrict the diffusion of molecules and the

extent to which they do so, specially in the *Drosophila* early embryo remains an open question. Molecules associated with organelles, cytoskeleton or the plasma membrane are known to compartmentalize to energids (Chowdhary et al., 2017; Frescas et al., 2006; Mavrakis et al., 2009a). This chapter focuses on how cytoplasm may be compartmentalized to energids.

Similar to our focus in Chapter 4, a method to distinctly label and track cytoplasmic population in the early embryo, is a convenient way to study cytoplasmic properties. However, our approach using photoactivatable probes may not capture the full range of cytoplasmic distributions that may occur during developmental time as it is restricted by the timing of activation. Another approach is to study molecular spread of cytoplasmic and membrane associated proteins produced locally through genetic interventions. This method would also capture the full range of cytoplasmic distribution changes that occur during development.

We can generate local gradients in the syncytial *Drosophila* embryo by producing them from a localized mRNA source. For example, the segmentation gene *fushi tarazu* (*ftz*) is expressed in a seven-banded pattern. By genetically tagging mRNA components which localize *ftz* to DNA encoding cytoplasmic probes like mRFP, we can expect mRFP to be restricted in a similar seven-banded fashion. However, the restriction of *ftz* coincides with cellularization (Edgar et al., 1987) and hence it is difficult to predict whether syncytial stages would also have similar restrictions.

The *bcd*-3'-UTR sequence of the mRNA is sufficient to anchor the *bcd* mRNA to the anterior of the embryo during oogenesis and embryogenesis (Berleth et al., 1988; Ephrussi and Lehmann, 1992). Previous studies have shown that adding *bcd*-3'-UTR to another transcription factor, Smaug, can form its antero-posterior gradient (Benoit et al., 2009). Anterior restriction of the giant-nuclei mRNA using the *bcd*-3'UTR, in an otherwise mutant background, forms a gradient of rescue of mutant defect in the AP axis (Zhang et al., 2004). However, a construct containing GFP with *bcd*-3'-UTR spreads throughout the syncytial embryo in the antero-posterior direction (Gregor et al., 2008). Together, these observations suggest that the *bcd*-3'-UTR can be used to anteriorly localize different types of proteins to assess their spread in the antero-posterior direction. Here, we examine the spread of cytoplasmic or membrane tagged

proteins to each energid. We address the question of how molecules may remain localized near each energid and how that changes their spread throughout the embryo. Since anterior localization using the *bcd*-3'-UTR is a well characterized way of locally enriching molecules, we used this approach to study the question of cytoplasmic restriction.

We discuss two cases of restriction to energids: cytoplasmic molecules of varied sizes and molecules that bind on and off the membrane by interaction with lipids in the plasma membrane and assess the extent of restriction. We found that whereas cytoplasmically expressed fluorescent proteins spread uniformly in the antero-posterior direction, membrane associated PH-PLC tagged to CFP is restricted and shows an exponentially shaped gradient similar to Bicoid.

5.2 Special notes on Materials and methods

Imaging

512 pixel X 512 pixel images were acquired after that with a scan speed of 1.56 seconds per frame.Mean line averaging of 2 was used. The gain and laser power were adjusted to be cover the dynamic range of each fluorescent tag and care was taken to not reach 255 on the 8 bit scale. Pinhole was kept open at 180µm.

FRAP experiments

For FRAPs at 5XGFP ,8XGFP and mRFP, the ROI size of 30.41µm^2 was used. The laser line used for bleaching and imaging was 488nm for 5X & 8XGFP and 561nm for mRFP. Bleaching was performed at 100 percent laser power and imaging was performed at a lower power using the same laser. Iterations were kept at 30 which corresponds to a bleaching time of 1.43 seconds.

8XGFP-*bcd*-3'UTR was found to be on the membrane at the anterior pole when stained with anti-GFP antibody, while live imaging showed very faint GFP signal. Hand de-vitellinization after fixation using PFA, preserves the GFP signal and was thus used to quantify the gradient.

5XGFP-*bcd*-3'UTR also shows weak GFP signal, but somehow signal in fixed images is substantial to be quantified.

PH-PLC-CFP-*bcd*-3'UTR was driven by *nanos*-Gal4 and *mat*-Gal4 at 18°C, 25°C and 28°C to check if expression levels could lead to differences in length scales. No observable difference were found as the lowest levels (*nanos*-Gal4,18°C) are enough to saturate the gradient.

5.3 Results

5.3.1 Anteriorly expressed fluorescent protein monomers or tandem multimers show a uniform spread as compared to Bicoid in syncytial *Drosophila* embryos

Restriction of different protein components to syncytial cells could occur due to differential molecular size in a crowded cytoplasm as seen in mammalian cells (Janson et al., 1996b; Luby-Phelps, 2000; Luby-Phelps and Taylor, 1988; Luby-Phelps et al., 1987; Luby-Phelps et al., 1988). It could also occur due to sequestration in different cellular regions or binding to the cellular architecture components. We assessed the extent of restriction of cytoplasmic and plasma membrane associated proteins across nucleo-cytoplasmic domains in the syncytial *Drosophila* embryo. Towards addressing this, we generated transgenes containing cytoplasmic or plasma membrane associated genes with the *bcd*-3'-UTR. The *bcd*-3'-UTR is known to be sufficient to target the anterior localization of mRNA and in turn generation of protein gradients in the antero-posterior direction. The shape of spread of molecules can be monitored to ascertain the degree of restriction in the antero-posterior axis in the syncytial blastoderm embryo. We first asked if fluorescent proteins (FP) of different sizes would give rise to an AP gradient and how the spread would differ from Bicoid (which provides an inherent control in these cases, being originally localized anteriorly using the *bcd*-3'UTR). For this we created constructs with mRFP (~25kDa), 5XGFP (~134kDa) and

8XGFP(~215kDa) and the *bcd*-3'-UTR under the control of inducible UASp promoter (Figure 5.1A). These transgenes were expressed to the same extent in oogenesis with the *mat*-Gal4-*vp16* and the resultant embryos were co-stained for Bicoid protein. We monitored the spread of these fluorescent proteins in the AP direction in the syncytial division cycles. We observed a uniform distribution of mRFP when measured in the antero-posterior axis in the embryo (Figure 5.1B,C, Movie Mov5.S1). This anteriorly expressed mRFP was not found in a gradient (Figure 5.1C). This was similar to the *bcd*>EGFP-*bcd*-3'UTR generated previously (Gregor et al., 2008). Interestingly, the 5XGFP (Figure 5.1D,E, Movie Mov5.S2) and 8XGFP (Figure 5.1F,G) were expressed in a gradient across the antero-posterior axis. However, the 5XGFP and 8XGFP showed gradients of varying slopes, which was quantified by fitting an exponential decay equation (Figure 5.1J).

The difference between mRFP and 5X/8XGFP could be attributed to the protein size of the freely diffusing protein involved in the gradient formation. Fluorescence recovery after photobleaching measurements showed that 5X and 8XGFP had higher diffusion values corresponding to slower recovery, proportional to their size in the syncytial embryo (Figure 5.1H,I). The higher diffusion values explain the slower spread of 5X and 8XGFP in the syncytial embryo and suggest that diffusion of these molecules is constrained due to molecular size. In summary, mRFP when expressed from the anterior of the embryo showed a uniform distribution and 5X/8XGFP were somewhat constrained due to molecular size.

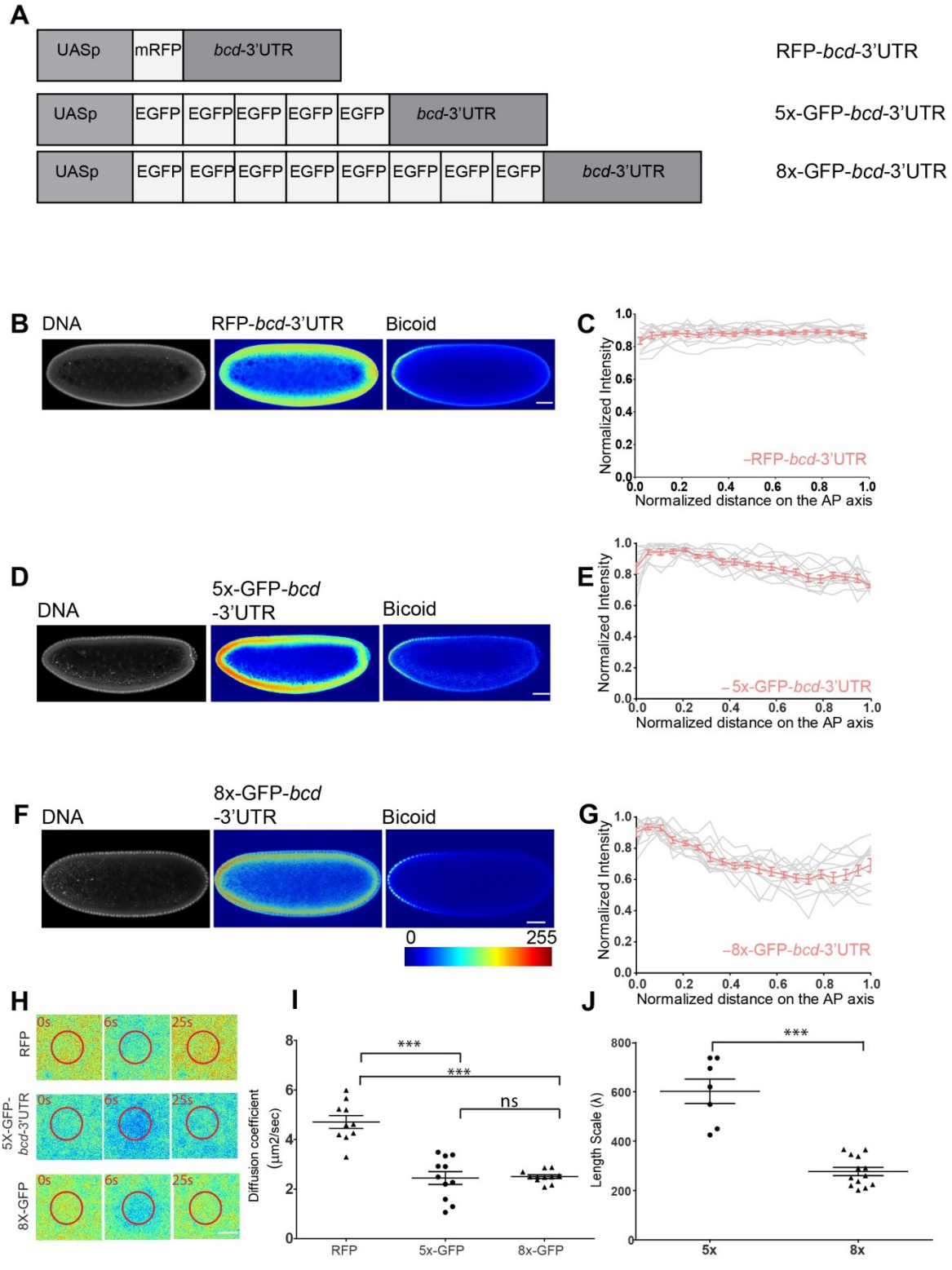

Figure 5.1: Fluorescent protein monomer and multimers expressed from constructs UASp-FP monomer/multimer-*bcd*-3'UTR spread uniformly as compared to Bicoid in syncytial embryos

(A). Graphical representation of the anteriorly localized FP constructs. The constructs contain the UASp promoter, the FP monomer, mRFP or multimer 5XGFP or 8XGFP gene followed by the *bcd*-3'UTR sequence.
(B-G). Differential gradients of anteriorly expressed mRFP, 5XGFP and 8XGFP. UASp-mRFP-*bcd*-3'UTR **(B)**, UASp-5XGFP-*bcd*-3'UTR **(D)** and UASp-8XGFP-*bcd*-3'UTR **(F)** when expressed with *mat*-Gal4 show a uniform mRFP spread and linear 5XGFP and 8XGFP protein gradients in the antero-posterior axis as compared to Bicoid. The pictures represent images from interphase of NC13 or NC14 **(B)**. The graphs for mRFP **(C)** 5XGFP **(E)** and 8XGFP **(G).**show quantification of anterior to posterior spread of fluorescent proteins and Bicoid in the same embryo. The raw data is shown in a lighter color and the averaged data is shown by a darker color, error bars represent standard error on mean (SEM). n=6 (mRFP), 6 (5XGFP), 6 (8XGFP) embryos. Scale bar= 50µm.
(H-I). FRAP analysis of FP monomer and multimer. Representative images of FRAP analysis for mRFP, 5XGFP and 8XGFP **(H)**. The graph shows diffusion coefficient values derived from different FRAP experiments for different FPs (mRFP, n=14 experiments in 4 embryos (14,4), 5XGFP-*bcd*-3'UTR, n=15,4, 8XGFP, n=10,3, One way ANOVA with Tukey's Multiple Comparison Test). Error bars represent $\pm$SEM. Scale bar=5µm.
(G).Graph shows scatter plot of length scale values **(G)** for anteriorly expressed 5X-GFP and 8X-GFP, extracted by fitting an exponential decay equation (n=7 observations from 5 cycle 14 embryos for anteriorly expressed 5X-GFP and 13 observations from 9 cycle 14 embryos for anteriorly expressed 8X-GFP, two-tailed non-parametric Mann Whitney test, p-value<0.0001).The images are shown in a 16 color intensity rainbow where Blue represents the lowest intensity and red represents the highest intensity.

5.3.2 Anteriorly expressed PIP2 binding protein PH-PLC-CFP shows an exponential gradient similar to Bicoid in syncytial *Drosophila* embryos

We next tested gradient formation using an anteriorly localized protein which contains a phospholipid binding domain. The PH domain of phospholipase C-δ (PH-PLC-δ) binds PIP2 and dynamically associates with the plasma membrane (Mavrakis et al., 2009a; Várnai and Balla, 1998). It marks the apical and lateral domains of the plasma membrane. A construct containing PH-PLC-CFP in tandem with the *bcd*-3'UTR, under the control of UASp promoter was created and expressed in the embryo using *mat-gal4-vp16* (Figure 5.2A). This transgene showed a similar localization to the polygonal plasma membrane in the syncytial embryo as the ubiquitously expressing transgene generated previously (Figure 5.2B) (Mavrakis et al, 2009). We imaged embryos containing PH-PLC-CFP gradient and compared it with Bicoid tagged to Venus in the interphase of syncytial cycles 11-14 (Figure 5.2C,D, Movie Mov5.S3). Bicoid has been shown previously to increase in amplitude across syncytial cycles (Abu-Arish et al., 2010). We found that living embryos containing the PH-PLC-CFP (Figure 5.2D) gradient showed an increase in amplitude across the syncytial cycles similar to Bicoid-Venus

embryos (Figure 5.2F, Movie Mov5.S4). An analysis of antero-posterior gradients for PH-PLC-CFP and Bicoid-Venus showed a similar exponential drop when compared in syncytial cycle 13 (Figure 5.2G,H). The length scale of the PH-PLC-CFP gradient was more than the Bicoid gradient (Bicoid=149$\pm$6.3 µm, PH-PLC-CFP=191$\pm$11.2 µm) (Figure 5.2I).

Thus we find that anteriorly expressed PH-PLC-CFP forms an exponential gradient. As per the SDD model, the "exponential-ness" and the length scale of any gradient depends on $\sqrt{\frac{Diffusion\ rate}{Degradation\ rate}}$ (Grimm et al., 2010). One explanation for the exponential spread of PH-PLC as compared to 5X/8XGFP is due to its binding to phospholipid PIP2 in the plasma membrane and other components of the cytoarchitecture, which can contribute towards lowering it's effective rate of diffusion. Previous studies have shown that molecules associated with the plasma membrane are compartmentalized to one energid. They diffuse freely within one energid and move across neighboring syncytial nucleo-cytoplasmic domains at a much slower rate (Mavrakis et al., 2009a). Hence binding of PH-PLC to PIP2 rich regions in the plasma membrane may contribute to the shape of its gradient.

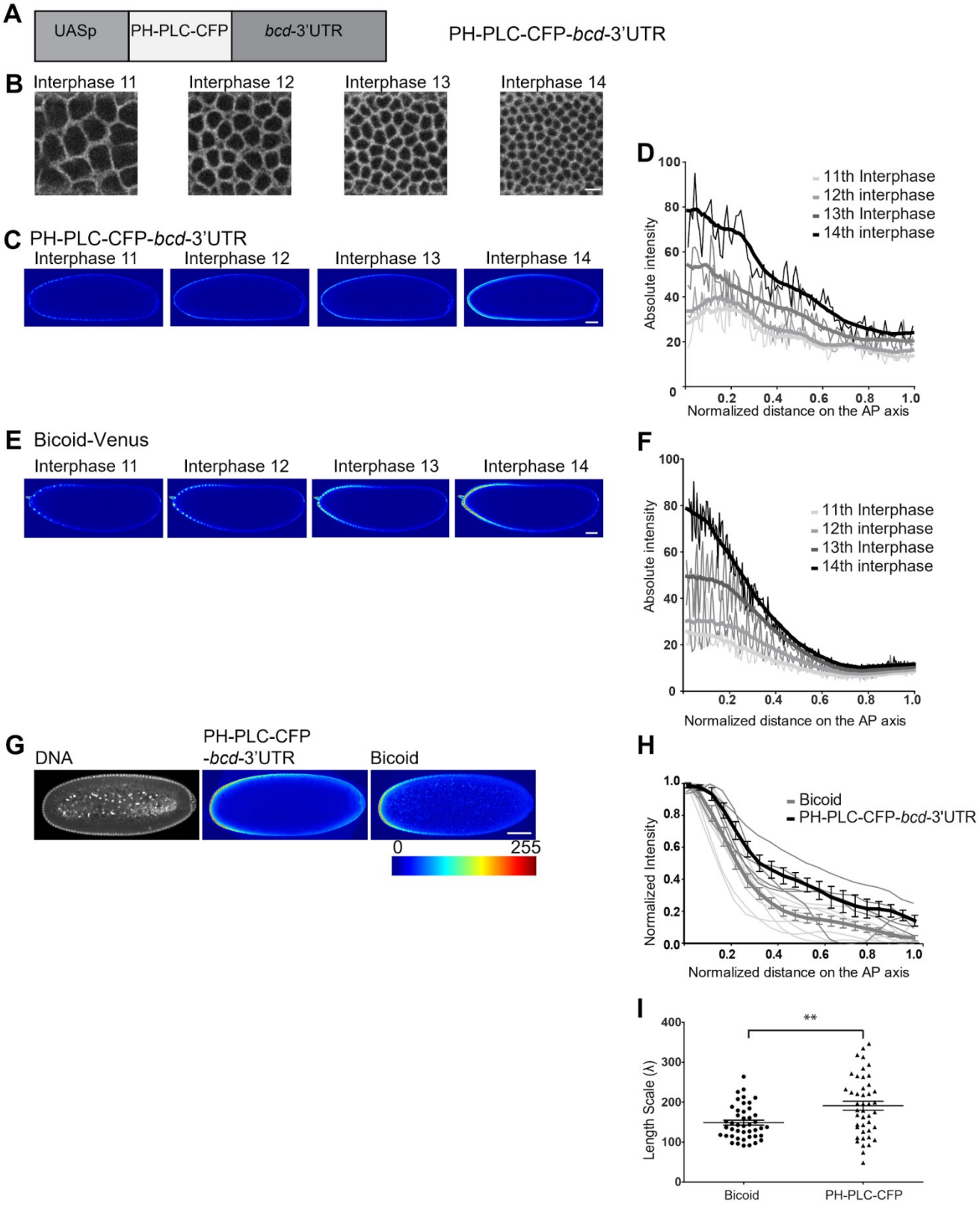

Figure 5.2: PH-PLC-CFP expressed anteriorly from the construct UASp-PH-PLC-CFP-*bcd*-3'UTR forms an exponential protein gradient similar to Bicoid in syncytial embryos

(A): Graphical representation of the anteriorly localized PH-PLC-CFP construct. The UASp promoter was added to the PH-PLC-CFP gene along with the *bcd*-3'UTR sequence.
(B-F): Formation of PH-PLC-CFP and Bicoid gradient in interphase of NC11-14.
Anteriorly expressed PH-PLC-CFP localizes to the plasma membrane **(B)**. Scale bar=10µm. PH-PLC-CFP**(C)** and Bicoid-Venus **(E)** images are shown from time lapse movies of living embryos from interphase of NC11-14 showing the development of the gradient across nuclear cycles. Graph shows representative line profile from anterior to posterior of the PH-PLC-CFP **(D)** and Bicoid **(F)** gradient from one embryo. The raw data is shown as a lighter color and smoothened curves are shown as thick lines. The same trend is observed in 6 embryos. Scale bar= 50µm.
(G-I): Anteriorly expressed PH-PLC-CFP shows an exponential protein gradient similar to Bicoid. Anteriorly expressing PH-PLC-CFP embryos are immunostained for Bicoid **(G)**. Graph shows quantification of both gradients**(H)** with the raw data in a lighter color (dark grey, PH-PLC-CFP; light grey, Bicoid) and the averaged data is shown in a darker color (grey, PH-PLC-CFP; black, Bicoid) error bars represent standard error on means (n=6 embryos for each, A.U., arbitrary units). Graph shows scatter plot of length scale values **(I)** extracted by fitting an exponential decay equation (n=22 embryos for Bicoid and 22 embryos for PH-PLC-CFP, two-tailed non-parametric Mann Whitney test, p-value=0.0058).Scale bar= 50µm.
The images are shown in a 16 color intensity rainbow where blue represents the lowest intensity and red represents the highest intensity.

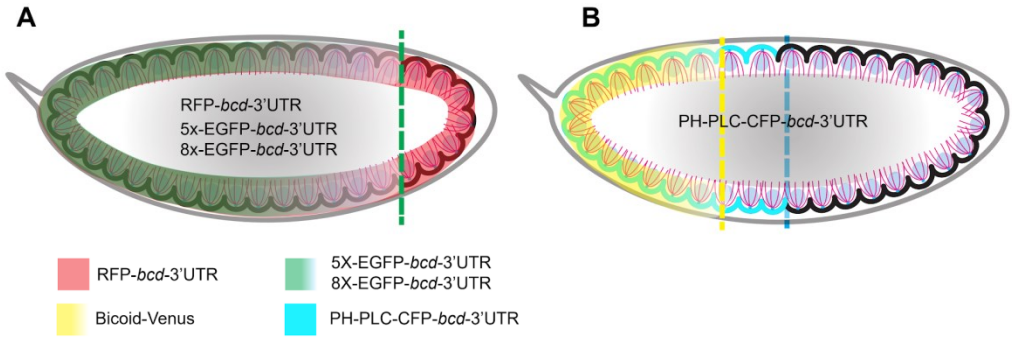

Figure 5.3: Schematic summarising the distribution of different proteins when expressed anteriorly by using the *bcd*-3'UTR sequence
Anteriorly expressed cytoplasmic proteins show a restriction of protein gradient spread based on size **(A)**. PH-PLC-CFP and Bicoid shows a similar exponential gradient from the anterior side **(B)**.

5.4 Discussion

In this study, we have compared molecules with different cytoplasmic properties as a readout to assess differential spread of proteins across energids, by using tools from the Bicoid gradient paradigm. We analyzed the extent of diffusion of free cytoplasmic proteins and plasma membrane associated PH-PLC-CFP when expressed anteriorly. We found that even though anteriorly expressed 5X/8XGFP created a gradient as compared to mRFP, it was not sufficient to form an exponential gradient. The steeper

gradient observed for anteriorly expressed PH-PLC-CFP showed an exponential spread. This suggests that the spread of proteins in the syncytial *Drosophila* embryo could be restricted depending on their interaction with the cytoarchitecture within each energid, than just size alone (Figure 5.3).

Restriction of molecules based on cellular localization

Energids in the early syncytial *Drosophila* blastoderm embryo are postulated to have nucleo-cytoplasmic zone of influence in which cellular components are restricted (Foe and Alberts, 1983). Earlier studies postulate that proteins may not mix freely in the syncytial cytoplasm and different proteins could become confined to the cytoplasmic domains that surround different nuclei (Foe and Alberts, 1983). An experimental cum simulation based study found that only 4% of hunchback (hb) transcripts exchanged between neighbouring cylindrical volumes which represented energids (Little et al., 2013). This restriction could occur due to mechanisms regulating the localization and partitioning of molecules. The microtubule cytoskeleton regulates *fushi tarazu* mRNA localization in the cytoplasm (Edgar et al., 1987). F-actin and plasma membrane block lateral movement of the *fushi tarazu* mRNA while microtubules confine it above the nucleus in the absence of plasma membrane boundaries. Further, modelling studies reinforce the argument that transient binding to microtubules is sufficient for segregating and restricting cytoplasmic components to spindle poles in absence of membrane based boundaries (Chen et al., 2012). Depolymerization of microtubules by nocodazole also leads to a greater diffusion of an ER lumenal probe across adjacent energids (Frescas et al., 2006). In addition, depolymerization of actin leads to a greater spread of a plasma membrane associated protein GAP43-mEos (Mavrakis et al., 2009a). Our analysis of ectopic protein gradients of Photoactivatable-GFP-Tubulin (PA-GFP-Tubulin) and Photoactivatable-GFP (PA-GFP) in the syncytial embryo shows that PA-GFP-Tubulin is more constrained as compared to PA-GFP. Changing the tubulin dynamics or disrupting furrows leads to an increased diffusion of PA-GFP-Tubulin and the extent of spread of PA-GFP-Tubulin approaches PA-GFP in these cases (Chapter 4). Thus, molecular interaction of cytoplasmic and plasma membrane proteins to the cytoskeleton

can contribute towards the generation of a compartmentalized cytoplasm even in the absence of plasma membrane boundaries.

This study suggests that there are multiple ways to create restriction of proteins to an energid in the syncytial embryo. Slowly moving proteins like 5XGFP and 8XGFP are retained near energids due to slow diffusivity, while fast diffusing mRFP forms no gradient. Even though based on molecular size, PH-PLC-CFP is closer to mRFP in diffusivity, it still forms an exponential gradient. When compared with 5X/8XGFP, this is unexpected as a fast diffusing probe is showing gradient properties, not exhibited by slowly diffusing probes. One explanation is the fact that PH-PLC-CFP binds on and off the membrane and therefore it's effective diffusivity is lower, which increases its retention near each energid. For Bicoid, a model which predicted such increase in retention time could predict the formation and dynamics of Bicoid like gradient (Kavousanakis et al., 2010). This same property seems to be captured by PH-PLC albeit by a different mechanism of retention near each energid.

Implications for Bicoid anterior-posterior gradient

Estimation of the size based diffusion coefficient of molecules in the syncytial *Drosophila* embryo has been carried out with fluorescently labelled dextran (Gregor et al., 2005). Dextran like mRFP and GFP provides information about diffusion of free molecules in the syncytial blastoderm embryo. Data in this study suggests that Bicoid protein spread is likely to be constrained by binding to the cytoarchitecture. This is not without precedence as studies with Homeobox transcription factors, Engrailed-1 and Engrailed-2 have shown specific non-nuclear subcellular localization (Joliot et al., 1997). The localization is dependent on a specific 11-amino acid sequence between the second and third helix of the homeodomain (Joliot et al., 1998). It would be interesting to test the domains of the Bicoid protein which are responsible for Bicoid association with cytoarchitecture.

Further, the *bcd*-3' UTR has been used to express transcription factors like Smaug and Gnu anteriorly (Benoit et al., 2009; Zhang et al., 2004). The shape of the Smaug gradient also matches Bicoid gradient shape to a large extent. In contrast to this, anteriorly produced nuclear localized EGFP (EGFP-NLS) did not yield a Bicoid like

gradient (Gregor et al., 2008), though it made the gradient steeper as compared to EGFP alone. This suggests that compartmentalizing EGFP-NLS can lead to changing effective diffusion coefficient as compared toEGFP alone. Contrasting the differences in the shapes of Smaug vs EGFP-NLS gradients, both being nuclear gradients, it can be said that gradient shapes are dependent on the mechanism of interaction with cyto-architecture. This is likely to increase their retention in a distinct location in an energid.

In summary, this study brings to light the importance of binding, cytoplasmic and cytoskeletal milieu and tortuosity in regulating how cytoplasm is restricted near energids in the syncytial *Drosophila* embryo.

5.5 Supplementary Movies

Mov5.S1: *mat*-*Gal4*>UASp-RFP-*bcd*-3'UTR Anteriorly localized UASp-RFP containing the bicoid *(bcd)* 3'UTR localization signal expressed using the *maternal*-Gal4 and imaged across the syncytial division cycles 11-14. Anterior is to the left. Note that RFP enters the nucleus.

Mov5.S2: *mat*-Gal4>UASp-5x-GFP-*bcd*-3'UTR

Anteriorly localized UASp-5X-GFP containing the bicoid *(bcd)* 3'UTR localization signal expressed using the maternal Gal4 and imaged across the syncytial division cycles 11-14. Anterior is to the left. A linear gradient could be seen.

Mov5.S3: *mat*-Gal4>UASp-PH-PLC-CFP-*bcd*-3'UTR

Anteriorly localized UASp-PH-PLC-CFP containing the bicoid *(bcd)* 3'UTR localization signal expressed using the maternal Gal4 and imaged across the syncytial division cycles 12-14. Anterior is to the left. PH-PLC-CFP labels the complete apical and lateral membrane.

Mov5.S4: Bicoid-Venus

Bicoid tagged to Venus under the Bicoid endogenous promoter imaged across the syncytial division cycles 10-14. Anterior is to the left. Bicoid gradient can be seen in the AP axis. Bicoid signal can be seen in the nucleus in interphase and cytoplasmic in metaphase.

Chapter 6: Bicoid gradient as a paradigm to study the cytoplasmic compartmentalization

Chapter 6 summary*: In this chapter, we have used the anterior-posterior gradient,Bicoid and the ectopic gradient of anteriorly tagged PH-PLC-CFP to test cyto-architectural components which may be restricting these gradients. We find that while actin perturbation disrupts both these gradients, pseudocleavage furrows perturbation leads to only PH-PLC gradient disruption but not that of Bicoid.*

6.1 Introduction

The early embryo has many paradigms to study the implications of binding, tortuosity and confinement on the cytoplasm. Morphogen gradients in the early embryo, namely, Bicoid, Dorsal and Torso are mostly cytoplasmic and therefore can be used as paradigms to test the implications of our understanding in these functional contexts.
A detailed introduction to the Dorsal and Bicoid gradients has already been provided in Chapter 1. Here we consider what these gradients can help us understand about cytoplasm of the early embryo.

The dorso-ventral gradient formed by Dorsal is compartmentalized to each nucleo-cytoplasmic domain (DeLotto et al., 2007). Modelling studies show that plasma membrane furrows could restrict Dorsal gradient spread (Daniels et al., 2012; Kanodia et al., 2009). The Dorsal gradient formation on the ventral side depends on specific binding partners on the ventral side (Carrell et al., 2017) and Dorsal import rate and its binding affinity to DNA varies across the DV axis (Asafen et al., 2018). These studies highlight how Dorsal is compartmentalized, can be restricted by cyto-architecture (furrows) and how binding affinities can change its diffusion in the embryo.
Bicoid forms a gradient in the antero-posterior axis, patterning the head of the embryo (Gregor et al., 2007). Bicoid gradient is formed due to a combination of synthesis, diffusion and degradation (SDD-model), which have currently be in studied in detail (Drocco et al., 2011; Durrieu et al., 2018; Gregor et al., 2007). There has been debate about whether Bicoid gradient is solely dependent on the shape of the bicoid mRNA

(which is also present as a gradient) (Spirov et al., 2009) but such claims have mostly been settled (Little et al., 2011) to include both mRNA shape and protein diffusion into consideration. There are various mechanisms involved in maintaining Bicoid protein localization. It is suggested that Bicoid might bind to actin to partition within energids (Lucchetta et al., 2008a), while the nuclei are not important for its compartmentalization (Grimm and Wieschaus, 2010). Towards the posterior pole, where Bicoid concentrations is sparse, Bicoid forms “hubs” of locally high density facilitating the rates at which it loads onto DNA (Mir et al., 2017).

We wanted to study more about Bicoid, its dynamics and localization and ultimately what all can contribute to its observable effective diffusion. Further, the anteriorly localized PH-PLC-CFP gradient, introduced in the last chapter, provided an inherent control as a gradient with different dynamics and present in the same direction. This gave us the opportunity to compare and contrast the properties of cytoplasmic restriction for these gradients.

It has already shown that PH-PLC is a restricted molecule that does not move across energids (Mavrakis et al., 2009a). What restricts it from crossing energid boundaries? To test the same, we can disrupt various components and use FLIP to check for greater exchange between energids, similar to Chapter 3 and earlier studies (Mavrakis et al., 2009a). The presence of an anterior-posterior gradient of PH-PLC-CFP provides a quick and easy way of testing the same without using FLIP. If energid boundaries get disrupted, then it would result in freely flowing PH-PLC and thereby the gradient shape would also be disrupted. Further, we expect that cytoarchitectural components which restrict PH-PLC-CFP gradient inside an energid might also be involved in restricting Bicoid.

Here we explain our observations on how Bicoid and PHLC are both cortically enriched, both gradients are invariant during interphase and metaphase and that Bicoid maybe associated with furrows.Finally, we show that pseudo cleavage furrows play a role in restriction of plasma membrane associated PH-PLC but not Bicoid.

6.2 Special notes on Materials and methods

Imaging

512 pixel X 512 pixel images were acquired after that with a scan speed of 1.56 seconds per frame.Mean line averaging of 2 was used. The gain and laser power were adjusted to be cover the dynamic range of each fluorescent tag and care was taken to not reach 255 on the 8 bit scale. Pinhole was kept open at 180µm.

FRAP experiments

Photobleaching of the region of interest (ROI) of size 21 μm^2 was carried out in syncytial embryos expressing Bicoid-Venus or PH-PLC-CFP with 514 nm or 458 nm laser, supplemented with 405 nm laser at 100% power and 30 iterations, while being imaged with the respective laser line at a lower power. 8 bit images were acquired with mean line averaging of 2, for 40 seconds with minimum interval between images, while gain and laser power were adjusted to be between the dynamic range of each fluorescent tag. Pin hole size was 334µm for Bicoid-Venus and 161µm for PH-PLC-CFP.

6.3 Results

6.3.1 Antero-posterior gradient of anteriorly expressed PH-PLC-CFP and Bicoid are similar in interphase and metaphase of the syncytial division cycle

The syncytial cytoarchitecture undergoes significant remodeling during the nuclear division cycles. Bicoid is concentrated in the nucleus in interphase and is cytoplasmic in metaphase (Gregor et al., 2007). The plasma membrane between the nuclei forms short furrows during interphase which elongate during metaphase (Holly et al., 2015; Mazumdar and Mazumdar, 2002). Nuclear localization of the dorso-ventral gradient, Dorsal during interphase and furrow based restriction of during metaphase, have been regarded important for the gradient shape maintenance (Daniels et al., 2012; DeLotto et al., 2007). Restriction of plasma membrane molecules to one energid is likely to be

due to local delivery of cargo to the plasma membrane, molecular machinery associated with lateral domain and cytoskeletal organization in the furrows (Frescas et al., 2006; Mavrakis et al., 2009a).

We first monitored the localization of anteriorly localized PH-PLC-CFP and Bicoid-Venus across the syncytial cycle in interphase and metaphase. The concentration of Bicoid has been shown to decrease in metaphase (Abu-Arish et al., 2010) possibly due to its spread and hence effective dilution across the whole energid. We imaged PH-PLC-CFP and Bicoid-Venus in the syncytial division cycles and found that PH-PLC-CFP, marks the short and long pseudocleavage furrows in interphase and metaphase respectively and Bicoid moves out of the nucleus during metaphase (Figure 6.1A). Even though PH-PLC-CFP and Bicoid-Venus had strikingly different cellular distributions, both of them remained near the cortex throughout the syncytial division cycles 11-13 (Figure 6.1B).

We next tested if the different cellular environments of interphase and metaphase could cause a change in the local diffusion of Bicoid-Venus and PH-PLC. Further, we tested if changes in cyto-architecture concomitant with cell-cycle could have an impact on overall gradient shape across the syncytial cycles in interphase and metaphase. To assess the change in local mobility in different stages of the syncytial cycle, we performed FRAP experiments on Bicoid-Venus and PH-PLC-CFP. We calculated the half time of recovery of the Bicoid-Venus (Figure 6.1C,D) and PH-PLC-CFP (Figure 6.1C,F) from FRAP experiments in interphase and metaphase. Noticeably, the local mobility as shown by t_{half} values was lower for Bicoid-Venus in the interphase as compared to metaphase of the syncytial division cycle (Figure 6.1D). On the other hand, PH-PLC-CFP did not show a significant difference in t_{half} between interphase and metaphase (Figure 6.1E). We measured the gradient shape in interphase and metaphase and found that the overall Bicoid (Figure 6.1F,G) and PH-PLC-CFP (Figure 6.1F,I) gradient shape and the corresponding length scales did not change (Figure 6.1S1J,L). We also looked at the gradient of a nuclear shuttling mutant of Bicoid (BicoidΔK50-57-Venus) which does not enter the nucleus in interphase. As reported earlier (Grimm and Wieschaus, 2010), we found that the gradient shape for BicoidΔK50-57-Venus remained the same across syncytial cycles (Figure 6.1F,H,6.1S1K, Movie

Mov6.S1) (Grimm and Wieschaus, 2010). Thus the changes in the mobility for Bicoid and cytoarchitecture of the syncytial division cycle did not impact the shape of the Bicoid and PH-PLC gradients.

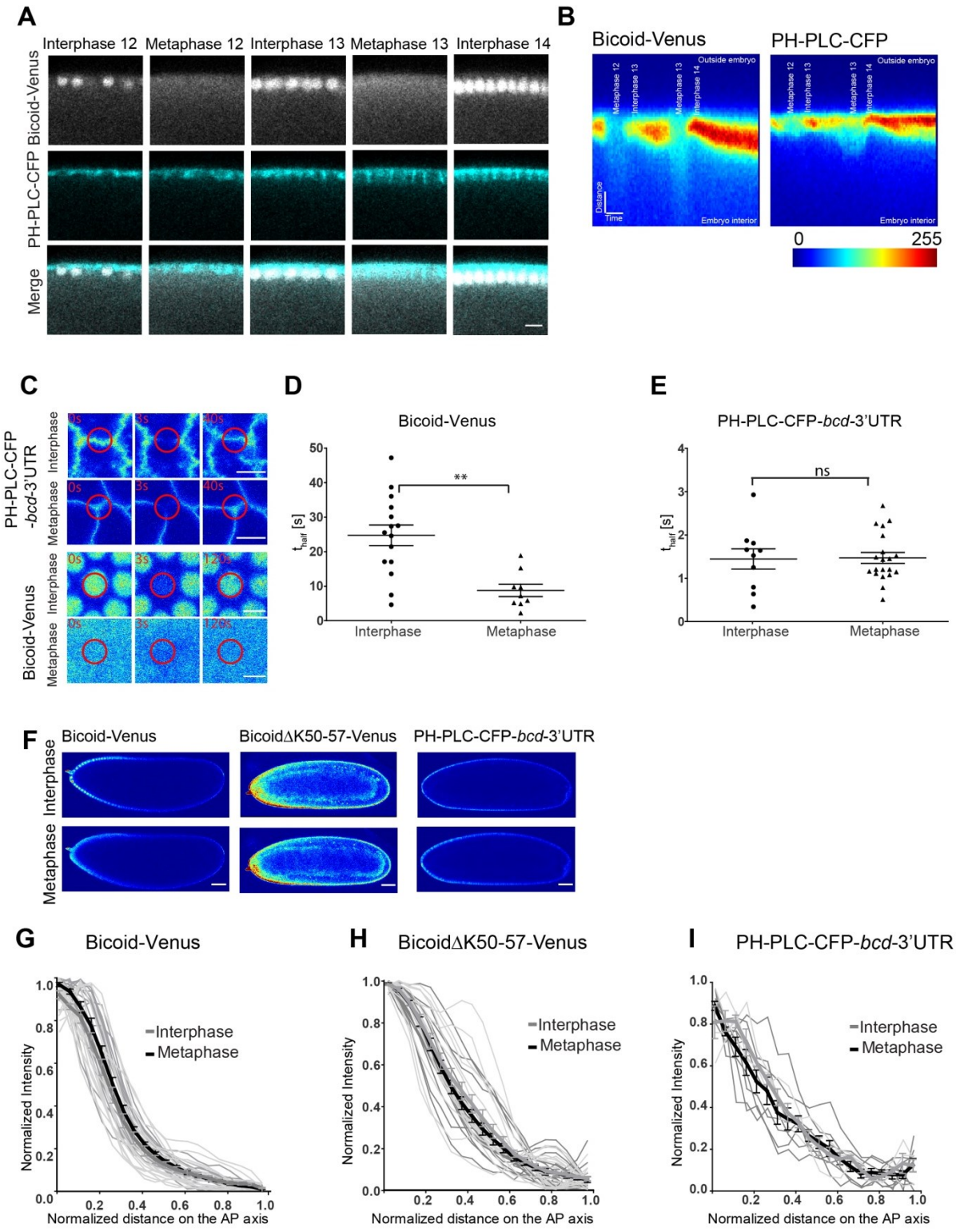

Figure 6.1: Anteriorly expressed PH-PLC-CFP and Bicoid gradients show an exponential spread in interphase and metaphase of the syncytial division cycle.

(A-B): PH-PLC-CFP and Bicoid gradient distribution in interphase of NC12-14 and metaphase of NC12-13. PH-PLC-CFP localizes to the furrow in between nuclei while Bicoid is inside nuclei during interphase. The furrows ingress to a greater depth in metaphase, while Bicoid is cytoplasmic. Scale bar= 10μm **(A)**. Kymograph shows cortical progression of intensity for Bicoid-Venus and PH-PLC-CFP across division cycles (marked) **(B)**. Scale bar= 5μm and 3.5 min.
(C-E): Bicoid shows faster mobility in metaphase. Representative time-lapse images for Bicoid-Venus and PH-PLC-CFP are shown for pre-bleach, bleach and post-bleach sections in interphase and metaphase blastoderm stages of NC13 **(C)**. FRAP analysis of Bicoid-Venus shows faster recovery in metaphase as compared to interphase (two-tailed non-parametric Mann Whitney test, p-value=0.0024) **(D)**, while PH-PLC-CFP shows similar recovery in both interphase and metaphase (two-tailed non-parametric Mann Whitney test, p-value=0.77) **(E)**. The graph shows t_{half} derived from different FRAP experiments during different phases of the cell cycle (Bicoid-Venus, n=15 experiments for interphase in 4 embryos, 9 experiments for metaphase in 4 embryos, PH-PLC-CFP, n=10 experiments for interphase in 4 embryos, n=20 experiments for metaphase in 4 embryos).
(F-I): Bicoid-Venus, BicoidΔK50-57-Venus and PH-PLC-CFP show an exponential gradient in interphase and metaphase of the syncytial cycle. Representative images **(F)** and quantification are shown in interphase and metaphase of the syncytial cycle. n=9 embryos for interphase and metaphase each for Bicoid-Venus **(G)**, n=3 embryos for BicoidΔK50-57-Venus **(H)** and n=4 embryos for PH-PLC-CFP **(I)**.Scale bar = 50μm.
The color scale used is a 16 color rainbow where blue represents the lowest intensity and red represents the highest intensity.

6.3.2 Bicoid equilibrates between pseudocleavage furrows in metaphase

Bicoid is present inside the nucleus in interphase, and becomes cytoplasmic in metaphase (Figure 6.1A). In interphase Bicoid in confined to each energid by the nucleus and adjacent nuclear intensity is known to be different (Gregor et al., 2007). In metaphase, the space between two furrows can be used to define an energid (Kanodia et al., 2009). Cytoplasmic Bicoid in metaphase, is mostly likely to be confined near each energid by the pseudocleavage furrows. How well does Bicoid diffuse between the furrows? There are two possible scenarios (Figure 6.2A). As Bicoid becomes cytoplasmic during metaphase, it can either equilibrate between furrows forming a stepwise gradient or form a gradient within each energid as well (Figure 6.2B). To test this, we imaged Bicoid along with phalloidin which marks actin and thereby the actin rich pseudocleavage furrows in metaphase (Figure 6.2B).We quantified the Bicoid gradient along with phalloidin, which marks the position of the pseudocleavage furrows (Figure 6.2C). We checked for the shape of the Bicoid gradient within each energid (two peaks of phalloidin intensity) (Figure 6.2C). We chose the steepest part of the gradient to study the same (Figure 6.2C (red boxes)). Zoomed in profiles of Bicoid and phalloidin (Figure

6.2D) seem to suggest that Bicoid equilibrates well between each set of furrows, suggesting an equilibration model. Further analysis needs to be done to check whether the furrows actively bind and restrict Bicoid or passively act as a barrier. A caveat towards this analysis is that since the scale at which Bicoid gradient falls between two furrows is already too shallow, it appears being uniform between furrows. It maybe that Bicoid profile in fact is drops sharply over two energids rather than one. We tried to test the same using Bicoid Delta K which is cytoplasmic during both interphase and metaphase, but did not get consistent results as staining and imaging DeltaK perturbed the signal and somehow led to a loss of the gradient.

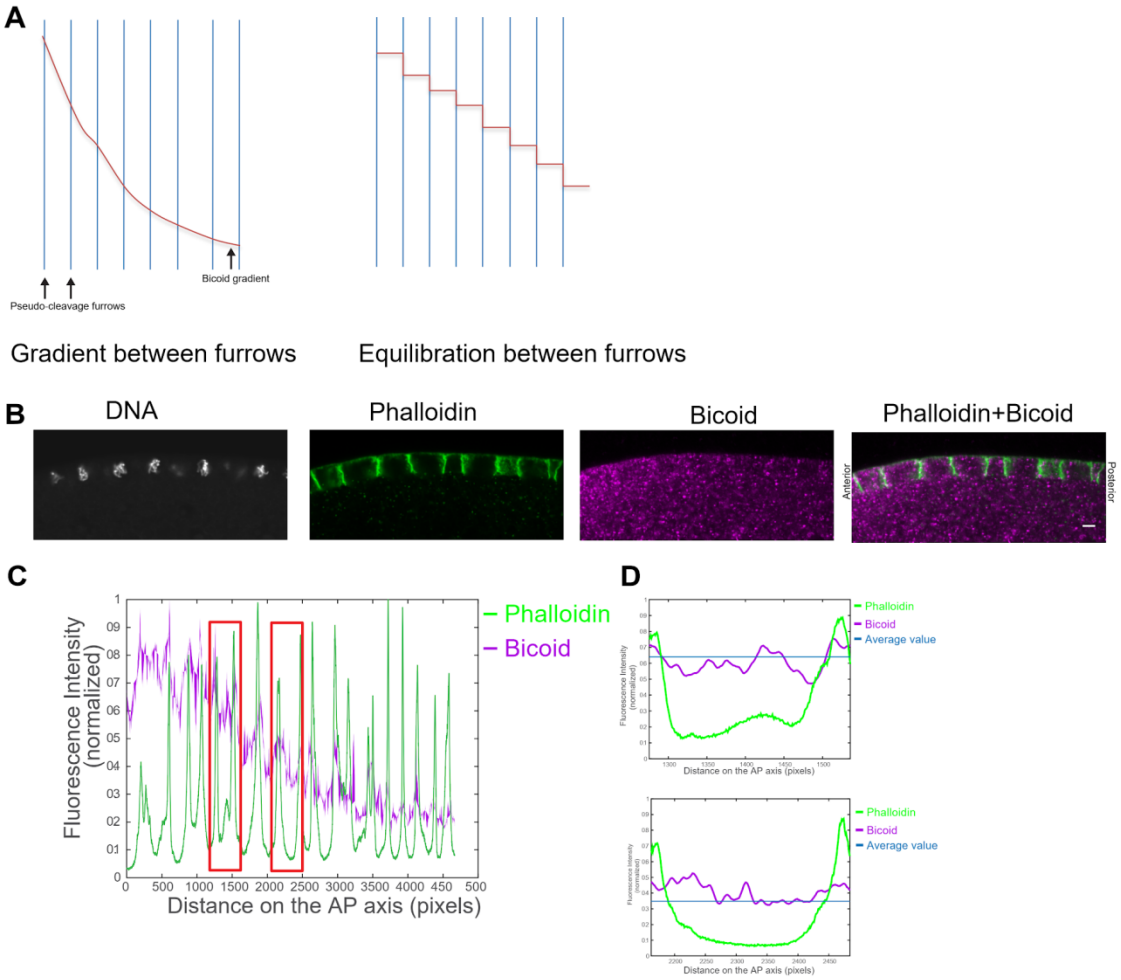

Figure 6.2: Cytoplasmic Bicoid equilibrates between metaphase pseudocleavage furrows

(A): Two models of Bicoid spread between pseudocleavage furrows. The vertical lines represent furrows, while the red line represents Bicoid gradient. The gradient can either be present in a graded fashion between furrows **(left)** or as a stepwise gradient by equilibrating between furrows **(right)**.

(B): Fixed imaging of Bicoid with Phalloidin. Bicoid is present in punctate form in metaphase, where the furrows can be seen as long vertical lines stained by phalloidin. Scale bar= 5μm.
(C): Anterior to posterior intensity profile of image shown in **(B)**. Bicoid profile can be seen to decrease gradually in the AP direction, while phalloidin intensity is highest at furrows showing as spikes followed by troughs which correspond to spaces between furrows.
(D): Zoomed in profiles between furrows shown in red boxes in **(C)**.Furrows are present on the right and left extremes of each graph while the raw Bicoid profile and averaged profile (of the first 100 pixels) is shown as the line parallel to X-axis. Notice the difference in the starting point of the Bicoid profiles in the two graphs, representing Bicoid profiles at different AP positions.

6.3.3 Bicoid is mildly enriched at pseudocleavage furrows

Upon imaging the pseudocleavage furrows with Bicoid, we observed that during metaphase, Bicoid staining looked punctate (Figure 6.2A: Bicoid). These punctae were present randomly scattered all across the metaphase cytoplasm, but showed preferential localization near the pseudocleavage furrows (Figure 6.3A). To test if this distribution was random and indeed Bicoid specific, we stained for Bicoid and phalloidin in an embryo containing cytoplasmic mRFP (Figure 6.3A). If the localization is specific for Bicoid, it would not correlate with mRFP, which should show constant signal everywhere between the furrows. To quantitative observe this enrichment, we marked an ROI and plotted an intensity profile across an energid (Figure 6.3A). We found that Bicoid showed enrichment near the furrows, while mRFP showed no such preference (Figure 6.3B). Further attempts to characterize these punctae were not pursued, though this can be tested by staining only using the secondary antibody to check if this is a non-specific signal. This could be followed by super-resolution based imaging of Bicoid in metaphase. A previous study has also suggested that Bicoid may be present near furrows (Lucchetta et al., 2008a).

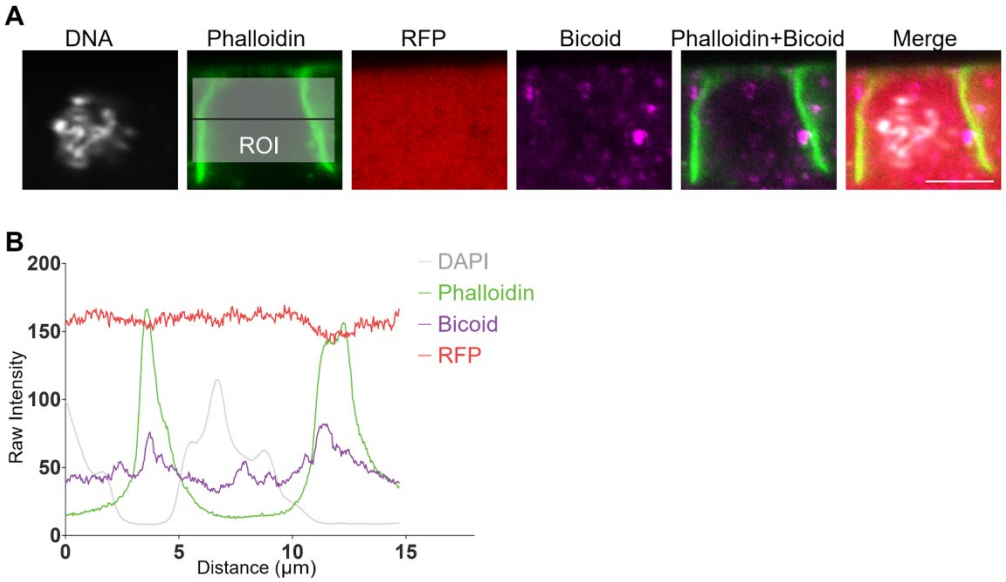

Figure 6.3: Cytoplasmic Bicoid is mildly enriched at pseudocleavage furrowsduring metaphase

(A): Zoomed in images of a metaphase embryo expressing mRFP showing one energid demarcated by phalloidin staining the metaphase furrows. Bicoid can be seen to be present as punctae. Scale bar=5µm.

(B): Intensity plots of the ROI (shown over phalloidin image in **(A)**. Notice DNA spike in the centre of the two green spikes representing phalloidin marked furrows. mRFP profile falls down slightly over furrows, while Bicoid seems to enrich near the furrows. Similar trends were seen for n=5 furrow pairs in 5 embryos.

6.3.4 The antero-posterior gradients of anteriorly expressed PH-PLC-CFP and Bicoid are restricted by actin dynamics

bicoid mRNA localization is regulated by cytoskeletal dynamics in oogenesis. In particular, actin filament organization by Swallow regulates *bicoid* mRNA maintenance at the anterior membrane in late stages of oogenesis (Weil et al., 2010). *swallow* mutant ovarioles show varied patterns of mRNA localization with spread to the lateral membranes during oogenesis (Weil et al., 2010). Also actin dynamics regulates the localization of *bicoid* mRNA in embryogenesis (Weil et al., 2008). We hence decided to test the gradient shapes of Bicoid and anteriorly expressed PH-PLC-CFP in embryos containing a perturbation of actin dynamics. Overexpression of fluorescently tagged actin is known to lead to a disruption of actin dynamics and depletion of F-actin. Expression of actin binding proteins also leads to disruption in actin polymerization in *Drosophila* oogenesis and other model systems (Aizawa et al., 1997; Hird, 1996; Röper et al., 2005; Spracklen et al., 2014). We overexpressed mRFP tagged Actin and imaged

syncytial *Drosophila* embryos for defects in the syncytial blastoderm cyto-architecture. In addition to the documented effects on actin remodelling on oogenesis by actin binding proteins, we found that 100% of the embryos obtained from maternal expression of mRFP-Actin with *nanos*-Gal4 were lethal at 24 hours. More specifically, mRFP-Actin expressing embryos caused furrow extension defects correlating with a defect in actin polymerization or remodelling (Figure 6.4A). The metaphase furrow was consistently shorter in mRFP-Actin overexpression embryos. Thus, in addition to previously reported defects on mRNA distribution of Bicoid, mRFP-Actin overexpressing embryos caused loss of furrows in the syncytial blastoderm embryo.

We next observed the gradient of Bicoid and anteriorly expressed PH-PLC-CFP in mRFP-Actin expressing embryos. An analysis of Bicoid protein gradient in fixed (Figure 6.4B,C) and living (Figure 6.4E,F, Movie Mov6.S2) embryos expressing mRFP-Actin showed an exponential gradient with a perturbed length scale greater than that seen in control embryos. Length scale analysis for spread of the exponential gradient from fixed and living embryos showed that Bicoid had an increased spread towards the posterior as compared to control embryos (Figure 6.4D,G). The extent of spread of the gradient also changed BicoidΔK50-57-Venus gradient in mRFP-Actin overexpressing embryos (Figure 6.4H,I). The length scale of the gradient changed significantly as compared to control in mRFP-Actin expressing embryos (Figure 6.4J). Most remarkably, anteriorly expressed PH-PLC-CFP gradient was severely perturbed as compared to Bicoid in mRFP-Actin overexpressing embryos as seen in an image from syncytial cycle 13 embryo (Figure 6.4K). The exponential gradient of anteriorly expressed PH-PLC-CFP (Figure 6.1) was no longer observed in mRFP-Actin overexpressing embryos and length scales could not be calculated from the distributions (Figure 6.4L, Movie Mov6.S3). These results collectively showed that overexpression of mRFP-Actin led to defects in the Bicoid and the anteriorly expressing PH-PLC-CFP gradient.

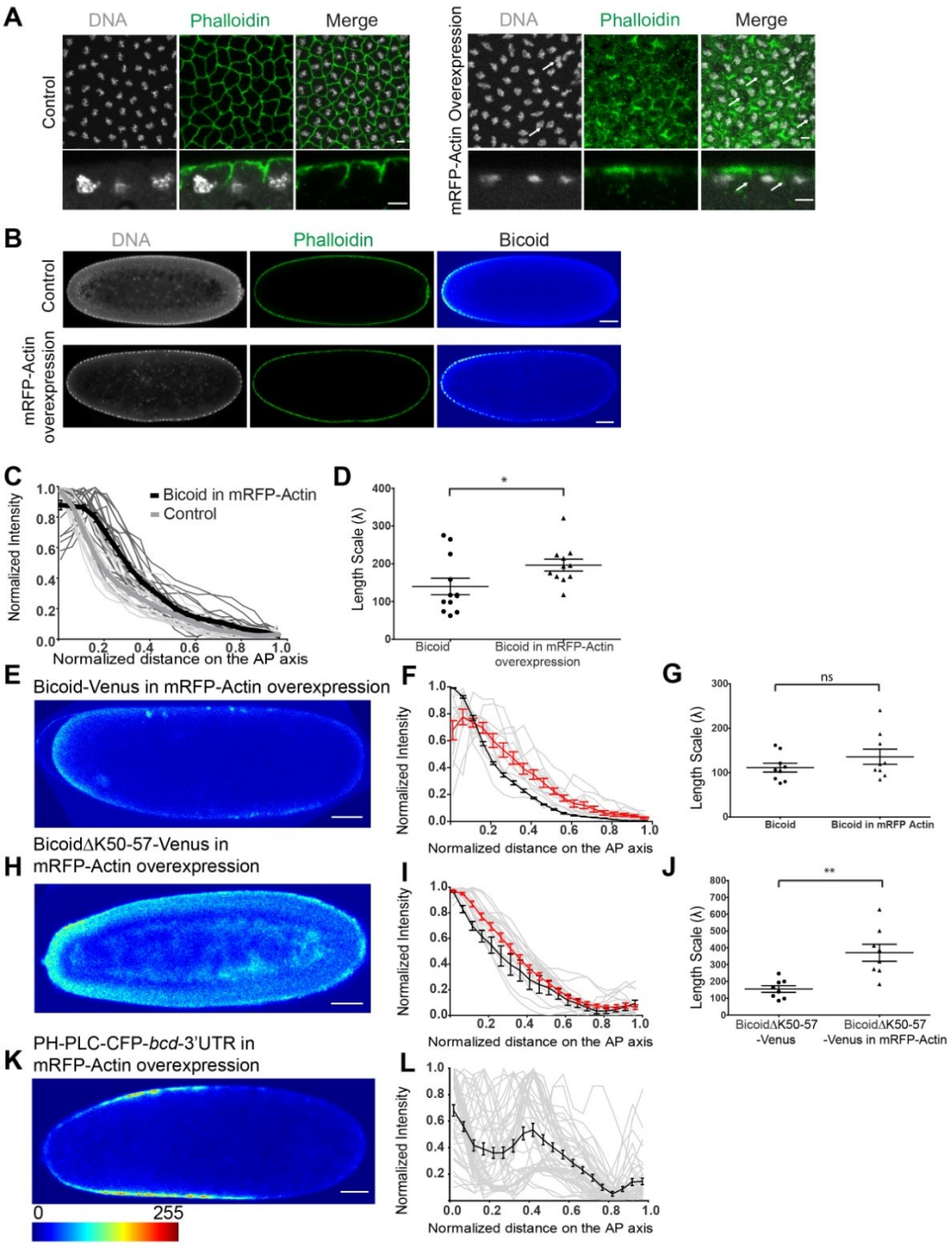

Figure 6.4: Anteriorly localized PH-PLC-CFP gradient is lost on over-expression of mRFP-Actin

(A): mRFP-Actin overexpression shows loss of metaphase furrows: Sagittal and surface view of embryos over-expressing mRFP-Actin, stained with DNA (grey) and Phalloidin (green) show shallow furrows with a loss of furrows in various locations (arrows) (n=70% of 30 embryos images showed this defect) Scale bar=5µm.

(B-D): Bicoid diffusion analysis in fixed embryos with mRFP-Actin overexpression. Bicoid (rainbow scale), Phalloidin (green) and DNA (grey) stained control embryos or embryos over-expressing mRFP-Actin **(B)** are shown. Line profile for measuring Bicoid gradient in control embryos or embryos expressing mRFP-Actin **(C)**. Grey lines in the

background show profiles across different embryos analysed, thick darker line represents average ±SEM. Graph shows scatter plot of length scale values **(D)** extracted by fitting an exponential decay equation. (n=6 embryos for control and n=6 embryos for mRFP-Actin overexpression, scale bar=50 μm, two-tailed non-parametric Mann Whitney test, p-value=0.0337,all embryos showed loss of furrow phenotype).
(E-G): Analysis of Bicoid-Venus in living embryos expressing mRFP-Actin. Bicoid-Venus expression is shown in a snapshot from a time lapse movie of an embryo overexpressing mRFP-Actin **(E)**. Quantification of the Bicoid-Venus gradient **(F)** with grey lines in the background showing line profiles across different embryos analysed, redline represents average for Bicoid-Venus in mRFP-Actin and black line represents average for control embryos. Error bars are ±SEM. Scatter plot shows length scale values extracted by fitting an exponential decay equation **(G)** (terminal time point analysed from n=6 embryos for control and n=8 embryos for Bicoid-Venus in mRFP-Actin, scale bar=50μm, two-tailed non-parametric Mann Whitney test, p-value=0.2973)
(H-J): Analysis of BicoidΔK50-57-Venus in living embryos expressing Actin-RFP. BicoidΔK50-57-Venus expression is shown in a snapshot from a time lapse movie of an embryo overexpressing mRFP-Actin **(H)**. Quantification of the BicoidΔK50-57-Venus gradient **(I)** with grey lines in the background showing line profiles (red line represents average±SEM) across different embryos analysed, black line represents average of control with ±SEM. Scatter plot shows length scale (λ) values extracted by fitting an exponential decay equation **(J)** (multiple time points from n=4 embryos, scale bar=50μm, two-tailed non-parametric Mann Whitney test, p-value=0.0011).
(K-L): Analysis of anteriorly expressed PH-PLC-CFP in living embryos expressing mRFP-Actin: PH-PLC-CFP-*bcd*-3'UTR expression is shown in a snapshot from a time lapse movie of an embryo overexpressing mRFP-Actin **(K)**. Quantification of the PH-PLC-CFP gradient with grey lines in the background showing line profiles across different embryos analysed, black line represents average with ±SEM **(L)** (n=5 embryos, Scale bar=50μm).

6.3.5 The antero-posterior gradient of anteriorly expressed PH-PLC-CFP is lost in pseudocleavage furrow mutant embryos

We further analysed the gradient of Bicoid and anteriorly expressed PH-PLC-CFP in embryos known to have a specific loss of pseudocleavage furrows. RalA is a component of the Ras signaling pathway (Colicelli, 2004; Harden, 2002). In syncytial *Drosophila* embryos, RalA functions through the exocyst complex to form pseudocleavage furrows. *ralA* mutants show distinct loss of furrows in metaphase (Holly et al., 2015). We expressed RNAi against *ralA* with *mat*-Gal4 and found that 60% of the embryos were lethal at 24 hours. We observed similar phenotypes of short furrows and loss of furrows in patches in metaphase of the syncytial division cycle as compared to the mutants of *ralA* (Figure 6.5A).

We went on to test the formation of Bicoid gradient by expressing Bicoid-Venus and cytoplasmic BicoidΔK50-57-Venus in embryos depleted of *ralA*. Bicoid-Venus(Figure 6.5B,C, Movie Mov6.S4) and BicoidΔK50-57-Venus (Figure 6.5E,F,

Movie Mov6.S5) showed a gradient similar to control gradients. An analysis of the length scale showed no significant change of the Bicoid-Venus and BicoidΔK50-57-Venus gradients in *ralA* RNAi background (Figure 6.5D,G) when compared with control embryos. Since the exponential gradient shape did not change drastically in these experiments, we conclude that furrows are not responsible for restricting the Bicoid gradient.

When anteriorly expressed PH-PLC-CFP gradient was monitored in *ralA* RNAi expressing embryos, there was a striking change in gradient shape. A snapshot in syncytial cycle 12 from such an embryo showed increased spread of PH-PLC-CFP towards the posterior (Figure 6.5H). A quantification of this gradient showed a complete loss of the gradient shape (Figure 6.5I, Movie Mov6.S6) as compared to the control (Figure 1) and length scales could not be calculated.

The presence of the GTPase exchange factor RhoGEF2 is required for pseudocleavage furrow extension. RhoGEF2 is localized at pseudocleavage furrowsand loss of *rhoGEF2* leads to decreased furrow length. *rhoGEF2* mutant embryos are likely to show a depletion of Rho-GTP and Myosin II activity. Increase in Myosin II activity like in embryos overexpressing RhoGEF2 leads to constriction of apical caps and loss of furrow formation (Zhang et al., 2018). We further tested if embryos showing an overexpression of RhoGEF2 could give rise to a perturbation of Bicoid and anteriorly expressed PH-PLC-CFP gradients. RhoGEF2 overexpression with *mat*-Gal4 gave embryos that were 87% lethal at 24 hours. RhoGEF2 overexpression led to short furrows throughout with patches of complete loss of furrows (Figure 6.6A). Bicoid-Venus and BicoidΔK50-57-Venus showed an exponential gradient in RhoGEF2 overexpressing embryos (Figure 6.6B,C,E,F). An analysis of the length scale of spread for this exponential gradient did not show any significant difference between control and RhoGEF2 overexpressing embryos (Figure 6.6D,G). Similar to *ralA* mutant embryos overexpression of RhoGEF2 also gave a disruption of the anteriorly expressed PH-PLC-CFP gradient. A snapshot from a movie of the RhoGEF2 overexpression embryo showed increase in PH-PLC-CFP signal towards the posterior (Figure 6.65H). A quantification of the PH-PLC-CFP gradient across multiple embryos showed a loss of the exponential nature of the gradient (Figure S1I).

Taken together, these experiments show that intact pseudocleavage furrows are responsible for the restriction anteriorly expressed PH-PLC-CFP gradient and do not play a significant role in giving rise to the exponential antero-posterior gradient of Bicoid protein. In addition, this suggests that the Bicoid gradient perturbation in mRFP-Actin background, involves a distinct mechanism independent of furrow perturbation

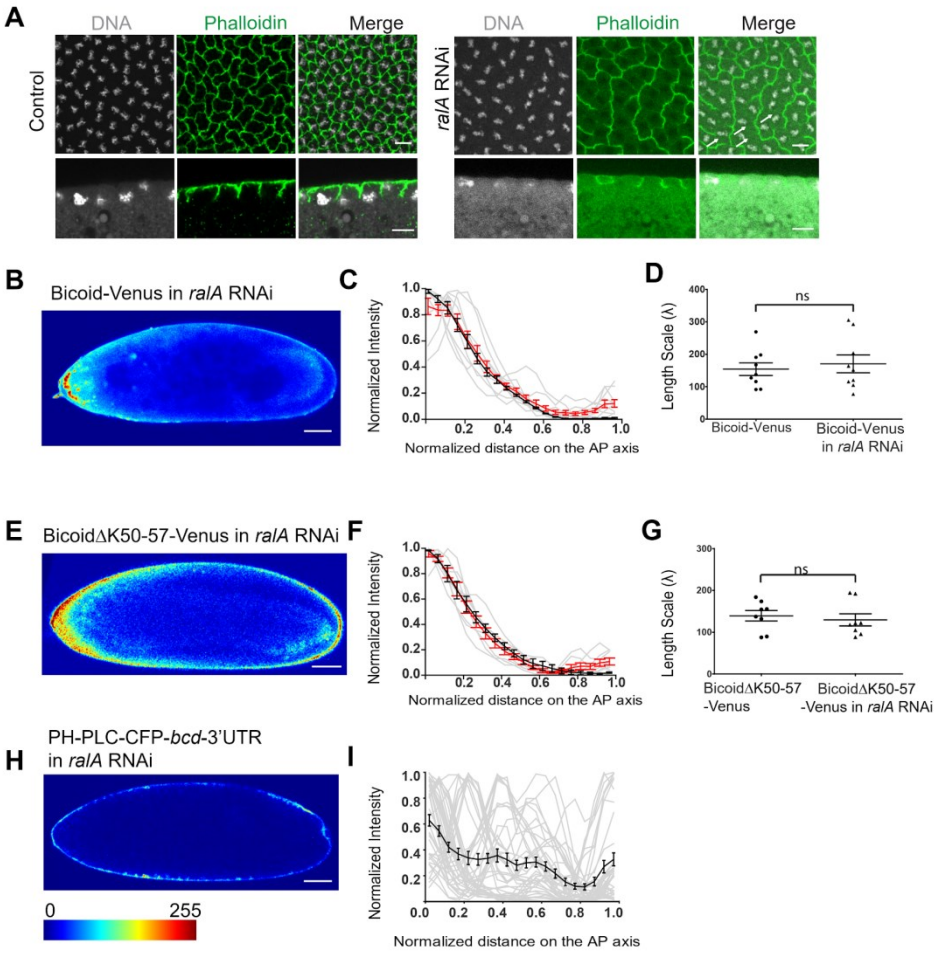

Figure 6.5: Anteriorly localized PH-PLC-CFP gradient is lost in *ralA* mutant embryos as compared to Bicoid
(A): *ralA* RNAi mediated knockdown embryos show loss of metaphase furrows: Sagittal and surface views of fixed control or *ralA* RNAi expressing embryos, stained with DNA (Grey) and Phalloidin (Green) , show intermittent loss of furrows upon *ralA* RNAi expression (n=80% of 30 embryos analysed show this effect). Scale bar=10µm.
(B-D): Analysis of Bicoid gradient in *ralA* RNAi expressing embryos. Bicoid-Venus expression is shown in a snapshot from a time lapse movie of an embryo expressing *ralA* RNAi **(B)**. Quantification of the Bicoid-Venus gradient with grey lines in the background (red line represents average±SEM) showing line profiles across different embryos analysed, black line represents average of control embryos with ±SEM **(C)**. Scatter plot shows length scale (λ) values extracted by fitting an exponential decay equation **(D)** (terminal time points from n=5 embryos each, Scale bar=50µm, two-tailed non-parametric Mann Whitney test, p-value=0.8633)

(E-G): Analysis of BicoidΔK50-57-Venus gradient in *ralA* RNAi expressing embryos. BicoidΔK50-57-Venus expression is shown in a snapshot from a time lapse movie of an embryo expressing *ralA* RNAi **(E)**. Quantification of the BicoidΔK50-57-Venus gradient with grey lines in the background (red line represents average±SEM) showing line profiles across different embryos analysed, black line represents average of control with ±SEM **(F)**. Scatter plot shows length scale (λ) values extracted by fitting an exponential decay equation **(G)** (terminal time points from n=4 embryos each, Scale bar=50µm, two-tailed non-parametric Mann Whitney test, p-value=0.6454).
(H-I): Analysis of anteriorly localized PH-PLC-CFP gradient in *ralA* RNAi expressing embryos. PH-PLC-CFP-*bcd*-3'UTR expression is shown in a snapshot from a time lapse movie of an embryo expressing *ralA* RNAi **(H)**. Quantification of the PH-PLC-CFP gradient with grey lines in the background showing line profiles across different embryos analysed, black line represents average with ±SEM**(I)**, scale bar=50µm, n=5 time points from each of the 5 embryos.
The color scale is a 16 color rainbow where blue represents the lowest intensity and red represents the highest intensity.

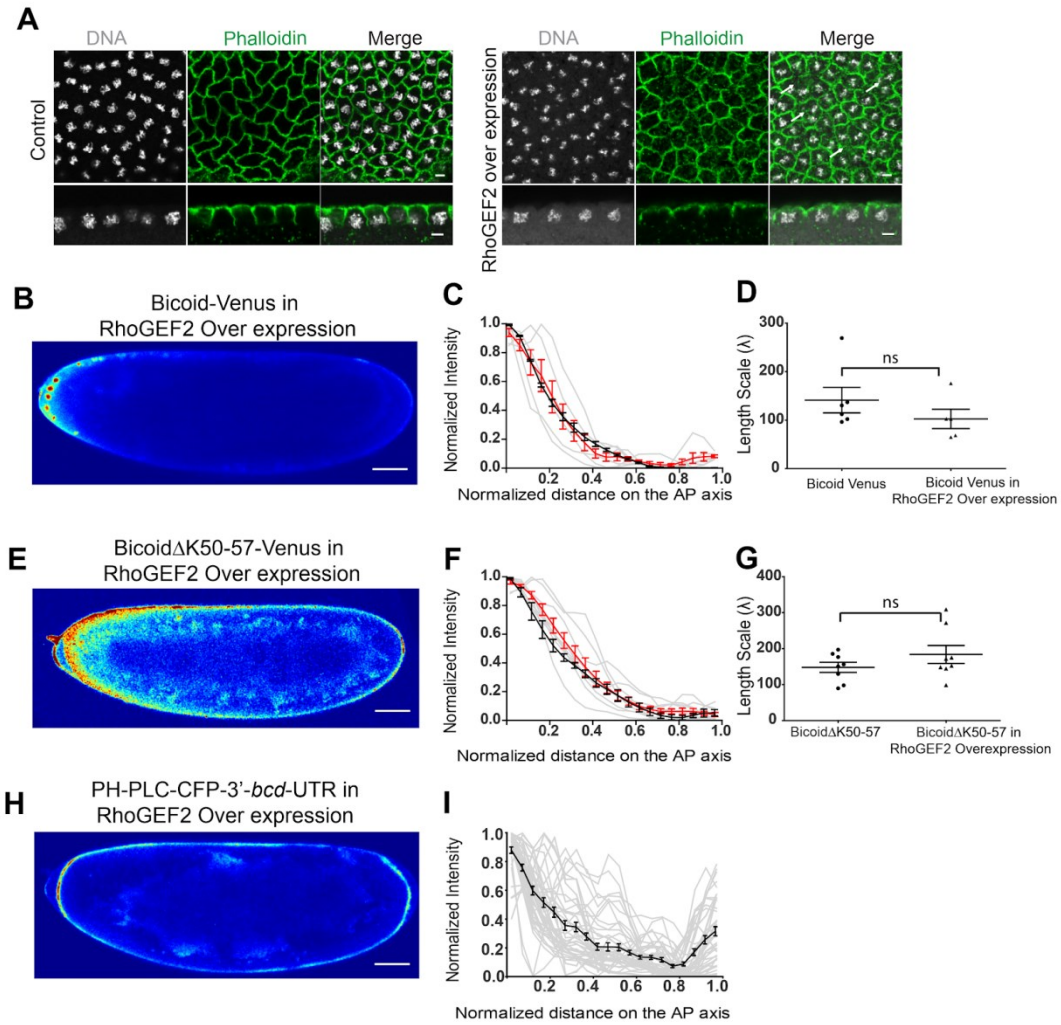

Figure 6.6: RhoGEF2 overexpression driven loss of metaphase furrows leads to loss of spread of anteriorly expressing PH-PLC-CFP gradient as compared to Bicoid

(A): Embryos overexpressing RhoGEF2show shorter metaphase furrows: Sagittal and surface views of fixed control or embryos overexpressing RhoGEF2, stained with DNA (Grey) and Phalloidin (Green), show shorter furrows upon RhoGEF2 overexpression (n=80% of 30 embryos analysed show this effect). Scale bar=10µm.
(B-D): Analysis of Bicoid gradient in embryos overexpressing RhoGEF2. Bicoid-Venus expression is shown in a snapshot from a time lapse movie of an embryo overexpressing RhoGEF2 **(B)**.Quantification of the Bicoid-Venus gradient with grey lines in the background (red line represents average±SEM) showing line profiles across different embryos analysed, black line represents average of control embryos with ±SEM **(C)**. Scatter plot shows length scale (λ) values extracted by fitting an exponential decay equation **(D)** (terminal multiple time points from n=3 embryos each, Scale bar=50µm, two-tailed non-parametric Mann Whitney test, p-value=0.2468)
(E-G): Analysis of BicoidΔK50-57-Venus gradient in embryos overexpressing RhoGEF2. BicoidΔK50-57-Venus expression is shown in a snapshot from a time lapse movie of an embryo expressing RhoGEF2 **(E)**. Quantification of the BicoidΔK50-57-Venus gradient with grey lines in the background (red line represents average±SEM) showing line profiles across different embryos analysed, black line represents average of control with ±SEM **(F)**. Scatter plot shows length scale (λ) values extracted by fitting an exponential decay equation **(G)**. (Terminal time points from n=4 embryos each, Scale bar=50µm, two-tailed non-parametric Mann Whitney test, p-value=0.5737)
(H-I): Analysis of anteriorly localized PH-PLC-CFP gradient in embryos overexpressing RhoGEF2. PH-PLC-CFP-*bcd*-3'UTR expression is shown in a snapshot from a time lapse movie of an embryo expressing RhoGEF2 **(H)**. Quantification of the PH-PLC-CFP gradient with grey lines in the background showing line profiles across different embryos analysed,black line represents average with ±SEM**(I)**, scale bar=50µm, n=15 time points from each of the 3 embryos.
The color scale is a 16 color rainbow where blue represents the lowest intensity and red represents the highest intensity.

6.3 Discussion

In this chapter, we have used the Bicoid gradient paradigm in syncytial *Drosophila* embryos as a model to test functional implications of cytoplasmic restriction and compartmentalization. We have compared it to plasma membrane associated PH-PLC-CFP which is expressed anteriorly like Bicoid. Anteriorly expressed PH-PLC-CFP and Bicoid gradient remained at the cortex even across the change in cytoarchitecture during each syncytial division cycle. Bicoid seems to equilibrate between furrow and also might bind to furrows or actin, though these observations are not yet rigorously tested. Actin remodelling regulated both PH-PLC-CFP and Bicoid gradients while pseudocleavage furrows affected the restriction of PH-PLC-CFP and not Bicoid (Figure 6.7).

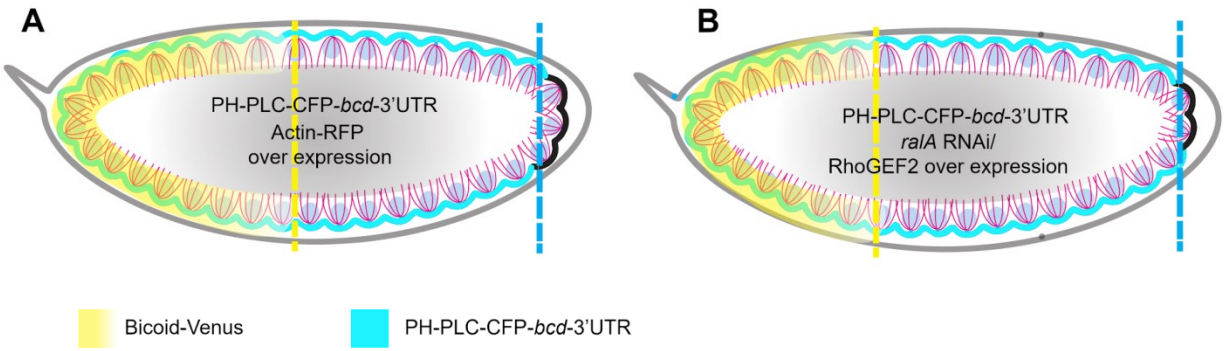

Figure 6.7: Schematic summarising the perturbation of PH-PLC and Bicoid gradient when cyto-architectural components are disrupted.

Anteriorly expressed cytoplasmic protein PH-PLC-CFP is restricted by plasma membrane furrows in mRFP-Actin **(A)** and RalA **(B)** as compared to Bicoid gradient.

Implications for Bicoid anterior-posterior gradient

The Bicoid gradient shows diffusion across energids and is not constrained by plasma membrane pseudocleavage furrows. The increased spread of the Bicoid gradient upon mRFP-Actin overexpression can be explained by considering the fact that the *bcd*-3'-UTR is tethered on actin (Weil et al., 2008). Actin polymerization defects may lead to decreased confinement of the *bicoid* mRNA thereby causing changes in the Bicoid gradient. Anteriorly expressed PH-PLC-CFP, similar to PH-PLC-CFP expressed throughout the embryo, is restricted by plasma membrane furrows (Mavrakis et al., 2009a). Therefore there are changes in its gradient shape under conditions that change furrow dynamics.

In addition to the SDD model, various cyto-architectural components in the early embryo may impinge on the effective diffusion of Bicoid. Bicoid might localize transiently or passively with actin (Lucchetta et al., 2008b), providing a possible mechanism leading to increase in the time spent near each energid and thus reducing its effective diffusion coefficient. Theoretical modelling studies show that presence of two rates, within and across energids, can account for the formation of Bicoid like gradient (Kavousanakis et al., 2010). Though these studies involve an obligate presence of nuclei, a Bicoid deletion mutant that abrogates nuclear shuttling, forms a gradient similar to the wild type (Grimm and Wieschaus, 2010). This suggests that the nuclei localization does not define the energids for Bicoid. We hypothesize that these two rates

are likely to come from free Bicoid and transient associations of Bicoid with the actin cytoskeleton. Though we show preliminary proof that Bicoid might associate with pseudocleavage furrows and equilibrates between furrows, the data strongly shows that pseudocleavage furrows are not the predominant contributor to the retention of Bicoid in each energid. Future analysis of disruption of other densely distributed cytoarchitectural components such as microtubules, ER or Golgi complexes (Frescas et al., 2006) will reveal if they impact the spread of Bicoid protein and mRNA in the syncytial blastoderm embryo.

Data in this study suggests that Bicoid protein spread is likely to be constrained by its interaction with various cytoplasmic/cytoarchitectural components, though not pseudocleavage furrows. This is not without precedence as studies with Homeobox transcription factors, Engrailed-1 and Engrailed-2 have shown specific non-nuclear subcellular localization (Joliot et al., 1997). The localization is dependent on a specific 11-amino acid sequence between the second and third helix of the homeodomain (Joliot et al., 1998). It would be interesting to test the domains of the Bicoid protein which are responsible for Bicoid association with cytoarchitecture.

Moreover, the presence of Bicoid (and PH-PLC) near the cortex across nuclear cycles also suggests that the effective volume in which Bicoid is diffusing might be much smaller than the whole embryo. This idea has been suggested earlier for Bicoid (Cai et al., 2017). We also know that cytoplasmic components are enriched cortically upto 35 to 40μm in the syncytial division cycles (Foe,Odell and Edgar, 1993; Chapter 3)

Implication for morphogen gradients

Even though this study uses the Bicoid gradient paradigm in the syncytial embryo, differential interactions of gradient molecules with cytoplasmic/extracellular components has implications for other gradients in other tissues. Dorsal , the dorso-ventral morphogen in the early embryo, is compartmentalized to nuclei in the syncytial embryo (Chen et al., 2012; DeLotto et al., 2007). Plasma membrane furrows and microtubules have been postulated to be important for the formation of its gradient through mathematical modelling. Moreover, monomeric versus weakly dimerizing GFP tagged to Dorsal causes a change in the gradient shape, implying a role for the protein size and

binding on gradient dynamics (Carrell et al., 2016). For another nuclear transcription factor Torso, nuclei are obligately involved for gradient shape. Disrupting nuclear patterning using *shakleton* mutants for example, can change the gradient shape (Coppey et al., 2008).

Fibroblast Growth Factor (FGF) gradient in zebrafish and cultured fibroblasts, also depends on extracellularly present Heparan sulfate proteoglycans (HPSGs). FGFs reversibly bind to HSPGs and disruption of this interaction leads to a dramatically increased spread (Balasubramanian and Zhang, 2016). In the wing disc, the formation of Dpp gradient is also postulated to depend on HSPGs, like Dally, which bind Dpp and may slow it down or prevent its movement out of the epithelial plane, thus reducing its effective diffusion (Müller et al., 2013). These studies imply a role on tortuosity and hindered diffusion as contributive factors for gradient spread (Müller et al., 2013). It would be interesting to see, for example, Dorsal gradient dynamics in a nuclear import deficient Dorsal mutant or when furrows or organelles like ER/Golgi are perturbed.

In summary, this chapter brings to light the importance of morphogen binding, cytoplasmic and cytoskeletal milieu and tortuosity in regulating Bicoid morphogen gradient spread in the syncytial *Drosophila* embryo.

6.4 Supplementary Movies

Mov6.S1: Bicoid-Venus-deltaK

BicoidΔK50-57 tagged to Venus under the Bicoid endogenous promoter imaged across the syncytial division cycles 11-14. Anterior is to the left. BicoidΔK50-57 gradient can be seen in the AP axis. BicoidΔK50-57 signal is seen in the cytoplasm in both interphase and metaphase.

Mov6.S2: Bicoid-Venus in Act-RFP OE

Bicoid-Venus expressed and imaged in an embryo over expressing Actin-RFP across syncytial cycles 11-13. Anterior is to the left. The embryo undergoes many rounds of contraction and the gradient is disrupted.

Mov6.S3: *nos*-Gal4>UASp-PH-PLC-CFP-*bcd*-3'UTR in Act-RFP OE

UASp-PH-PLC-CFP-*bcd*-3'UTR expressed and imaged in an embryo over expressing Actin-RFP across syncytial cycles 11-13. Anterior is to the left. The interphase and metaphase furrows are absent in most of the embryo. The embryo undergoes contraction and the gradient is disrupted.

Mov6.S4: Bicoid-Venus in *ralA* RNAi
Bicoid-Venus expressed and imaged in an embryo expressing *ralA* RNAi across syncytial cycles 12-14. Anterior is to the left. Even though the embryo undergoes many rounds of contraction, the gradient is not disrupted.

Mov6.S5: BicoidΔK50-57-Venus in *ralA* RNAi
BicoidΔK50-57-Venus expressed and imaged in an embryo expressing *ralA* RNAi across syncytial cycles 12-14. Anterior is to the left. Even though the embryo undergoes many rounds of contraction, the gradient is not disrupted.

Mov6.S6: *mat*-Gal4>UASp-PH-PLC-CFP-*bcd*-3'UTR in *ralA* RNAi
UASp-PH-PLC-CFP-*bcd*-3'UTR expressed and imaged in an embryo expressing *ralA* RNAi across syncytial cycles 11-14. Anterior is to the left. The interphase and metaphase furrows are absent in most of the embryo. The embryo undergoes contraction and the gradient is disrupted.

Thesis Summary and Future perspective

Significance of the work

Our understanding of the cytoplasm as a complex, inhomogeneous, gel-like medium has evolved since the 1980's (Luby-Phelps, 2000; Luby-Phelps, 2013). Seminal studies on size based restriction and compartmentalization of inert tracers (Luby-Phelps et al., 1987), followed by characterization of cellular components which mediate this (Provance et al., 1993), have helped us understand the complexities of cytoplasm inside cells. Studies on diffusion and viscosity changes inside cells (Baum et al., 2014) and in the early *Drosophila* embryo syncytium (Gregor et al., 2005; Wessel et al., 2015) have also helped characterize general cytoplasmic properties. However, there seemed to be a need for a detailed understanding of cytoplasmic distribution, diffusion & restriction and how these properties correlate with developmental stages of the embryo. Our work address these aspects in a simplified way (Chapter 3).

Some aspects of cell theory, centered on understanding the origins of eukaryotic cell postulated models like "inside out model of the cell" and energids (Baum et al., 2014; Sachs, 1892), wherein a single nucleus has influence over a region of cytoplasm with or without the presence of cell boundaries. This concept has been well studied in syncytia where the absence of concrete boundaries between cells allow testing for cytoplasmic compartmentalization. Compartmentalization has been studied in plant endosperm (Boisnard-Lorig et al., 2001), muscle cells (Pavlath et al., 1989) and fungi (Gladfelter et al., 2006), while in the embryo compartmentalization is known for ER, Golgi (Frescas et al., 2006) and plasma membrane (Mavrakis et al., 2009a). Cytoplasmic compartmentalization is known from certain long germ band insects, though not through studies on cytoplasmic dynamics (Ho et al., 1997). We attempted to test diffusion and restriction of cytoplasm in the early *Drosophila* embryo (Chapter 3).

Another postulate of cytoplasmic restriction and presence of energids is that binding to existing cyto-architectural structures can mediate restriction. Modelling studies have predicted that microtubule based association is sufficient for compartmentalizing the cytoplasm (Chen et al., 2012). Binding and size based

restriction of diffusion has been shown for some morphogens in the embryo (Asafen et al., 2018). We have tried to test this idea in detail in this study with our experiments using Lifeact-GFP (Chapter 3), PA-GFP-Tubulin (Chapter 4) and ectopic gradients (Chapter 5).

The role of yolk in the early embryo has also been studied earlier. It is known how yolk functions as an energy source, how it is developmentally deposited in the egg, and how it is used in the egg to release energy (DiMario and Mahowald, 1987; Fagotto, 1995; Kuhn et al., 2015). However the role of yolk as a passive barriers to cytoplasm and as an inert biophysical component which is subject to mechanical forces in the embryo is not yet well characterized, except in zebrafish (Shamipour et al., 2019). Our work is an attempt towards a deeper understanding of the same (Chapter 3).

Graded distribution of molecules is a well studied feature of reaction diffusion systems and inherently provides opportunities for studying cytoplasmic restriction. Many studies have used the anterior localization of molecules to create such graded distribution (Benoit et al., 2009; Gregor et al., 2008; Zhang et al., 2004). The major focus of such studies have been the molecules in question per se, rather than the implications of such experiments on the cytoplasm in general. Our study using photoactivation at the anterior pole (Chapter 4) and genetically targeting of fluorescent probes at the anterior pole (Chapter 5) have helped us understand general properties of the cytoplasm and how size and binding based restriction takes place.

Studies on the anterior-posterior morphogen gradient Bicoid have been instrumental in dissecting the role of nuclei (Grimm and Wieschaus, 2010) and actin (Lucchetta et al., 2008a) in the formation of this gradient, while theoretical modelling based studies have suggested formation of Bicoid in context of the energids (Kavousanakis et al., 2010). We have elucidated the role that cytoplasmic restriction and diffusion play in formation of Bicoid gradient (Chapter 6).

Results and future perspectives

Distribution and dynamics of cytoplasm in the embryo

Our results using sagittal imaging of various fluorescently tagged transgenes over developmental time in the early embryo (Chapter 3) show that during the syncytial blastoderm nuclear cycles 10 to 13, cytoplasm is enriched near the cortex. The extent of the depth as well as the intensity (and hence the concentration) increases as the nuclear cycles progress. This is also correlated with our observation of PA-GFP and PA-GFP-Tubulin enrichment in these regions during the same cycles (Chapter 4). The formation of these phases over the bulk yolk is similar to cytoplasmic restriction of tracers of various sizes seen in cells (Luby-Phelps et al., 1987). How does the cytoplasm get enriched cortically? This is an interesting direction to follow in the future. Studies in Medaka, highlight the separation of cytoplasm from the bulk of the embryo, including the movement of lipid droplets (Abraham et al., 1993). It is also known that myosin contractility positions the mouse nucleus in the oocyte in the absence of centrosomes, and this leads to fluidization of the cytoplasm (Almonacid et al., 2015).

In the early *Drosophila* embryo, it will be exciting to use mutants and test for disruption of this cortical enrichment, such as *halo* wherein the lipid droplets remain apically enriched (Arora et al., 2016) or microtubule mutants like *eb1* (Chapter 4) where the extent of yolk compaction might become limited. These will be a good starting point to check if such cortical enrichment is of any functional significance.

Further, our results suggest that local diffusion is generally similar across various depths in the syncytial blastoderm near the cortex (Chapter 3). This is contrary to the observation that the viscosity of the cytoplasm is ~1000 times that of water in the region between the nuclear layer and the yolk (Wessel et al., 2015). It would be interesting to use sensitive methods like FCS to check diffusion at different depths during this phase. One can also elucidate contributors to this viscosity by perturbing specific cyto-architectural components. It is also worthwhile to probe the functional implications of viscosity in the embryo. For example, unlike *Drosophila* embryo, C.elegans embryos are known to not vary in viscoelasticity in the AP axis and therefore their mitotic spindle positioning is driven by asymmetric forces rather than asymmetric viscosity (Daniels et

al., 2006).

The observations of yolk compaction and its dynamics are the first characterization of this phenomenon in the *Drosophila* embryo, to our knowledge (Chapter 3). We find that yolk particles become gradually compacted towards the centre of the embryo over nuclear cycles 10 to 13. We also notice that this motion is not sudden but instead proceeds gradually during each interphase and metaphase, only to relax and move cortically during telophase, before finally compacting again. Further characterization of this motion can include finding cyto-architectural components which mediate this compaction. Are furrows/ microtubules/ microtubule based motors involved in this phenomenon? It is also known that yolk particles change shape under shear stresses and thereby are excluded from the cytoplasmic phase in Zebrafish embryos (Beams et al., 1985). Functionally how does this affect cytoplasmic enrichment and moreover, morphogen gradients is also an important question.

Role of cyto-architecture in restricting diffusion

Our results suggest that apical diffusion between energids is restricted while diffusion basally is generally free, during interphase (Chapter 3). What impact does the nascent plasma membrane have on this diffusion?Is this mediated by microtubule based crowding? Using mutants such as *ralA* (Holly et al., 2015), which restricts the formation of these membranes, it is possible to tease apart the relative contributions of cytoarchitecture on diffusion.

Our photoactivation experiments suggest that binding to architecture can impede diffusion and thereby spread of probes, as illustrated by PA-GFP-Tubulin spreading less than PA-GFP in the AP direction (Chapter 4). Though this does not control for the size of the probes, it corroborates our results with LifeAct-GFP and mRFP, where LifeAct-GFP is on the same size scale as mRFP and yet is more restricted to each energid (Chapter 3). Moreover, the comparison of anteriorly localized PH-PLC with anteriorly localized mRFP, 5XGFP and 8XGFP gradients (Chapter 5) also indicates that binding restricts the spread of molecules to near each energid.

Taken together, these results suggest that binding to existing architecture is a way to compartmentalize the cytoplasm. Future questions in this direction can include

checking if further restriction in diffusion would lead to smaller length scales. PA-Toll is another probe which has been used earlier in the embryo (Mavrakis et al., 2009a) and can be used in this regard.

Interestingly the length scale observed upon activation at the centre is significantly and consistently different from that of the anterior and posterior activation. How this is brought about is another interesting direction, which will include using embryos of different aspect ratios, as reported earlier (Rupprecht et al., 2017). Another important question is to test the role of degradation in these ectopic gradient ofphotoactivated probes, and anteriorly tagged ectopic probes. These can be performed by using injection of proteasomal inhibitors, which have been seen to perturb the Bicoid gradient in a related study (Durrieu et al., 2018).

Cyto-architecture and its impact on morphogen gradients

Finally, our analysis of the Bicoid gradient, shows that it is enriched cortically (Chapter 6) similar to other cytoplasmic probes (Chapter 3) and Photoactivatable probes (Chapter 4). It also corroborates previous results which show such cortical enrichment of Bicoid, though under hypoxic conditions (Cai et al., 2017). What biological significance does this enrichment have? It would be interesting to look for mutants which show reduction in the size of this cortical region of enrichment. This can be followed by observation of developmental changes in these mutants, if any, that may be brought about due to change in concentration of morphogens, namely Biocid and Dorsal, in the cortical region. One may also conduct interesting experiments by injecting high molecular weight, diffusion hindering molecules like Ficoll (Luby-Phelps et al., 1987). This could reduce the effective volume of diffusion in the cortical region and it can be observed how these gradients maneuver around the ficoll based obstruction to spread in the embryo.

Our analysis did not find any significant change in Bicoid gradient spread when the pseudo-cleavage furrows are perturbed. This may suggests that pseudo-cleavage furrows play only a minor role in limiting the extent of diffusion in the cortical region of the early embryo. We know that the developmental time spent in metaphase (where these furrows are seen) is much smaller when compared to time spent in interphase

(Foe and Alberts, 1983; Gregor et al., 2007). The diffusion of morphogens might be taking place predominantly in interphase and hence we observed no effect of this perturbation. In the future, experiments can be performed to observe Bicoid gradient dynamics in gradients which perturb ER or Golgi architecture as these occupy significant volume of the cortical cytoplasmic space (Frescas et al., 2006).

Limitations of the study

Our compilation currently has the limitation of not using any embryo injection based experiments. This can be pursued in the future as compartmentalization can be easily tested upon injection of fluorescent beads or tracers of different sizes. This has been done earlier but with a different experimental focus (Roth, 1993). Also our understanding of the mechanism of gradient formation for photoactivatable and anteriorly tagged probes is limited by not being able to perturb degradation rates, as has been done elsewhere (Durrieu et al., 2018). Hence we assume the applicability of SDD model and its resultant equations, or assume low degradation rates, considering these are ectopic probes. This can be verified by injection based inhibition of degradation. Further, our current estimates of the Bicoid length scale vary systematically from reported values, probably due to some microscopy based corrections which have not yet been considered. We are currently trying to improve our estimates in consultation with our collaborators.

In conclusion, we have attempted to characterize the cytoplasmic distribution, dynamics and the role of cyto-architecture on these properties in the *Drosophila* early syncytial embryo.Our study highlights how intra-cellular crowding, binding & association with cyto-architecture and restricted diffusion, together define cytoplasmic properties which ultimately characterize functional properties in the cell.

References

Abraham, V. C., Gupta, S. and Fluck, R. A.(1993). Ooplasmic Segregation in the Medaka (Oryzias latipes) Egg.*Biol. Bull.***184**, 115–124.

Abu-Arish, A., Porcher, A., Czerwonka, A., Dostatni, N. and Fradin, C. (2010). High mobility of bicoid captured by fluorescence correlation spectroscopy: implication for the rapid establishment of its gradient. *Biophys.J.***99**, L33–5.

Aizawa, H., Sameshima, M. and Yahara, I.(1997). A Green Fluorescent Protein-actin Fusion Protein Dominantly Inhibits Cytokinesis, Cell Spreading, and Locomotion in Dictyostelium.*Cell Struct.Funct.***22**, 335–345.

Ali-Murthy, Z. and Kornberg, T. B. (2016). Bicoid gradient formation and function in the *Drosophila* pre-syncytial blastoderm. *Elife***5**,.

Almonacid, M., Ahmed, W. W., Bussonnier, M., Mailly, P., Betz, T., Voituriez, R., Gov, N. S. and Verlhac, M.-H. (2015). Active diffusion positions the nucleus in mouse oocytes. *Nat. Cell Biol.***17**, 470–479.

Anderson, C. A., Eser, U., Korndorf, T., Borsuk, M. E., Skotheim, J. M. and Gladfelter, A. S. (2013). Nuclear Repulsion Enables Division Autonomy in a Single Cytoplasm. *Current Biology***23**, 1999–2010.

Apel, E. D., Lewis, R. M., Grady, R. M. and Sanes, J. R. (2000). Syne-1, a dystrophin- and Klarsicht-related protein associated with synaptic nuclei at the neuromuscular junction. *J. Biol. Chem.***275**, 31986–31995.

Arora, G. K., Tran, S. L., Rizzo, N., Jain, A. and Welte, M. A. (2016). Temporal control of bidirectional lipid-droplet motion in *Drosophila* depends on the ratio of kinesin-1 and its co-factor Halo. *J. Cell Sci.***129**, 1416–1428.

Asafen, H. A., Al Asafen, H., Clark, N. M., Jacobsen, T., Sozzani, R. and Reeves, G. (2018). Dorsal/NF-κB exhibits a dorsal-to-ventral mobility gradient in the *Drosophila* embryo.

Ault, J. G., DeMarco, A. J., Salmon, E. D. and Rieder, C. L. (1991). Studies on the ejection properties of asters: astral microtubule turnover influences the oscillatory behavior and positioning of mono-oriented chromosomes. *J. Cell Sci.***99(Pt 4)**, 701–710.

Balasubramanian, R. and Zhang, X.(2016). Mechanisms of FGF gradient formation during embryogenesis.*Semin. Cell Dev. Biol.***53**, 94–100.

Baluska, F., Volkmann, D. and Barlow, P. W. (2004). Eukaryotic cells and their cell bodies: Cell Theory revised. *Ann. Bot.***94**, 9–32.

Baluska, F., Volkmann, D. and Barlow, P. W.(2006). Cell-Cell Channels and Their Implications for Cell Theory. In *Cell-Cell Channels* (ed. Baluska, F.), Volkmann, D.), and Barlow, P. W.), pp. 1–18. New York, NY: Springer New York.

Barmchi, M. P., Rogers, S. and Häcker, U. (2005). DRhoGEF2 regulates actin organization and contractility in the *Drosophila* blastoderm embryo. *J. Cell Biol.***168**, 575–585.

Baum, D. A. and Baum, B. (2014). An inside-out origin for the eukaryotic cell. *BMC Biol.***12**, 76.

Baum, M., Erdel, F., Wachsmuth, M. and Rippe, K. (2014). Retrieving the intracellular topology from multi-scale protein mobility mapping in living cells. *Nat. Commun.***5**, 4494.

Beams, H. W., Kessel, R. G., Shih, C. Y. and Tung, H. N. (1985). Scanning electron microscope studies on blastodisc formation in the zebrafish,Brachydanio rerio. *J. Morphol.***184**, 41–49.

Benoit, B., He, C. H., Zhang, F., Votruba, S. M., Tadros, W., Westwood, J. T., Smibert, C. A., Lipshitz, H. D. and Theurkauf, W. E. (2009). An essential role for the RNA-binding protein Smaug during the *Drosophila* maternal-to-zygotic transition. *Development***136**, 923–932.

Bergmann, S., Sandler, O., Sberro, H., Shnider, S., Schejter, E., Shilo, B.-Z. and Barkai, N.(2007). Pre-steady-state decoding of the Bicoid morphogen gradient.*PLoS Biol.***5**, e46.

Berleth, T., Burri, M., Thoma, G., Bopp, D., Richstein, S., Frigerio, G., Noll, M. and Nüsslein-Volhard, C. (1988). The role of localization of bicoid RNA in organizing the anterior pattern of the *Drosophila* embryo. *EMBO J.***7**, 1749–1756.

Blankenship, J. T. and Wieschaus, E.(2001). Two new roles for the *Drosophila* AP patterning system in early morphogenesis.*Development***128**, 5129–5138.

Boisnard-Lorig, C., Colon-Carmona, A., Bauch, M., Hodge, S., Doerner, P., Bancharel, E., Dumas, C., Haseloff, J. and Berger, F. (2001). Dynamic analyses of the expression of the HISTONE::YFP fusion protein in arabidopsis show that syncytial endosperm is divided in mitotic domains. *Plant Cell***13**, 495–509.

Bownes, M., Dempster, M. and Blair, M.(1983). Expression of the yolk-protein genes in the mutant doublesex dominant (dsxD) of *Drosophila* melanogaster.*J. Embryol. Exp. Morphol.***75**, 241–257.

Bownes, M., Lineruth, K. and Mauchline, D. (1991). Egg production and fertility in *Drosophila* depend upon the number of yolk-protein gene copies. *Mol. Gen. Genet.***228**, 324–327.

Bownes, M., Hurd, H., Busgen, T., Servay, D., Alvis, S., Popovic, B., Bruce, S., Burns, I., Rothwell, K. and Walkinshaw, M. (2002). *Drosophila* yolk protein produced in E. coli is accumulated by mosquito ovaries. *Insect Molecular Biology***11**, 487–496.

Bownes M, E. al (1983). Expression of the yolk-protein genes in the mutant doublesex dominant (dsxD) of *Drosophila* melanogaster.

Brenner, H. R., Witzemann, V. and Sakmann, B. (1990). Imprinting of acetylcholine receptor messenger RNA accumulation in mammalian neuromuscular synapses. *Nature***344**, 544–547.

Brown, R. C. and Lemmon, B. E.(2008). Microtubules in early development of the megagametophyte of Ginkgo biloba.*J. Plant Res.***121**, 397–406.

Brown, R. C., Lemmon, B. E. and Nguyen, H. (2003). Events during the first four rounds of mitosis establish three developmental domains in the syncytial endosperm of Arabidopsis thaliana. *Protoplasma***222**, 167–174.

Butterworth, F. M. (1999). A yolk protein mutant leads to defects in the secretion machinery of*Drosophila* melanogaster. *Tissue and Cell***31**, 212–222.

Cai, X., Akber, M., Spirov, A. and Baumgartner, S. (2017). Cortical movement of Bicoid in early *Drosophila* embryos is actin- and microtubule-dependent and disagrees with the SDD diffusion model. *PLoS One***12**, e0185443.

Cao, J., Albertson, R., Riggs, B., Field, C. M. and Sullivan, W. (2008). Nuf, a Rab11 effector, maintains cytokinetic furrow integrity by promoting local actin polymerization. *J. Cell Biol.***182**, 301–313.

Cao, J., Crest, J., Fasulo, B. and Sullivan, W. (2010). Cortical actin dynamics facilitate early-stage centrosome separation. *Curr.Biol.***20**, 770–776.

Carrell, S. N., O'Connell, M. D., Allen, A. E., Smith, S. M. and Reeves, G. (2016). A Facilitated Diffusion Mechanism Establishes the *Drosophila* Dorsal Gradient.

Carrell, S. N., O'Connell, M. D., Jacobsen, T., Allen, A. E., Smith, S. M. and Reeves, G. T. (2017). A facilitated diffusion mechanism establishes the *Drosophila* Dorsal gradient. *Development* dev.155549.

Chen, J., Lippincott-Schwartz, J. and Liu, J.(2012). Intracellular spatial localization regulated by the microtubule network.*PLoS One***7**, e34919.

Chowdhary, S., Tomer, D., Dubal, D., Sambre, D. and Rikhy, R.(2017). Analysis of mitochondrial organization and function in the *Drosophila* blastoderm embryo.*Sci. Rep.***7**, 5502.

Christian, J. L. (2012). Morphogen gradients in development: from form to function. *Wiley Interdiscip. Rev. Dev. Biol.***1**, 3–15.

Colicelli, J.(2004). Human RAS Superfamily Proteins and Related GTPases.*Sci. Signal.***2004**, re13–re13.

Coppey, M., Boettiger, A. N., Berezhkovskii, A. M. and Shvartsman, S. Y. (2008). Nuclear trapping shapes the terminal gradient in the *Drosophila* embryo. *Curr.Biol.***18**, 915–919.

Couteaux, R. and Pécot-Dechavassine, M.(1973). [Ultrastructural and cytochemical data on the mechanism of acetylcholine release in synaptic transmission]].*Arch. Ital. Biol.***111**, 231–262.

Crest, J., Concha-Moore, K. and Sullivan, W. (2012). RhoGEF and Positioning of Rappaport-like Furrows in the Early *Drosophila* Embryo. *Curr.Biol.***22**, 2037–2041.

Crick, F.(1970). Diffusion in embryogenesis.

Cutler, A. A., Jackson, J. B., Corbett, A. H. and Pavlath, G. K.(2018). Non-equivalence of nuclear import among nuclei in multinucleated skeletal muscle cells.*Journal of Cell Science***131**, jcs207670.

Daniels, B. R., Masi, B. C. and Wirtz, D. (2006). Probing single-cell micromechanics in vivo: the microrheology of C. elegans developing embryos. *Biophys.J.***90**, 4712–4719.

Daniels, B. R., Rikhy, R., Renz, M., Dobrowsky, T. M. and Lippincott-Schwartz, J.(2012). Multiscale diffusion in the mitotic *Drosophila* melanogaster syncytial blastoderm.*Proc. Natl. Acad. Sci. U. S. A.***109**, 8588–8593.

DeLotto, R., DeLotto, Y., Steward, R. and Lippincott-Schwartz, J. (2007). Nucleocytoplasmic shuttling mediates the dynamic maintenance of nuclear Dorsal levels during *Drosophila* embryogenesis. *Development***134**, 4233–4241.

DiMario, P. J. and Mahowald, A. P. (1987). Female sterile (1) yolkless: a recessive female sterile mutation in *Drosophila* melanogaster with depressed numbers of coated pits and coated vesicles within the developing oocytes. *J. Cell Biol.***105**, 199–206.

Driever, W. and Nüsslein-Volhard, C.(1988a). A gradient of bicoid protein in *Drosophila* embryos.*Cell***54**, 83–93.

Driever, W. and Nüsslein-Volhard, C. (1988b). The bicoid protein determines position in the *Drosophila* embryo in a concentration-dependent manner. *Cell***54**, 95–104.

Drocco, J. A., Grimm, O., Tank, D. W. and Wieschaus, E. (2011). Measurement and perturbation of morphogen lifetime: effects on gradient shape. *Biophys.J.***101**, 1807–1815.

Dubrulle, J. and Pourquié, O. (2004). fgf8 mRNA decay establishes a gradient that couples axial elongation to patterning in the vertebrate embryo. *Nature***427**, 419–422.

Dundon, S. E. R., Chang, S.-S., Kumar, A., Occhipinti, P., Shroff, H., Roper, M. and Gladfelter, A. S. (2016). Clustered nuclei maintain autonomy and nucleocytoplasmic ratio control in a syncytium. *Molecular Biology of the Cell***27**, 2000–2007.

Durrieu, L., Kirrmaier, D., Schneidt, T., Kats, I., Raghavan, S., Hufnagel, L., Saunders, T. E. and Knop, M.(2018). Bicoid gradient formation mechanism and dynamics revealed by protein lifetime analysis.*Mol. Syst. Biol.***14**, e8355.

Edgar, B. A., Odell, G. M. and Schubiger, G.(1987). Cytoarchitecture and the patterning of fushi tarazu expression in the *Drosophila* blastoderm.*Genes Dev.***1**, 1226–1237.

Entchev, E. V., Schwabedissen, A. and González-Gaitán, M.(2000). Gradient formation of the TGF-beta homolog Dpp. *Cell***103**, 981–991.

Ephrussi, A. and Lehmann, R. (1992). Induction of germ cell formation by oskar. *Nature***358**, 387–392.

Fagotto, F.(1995). Regulation of yolk degradation, or how to make sleepy lysosomes.*J. Cell Sci.***108(Pt 12)**, 3645–3647.

Fahmy, K., Akber, M., Cai, X., Koul, A., Hayder, A. and Baumgartner, S. (2014). αTubulin 67C and Ncd are essential for establishing a cortical microtubular network and formation of the Bicoid mRNA gradient in *Drosophila*. *PLoS One***9**, e112053.

Figard, L., Xu, H., Garcia, H. G., Golding, I. and Sokac, A. M. (2013). The plasma membrane flattens out to fuel cell-surface growth during *Drosophila* cellularization. *Dev. Cell***27**, 648–655.

Foe, V. E. and Alberts, B. M.(1983). Studies of nuclear and cytoplasmic behaviour during the

five mitotic cycles that precede gastrulation in *Drosophila* embryogenesis.*J. Cell Sci.***61**, 31–70.

Foe, V. E., Field, C. M. and Odell, G. M. (2000). Microtubules and mitotic cycle phase modulate spatiotemporal distributions of F-actin and myosin II in *Drosophila* syncytial blastoderm embryos. *Development*.

Foe,Odell and Edgar (1993). Mitosis and morphogenesis in the *Drosophila* embryo: point and counterpoint. In *The Development of Drosophila melanogaster* (ed. Michael Bates, A. M. A.), pp. 149–300.Cold Spring Harbor Laboratory Press.

Fontaine, B.(1989). Localization of nicotinic acetylcholine receptor alpha-subunit transcripts during myogenesis and motor endplate development in the chick.*The Journal of Cell Biology***108**, 1025–1037.

Frescas, D., Mavrakis, M., Lorenz, H., Delotto, R. and Lippincott-Schwartz, J. (2006). The secretory membrane system in the *Drosophila* syncytial blastoderm embryo exists as functionally compartmentalized units around individual nuclei. *J. Cell Biol.***173**, 219–230.

Gauthier-Kemper, A., Weissmann, C., Reyher, H.-J.and Brandt, R. (2012). Monitoring cytoskeletal dynamics in living neurons using fluorescence photoactivation. *Methods Enzymol.***505**, 3–21.

Gladfelter, A. S. (2006). Nuclear anarchy: asynchronous mitosis in multinucleated fungal hyphae. *Curr.Opin.Microbiol.***9**, 547–552.

Gladfelter, A. S., Hungerbuehler, A. K. and Philippsen, P.(2006). Asynchronous nuclear division cycles in multinucleated cells.*J. Cell Biol.***172**, 347–362.

Goff, L. J. and Coleman, A. W. (1987). The solution to the cytological paradox of isomorphy. *J. Cell Biol.***104**, 739–748.

Goldman, R. D., Spector, D. L. and Masters, B. R.(2006). Live Cell Imaging, A Laboratory Manual.*Journal of Biomedical Optics***11**, 019901.

Goodsell, D. S. (2009). Miniseries: illustrating the machinery of life. *Escherichia coli.Biochem. Mol. Biol. Educ.***37**, 325–332.

Goodsell, D. S.(2011). Eukaryotic cell panorama.*Biochem. Mol. Biol. Educ.***39**, 91–101.

Goodsell, D. S. (2013). *The Machinery of Life*. Springer Science & Business Media.

Gregor, T., Bialek, W., de Ruyter van Steveninck, R. R., Tank, D. W. and Wieschaus, E. F.(2005). Diffusion and scaling during early embryonic pattern formation.*Proc. Natl. Acad. Sci. U. S. A.***102**, 18403–18407.

Gregor, T., Wieschaus, E. F., McGregor, A. P., Bialek, W. and Tank, D. W.(2007). Stability and nuclear dynamics of the bicoid morphogen gradient.*Cell***130**, 141–152.

Gregor, T., McGregor, A. P. and Wieschaus, E. F.(2008). Shape and function of the Bicoid morphogen gradient in dipteran species with different sized embryos.*Dev. Biol.***316**, 350–358.

Grimm, O. and Wieschaus, E. (2010). The Bicoid gradient is shaped independently of nuclei. *Development***137**, 2857–2862.

Grimm, O., Coppey, M. and Wieschaus, E. (2010). Modelling the Bicoid gradient. *Development***137**, 2253–2264.

Gritsman, K., Talbot, W. S. and Schier, A. F. (2000). Nodal signaling patterns the organizer. *Development***127**, 921–932.

Gura Sadovsky, R., Brielle, S., Kaganovich, D. and England, J. L.(2017). Measurement of Rapid Protein Diffusion in the Cytoplasm by Photo-Converted Intensity Profile Expansion.*Cell Rep.***18**, 2795–2806.

Hall, Z. W. and Ralston, E.(1989). Nuclear domains in muscle cells.*Cell***59**, 771–772.

Harden, N. (2002). Signaling pathways directing the movement and fusion of epithelial sheets: lessons from dorsal closure in *Drosophila*. *Differentiation***70**, 181–203.

He, F., Wen, Y., Cheung, D., Deng, J., Lu, L. J., Jiao, R. and Ma, J.(2010). Distance measurements via the morphogen gradient of Bicoid in *Drosophila* embryos.*BMC Dev. Biol.***10**, 80.

Hird, S.(1996). Cortical actin movements during the first cell cycle of the Caenorhabditis elegans embryo.*J. Cell Sci.***109(Pt 2)**, 525–533.

Ho, K., Dunin-Borkowski, O. M. and Akam, M. (1997). Cellularization in locust embryos occurs before blastoderm formation. *Development***124**, 2761–2768.

Holly, R. M., Mavor, L. M., Zuo, Z. and Blankenship, J. T. (2015). A rapid, membrane-dependent pathway directs furrow formation through RalA in the early *Drosophila* embryo. *Development***142**, 2316–2328.

Hotani, H. and Miyamoto, H.(1990). Dynamic features of microtubules as visualized by dark-field microscopy.*Adv. Biophys.***26**, 135–156.

Houchmandzadeh, B., Wieschaus, E. and Leibler, S.(2002). Establishment of developmental precision and proportions in the early *Drosophila* embryo.*Nature***415**, 798–802.

Houchmandzadeh, B., Wieschaus, E. and Leibler, S.(2005). Precise domain specification in the developing *Drosophila* embryo.*Phys. Rev. E Stat. Nonlin. Soft Matter Phys.***72**, 061920.

Huettner, A. F. (1923). The origin of the germ cells in *Drosophila* melanogaster. *J. Morphol.***37**, 385–423.

Hungerbuehler, A. K., Philippsen, P. and Gladfelter, A. S.(2007). Limited functional redundancy and oscillation of cyclins in multinucleated Ashbya gossypii fungal cells.*Eukaryot. Cell***6**, 473–486.

Janson, L. W., Ragsdale, K. and Luby-Phelps, K.(1996a). Mechanism and size cutoff for steric exclusion from actin-rich cytoplasmic domains.*Biophys.J.***71**, 1228–1234.

Janson, L. W., Ragsdale, K. and Luby-Phelps, K.(1996b). Mechanism and size cutoff for steric exclusion from actin-rich cytoplasmic domains.*Biophys.J.***71**, 1228–1234.

Jasmin, B. J., Lee, R. K. and Rotundo, R. L.(1993). Compartmentalization of acetylcholinesterase mRNA and enzyme at the vertebrate neuromuscular junction.*Neuron***11**, 467–477.

Joliot, A., Trembleau, A., Raposo, G., Calvet, S., Volovitch, M. and Prochiantz, A.(1997). Association of Engrailed homeoproteins with vesicles presenting caveolae-like properties.*Development***124**, 1865–1875.

Joliot, A., Maizel, A., Rosenberg, D., Trembleau, A., Dupas, S., Volovitch, M. and Prochiantz, A.(1998). Identification of a signal sequence necessary for the unconventional secretion of Engrailed homeoprotein.*Curr.Biol.***8**, 856–863.

Kanodia, J. S., Rikhy, R., Kim, Y., Lund, V. K., DeLotto, R., Lippincott-Schwartz, J. and Shvartsman, S. Y.(2009). Dynamics of the Dorsal morphogen gradient.*Proc. Natl. Acad. Sci. U. S. A.***106**, 21707–21712.

Karr, T. L.(1986). Organization of the cytoskeleton in early *Drosophila* embryos.*J. Cell Biol.***102**, 1494–1509.

Kavousanakis, M. E., Kanodia, J. S., Kim, Y., Kevrekidis, I. G. and Shvartsman, S. Y.(2010). A compartmental model for the bicoid gradient.*Dev. Biol.***345**, 12–17.

Kellogg, D. R., Mitchison, T. J. and Alberts, B. M.(1988). Behaviour of microtubules and actin filaments in living *Drosophila* embryos.*Development***103**, 675–686.

Kinsey, S. T., Locke, B. R. and Dillaman, R. M. (2011). Molecules in motion: influences of diffusion on metabolic structure and function in skeletal muscle. *Journal of Experimental Biology***214**, 263–274.

Kuhn, H., Sopko, R., Coughlin, M., Perrimon, N. and Mitchison, T. (2015). The Atg1-Tor pathway regulates yolk catabolism in *Drosophila* embryos. *Development***142**, 3869–3878.

Kuimova, M. K., Botchway, S. W., Parker, A. W., Balaz, M., Collins, H. A., Anderson, H. L., Suhling, K. and Ogilby, P. R. (2009). Imaging intracellular viscosity of a single cell during photoinduced cell death. *Nat. Chem.***1**, 69–73.

Lander, A. D., Nie, Q. and Wan, F. Y. M. (2002). Do morphogen gradients arise by diffusion? *Dev. Cell***2**, 785–796.

Lécuyer, E., Yoshida, H., Parthasarathy, N., Alm, C., Babak, T., Cerovina, T., Hughes, T. R., Tomancak, P. and Krause, H. M. (2007). Global analysis of mRNA localization reveals a prominent role in organizing cellular architecture and function. *Cell***131**, 174–187.

Lee, C., Zhang, H., Baker, A. E., Occhipinti, P., Borsuk, M. E. and Gladfelter, A. S. (2013). Protein aggregation behavior regulates cyclin transcript localization and cell-cycle control. *Dev. Cell***25**, 572–584.

Lippincott-Schwartz, J. and Patterson, G. H.(2003). Development and use of fluorescent protein markers in living cells.*Science***300**, 87–91.

Little, S. C., Tkačik, G., Kneeland, T. B., Wieschaus, E. F. and Gregor, T. (2011). The formation of the Bicoid morphogen gradient requires protein movement from anteriorly localized mRNA. *PLoS Biol.***9**, e1000596.

Little, S. C., Tikhonov, M. and Gregor, T. (2013). Precise developmental gene expression arises from globally stochastic transcriptional activity. *Cell***154**, 789–800.

Luby-Phelps, K. (2000). Cytoarchitecture and physical properties of cytoplasm: volume, viscosity, diffusion, intracellular surface area. *Int. Rev. Cytol.***192**, 189–221.

Luby-Phelps, K. (2013). The physical chemistry of cytoplasm and its influence on cell function: an update. *Mol. Biol. Cell***24**, 2593–2596.

Luby-Phelps, K. and Taylor, D. L.(1988). Subcellular compartmentalization by local differentiation of cytoplasmic structure.*Cell Motil. Cytoskeleton***10**, 28–37.

Luby-Phelps, K., Taylor, D. L. and Lanni, F. (1986a). Probing the structure of cytoplasm. *J. Cell Biol.***102**, 2015–2022.

Luby-Phelps, K., Taylor, D. L. and Lanni, F. (1986b). Probing the structure of cytoplasm. *J. Cell Biol.***102**, 2015–2022.

Luby-Phelps, K., Castle, P. E., Taylor, D. L. and Lanni, F.(1987). Hindered diffusion of inert tracer particles in the cytoplasm of mouse 3T3 cells.*Proc. Natl. Acad. Sci. U. S. A.***84**, 4910–4913.

Luby-Phelps, K., Lanni, F. and Taylor, D. L. (1988). The submicroscopic properties of cytoplasm as a determinant of cellular function. *Annu. Rev. Biophys. Biophys.Chem.***17**, 369–396.

Lucchetta, E. M., Vincent, M. E. and Ismagilov, R. F. (2008a). A Precise Bicoid Gradient Is Nonessential during Cycles 11–13 for Precise Patterning in the *Drosophila* Blastoderm. *PLoS ONE***3**, e3651.

Lucchetta, E. M., Vincent, M. E. and Ismagilov, R. F. (2008b). A precise Bicoid gradient is nonessential during cycles 11-13 for precise patterning in the *Drosophila* blastoderm. *PLoS One***3**, e3651.

Maddox, P. S. and Ladouceur, A.-M. (2015). Concentrating on the mitotic spindle. *The Journal of Cell Biology***210**, 691–693.

Mavrakis, M., Rikhy, R. and Lippincott-Schwartz, J. (2009a). Plasma membrane polarity and compartmentalization are established before cellularization in the fly embryo. *Dev. Cell***16**, 93–104.

Mavrakis, M., Rikhy, R. and Lippincott-Schwartz, J. (2009b). Cells within a cell: Insights into cellular architecture and polarization from the organization of the early fly embryo. *Commun.Integr.Biol.***2**, 313–314.

Mazumdar, A. and Mazumdar, M. (2002). How one becomes many: blastoderm cellularization in *Drosophila* melanogaster. *Bioessays***24**, 1012–1022.

Mir, M., Reimer, A., Haines, J. E., Li, X.-Y., Stadler, M., Garcia, H., Eisen, M. B. and Darzacq, X. (2017). Dense Bicoid hubs accentuate binding along the morphogen gradient. *Genes Dev.***31**, 1784–1794.

Moffatt, C. B. and Cohen-Fix, O. (2019). The Multiple Ways Nuclei Scale on a Multinucleated

Muscle Cell Scale. *Dev. Cell***49**, 3–5.

Moscoso, L. M., Chu, G. C., Gautam, M., Noakes, P. G., Merlie, J. P. and Sanes, J. R.(1995). Synapse-associated expression of an acetylcholine receptor-inducing protein, ARIA/heregulin, and its putative receptors, ErbB2 and ErbB3, in developing mammalian muscle.*Dev. Biol.***172**, 158–169.

Müller, P., Rogers, K. W., Yu, S. R., Brand, M. and Schier, A. F.(2013). Morphogen transport.*Development***140**, 1621–1638.

Newlands, S., Levitt, L. K., Robinson, C. S., Karpf, A. B., Hodgson, V. R., Wade, R. P. and Hardeman, E. C. (1998). Transcription occurs in pulses in muscle fibers. *Genes Dev.***12**, 2748–2758.

Ono, T., Ono, K., Mizukawa, K., Ohta, T., Tsuchiya, T. and Tsuda, M.(1994). Limited diffusibility of gene products directed by a single nucleus in the cytoplasm of multinucleated myofibres.*FEBS Lett.***337**, 18–22.

Otegui, M. and Staehelin, L. A. (2000). Cytokinesis in flowering plants: more than one way to divide a cell. *Curr.Opin. Plant Biol.***3**, 493–502.

Parry, B., Surovtsev, I., Cabeen, M., O'Hern, C., Dufresne, E. and Jacobs-Wagner, C. (2014a). Cellular Metabolism Fluidizes the Glassy Bacterial Cytoplasm. *Biophysical Journal***106**, 313a.

Parry, B. R., Surovtsev, I. V., Cabeen, M. T., O'Hern, C. S., Dufresne, E. R. and Jacobs-Wagner, C. (2014b). The bacterial cytoplasm has glass-like properties and is fluidized by metabolic activity. *Cell***156**, 183–194.

Pavlath, G. K., Rich, K., Webster, S. G. and Blau, H. M.(1989). Localization of muscle gene products in nuclear domains.*Nature***337**, 570–573.

Pickett-Heaps, J. D., Gunning, B. E., Brown, R. C., Lemmon, B. E. and Cleary, A. L. (1999). The cytoplast concept in dividing plant cells: cytoplasmic domains and the evolution of spatially organized cell. *Am. J. Bot.***86**, 153–172.

Porcher, A. and Dostatni, N. (2010). The bicoid morphogen system. *Curr.Biol.***20**, R249–54.

Provance, D. W., Jr, McDowall, A., Marko, M. and Luby-Phelps, K.(1993). Cytoarchitecture of size-excluding compartments in living cells.*J. Cell Sci.***106(Pt 2)**, 565–577.

Riedl, J., Crevenna, A. H., Kessenbrock, K., Yu, J. H., Neukirchen, D., Bista, M., Bradke, F., Jenne, D., Holak, T. A., Werb, Z., et al. (2008). Lifeact: a versatile marker to visualize F-actin. *Nat. Methods***5**, 605–607.

Rogers, K. W. and Schier, A. F. (2011). Morphogen gradients: from generation to interpretation. *Annu. Rev. Cell Dev. Biol.***27**, 377–407.

Rogers, S. L., Rogers, G. C., Sharp, D. J. and Vale, R. D. (2002). *Drosophila* EB1 is important for proper assembly, dynamics, and positioning of the mitotic spindle. *J. Cell Biol.***158**, 873–884.

Röper, K., Mao, Y. and Brown, N. H.(2005). Contribution of sequence variation in

*Drosophila*actins to their incorporation into actin-based structures in vivo.*J. Cell Sci.***118**, 3937–3948.

Roth, S.(1993). Mechanisms of dorsal-ventral axis determination in *Drosophila* embryos revealed by cytoplasmic transplantations.*Development***117**, 1385–1396.

Roth, S., Stein, D. and Nüsslein-Volhard, C. (1989). A gradient of nuclear localization of the dorsal protein determines dorsoventral pattern in the *Drosophila* embryo. *Cell***59**, 1189–1202.

Ruiwen Wang, M. G. B. (2007). The maximal size of protein to diffuse through the nuclear pore is larger than 60kDa. *FEBS Lett.***581**, 3164.

Rupprecht, J.-F., Ong, K. H., Yin, J., Huang, A., Dinh, H.-H.-Q., Singh, A. P., Zhang, S., Yu, W. and Saunders, T. E. (2017). Geometric constraints alter cell arrangements within curved epithelial tissues. *Mol. Biol. Cell***28**, 3582–3594.

Rusan, N. M. and Peifer, M.(2007). A role for a novel centrosome cycle in asymmetric cell division.*J. Cell Biol.***177**, 13–20.

Sachs, J.(1892). Beiträge zur Zellentheorie.Energiden und Zellen.*Flora***75**, 57–67.

Schmidt, A. and Grosshans, J.(2018). Dynamics of cortical domains in early development.*J. Cell Sci.***131**,.

Schonbaum, C. P., Perrino, J. J. and Mahowald, A. P.(2000). Regulation of the vitellogenin receptor during *Drosophila* melanogaster oogenesis.*Mol. Biol. Cell***11**, 511–521.

Schweizer, N., Pawar, N., Weiss, M. and Maiato, H. (2015). An organelle-exclusion envelope assists mitosis and underlies distinct molecular crowding in the spindle region. *J. Cell Biol.***210**, 695–704.

Shamipour, S., Kardos, R., Xue, S.-L., Hof, B., Hannezo, E. and Heisenberg, C.-P.(2019). Bulk Actin Dynamics Drive Phase Segregation in Zebrafish Oocytes.*Cell***177**, 1463–1479.e18.

Shepherd, V. A. (2006). The cytomatrix as a cooperative system of macromolecular and water networks. *Curr.Top. Dev. Biol.***75**, 171–223.

Sherlekar, A. and Rikhy, R. (2016). Syndapin promotes pseudocleavage furrow formation by actin organization in the syncytial *Drosophila* embryo. *Mol. Biol. Cell***27**, 2064–2079.

Sommer, B., Oprins, A., Rabouille, C. and Munro, S. (2005). The exocyst component Sec5 is present on endocytic vesicles in the oocyte of*Drosophila* melanogaster. *The Journal of Cell Biology***169**, 953–963.

Sonnenblick, B. P.(1941). Germ Cell Movements and Sex Differentiation of the Gonads in the *Drosophila* Embryo.*Proc. Natl. Acad. Sci. U. S. A.***27**, 484–489.

Spirov, A., Fahmy, K., Schneider, M., Frei, E., Noll, M. and Baumgartner, S. (2009). Formation of the bicoid morphogen gradient: an mRNA gradient dictates the protein gradient. *Development***136**, 605–614.

Spracklen, A. J., Fagan, T. N., Lovander, K. E. and Tootle, T. L. (2014). The pros and cons of common actin labeling tools for visualizing actin dynamics during *Drosophila* oogenesis. *Dev. Biol.***393**, 209–226.

Staller, M. V., Yan, D., Randklev, S., Bragdon, M. D., Wunderlich, Z. B., Tao, R., Perkins, L. A., DePace, A. H. and Perrimon, N.(2013). Depleting Gene Activities in Early *Drosophila* Embryos with the “Maternal-Gal4–shRNA” System.*Genetics***193**, 51–61.

Stasevich, T. J., Mueller, F., Michelman-Ribeiro, A., Rosales, T., Knutson, J. R. and McNally, J. G. (2010). Cross-validating FRAP and FCS to quantify the impact of photobleaching on in vivo binding estimates. *Biophys.J.***99**, 3093–3101.

Struhl, G., Struhl, K. and Macdonald, P. M. (1989). The gradient morphogen bicoid is a concentration-dependent transcriptional activator. *Cell***57**, 1259–1273.

Sullivan, W. and Theurkauf, W. E. (1995). The cytoskeleton and morphogenesis of the early *Drosophila* embryo. *Curr.Opin. Cell Biol.***7**, 18–22.

Teleman, A. A. and Cohen, S. M.(2000). Dpp gradient formation in the *Drosophila* wing imaginal disc.*Cell***103**, 971–980.

Thukral, S., Kaity, B., Dey, B., Sharma, S., Nandi, A., Mitra, M. and Rikhy, R. (2019). Cyto-architecture constrains a photoactivation induced tubulin gradient in the syncytial *Drosophila* embryo. *bioRxiv***520031**,.

Trembecka, D. O., Kuzak, M. and Dobrucki, J. W. (2010). Conditions for using FRAP as a quantitative technique--influence of the bleaching protocol. *Cytometry A***77**, 366–370.

Tsuruhara, T., Koenig, J. H. and Ikeda, K. (1990). Synchronized endocytosis studied in the oocyte of a temperature-sensitive mutant of *Drosophila* melanogaster. *Cell Tissue Res.***259**, 199–207.

Turing, A. M. (1952). The chemical basis of morphogenesis.

Turner, F. R. and Mahowald, A. P. (1976). Scanning electron microscopy of *Drosophila* embryogenesis: 1. The structure of the egg envelopes and the formation of the cellular blastoderm. *Dev. Biol.***50**, 95–108.

Várnai, P. and Balla, T. (1998). Visualization of phosphoinositides that bind pleckstrin homology domains: calcium- and agonist-induced dynamic changes and relationship to myo-[3H]inositol-labeled phosphoinositide pools. *J. Cell Biol.***143**, 501–510.

Verkman, A. S. (1999). [22] Green fluorescent protein as a probe to study intracellular solute diffusion. In *Methods in Enzymology*, pp. 250–264.Academic Press.

Wahli, W.(1988). Evolution and expression of vitellogenin genes.

Warn, R. M. (1986). The cytoskeleton of the early *Drosophila* embryo. *J. Cell Sci. Suppl.***5**, 311–328.

Weil, T. T., Parton, R., Davis, I. and Gavis, E. R. (2008). Changes in bicoid mRNA anchoring highlight conserved mechanisms during the oocyte-to-embryo transition. *Curr.Biol.***18**, 1055–1061.

Weil, T. T., Xanthakis, D., Parton, R., Dobbie, I., Rabouille, C., Gavis, E. R. and Davis, I.(2010). Distinguishing direct from indirect roles for bicoid mRNA localization factors.*Development***137**, 169–176.

Welte, M. A. (2015). As the fat flies: The dynamic lipid droplets of *Drosophila* embryos. *Biochim.Biophys. Acta***1851**, 1156–1185.

Welte, M. A., Gross, S. P., Postner, M., Block, S. M. and Wieschaus, E. F. (1998). Developmental regulation of vesicle transport in *Drosophila* embryos: forces and kinetics. *Cell***92**, 547–557.

Wessel, A. D., Gumalla, M., Grosshans, J. and Schmidt, C. F. (2015). The mechanical properties of early *Drosophila* embryos measured by high-speed video microrheology. *Biophys.J.***108**, 1899–1907.

Windner, S. E., Manhart, A., Brown, A., Mogilner, A. and Baylies, M. K. (2019). Nuclear Scaling Is Coordinated among Individual Nuclei in Multinucleated Muscle Fibers. *Dev. Cell***49**, 48–62.e3.

Wolpert, L.(1969). Positional information and the spatial pattern of cellular differentiation.*Journal of Theoretical Biology***25**, 1–47.

Yao, C., Rath, U., Maiato, H., Sharp, D., Girton, J., Johansen, K. M. and Johansen, J. (2012). A nuclear-derived proteinaceous matrix embeds the microtubule spindle apparatus during mitosis. *Mol. Biol. Cell***23**, 3532–3541.

Yao, C., Wang, C., Li, Y., Zavortink, M., Archambault, V., Girton, J., Johansen, K. M. and Johansen, J.(2018). Evidence for a role of spindle matrix formation in cell cycle progression by antibody perturbation.*PLoS One***13**, e0208022.

Yguerabide, J., Schmidt, J. A. and Yguerabide, E. E.(1982). Lateral mobility in membranes as detected by fluorescence recovery after photobleaching.*Biophys.J.***40**, 69–75.

Yu, S. R., Burkhardt, M., Nowak, M., Ries, J., Petrásek, Z., Scholpp, S., Schwille, P. and Brand, M.(2009). Fgf8 morphogen gradient forms by a source-sink mechanism with freely diffusing molecules.*Nature***461**, 533–536.

Zhang, J., Houston, D. W., King, M. L., Payne, C., Wylie, C. and Heasman, J. (1998). The role of maternal VegT in establishing the primary germ layers in Xenopus embryos. *Cell***94**, 515–524.

Zhang, X.-H., Axton, J. M., Drinjákovic, J., Lorenz, L., White-Cooper, H. and Renault, A. D.(2004). Spatial and temporal control of mitotic cyclins by the Gnu regulator of embryonic mitosis in *Drosophila*.*J. Cell Sci.***117**, 3571–3578.

Zhang, Y., Yu, J. C., Jiang, T., Fernandez-Gonzalez, R. and Harris, T. J. C.(2018). Collision of Expanding Actin Caps with Actomyosin Borders for Cortical Bending and Mitotic Rounding in a Syncytium.*Dev. Cell***45**, 551–564.e4.